



HAL
open science

Study by simulation and measure of a system of exhibition of animals in the radio waves led by the Wi-Fi systems

Tongning Wu

► **To cite this version:**

Tongning Wu. Study by simulation and measure of a system of exhibition of animals in the radio waves led by the Wi-Fi systems. Other. Université Paris-Est, 2009. English. NNT : 2009PEST1018 . tel-00512334

HAL Id: tel-00512334

<https://theses.hal.science/tel-00512334v1>

Submitted on 30 Aug 2010

HAL is a multi-disciplinary open access archive for the deposit and dissemination of scientific research documents, whether they are published or not. The documents may come from teaching and research institutions in France or abroad, or from public or private research centers.

L'archive ouverte pluridisciplinaire **HAL**, est destinée au dépôt et à la diffusion de documents scientifiques de niveau recherche, publiés ou non, émanant des établissements d'enseignement et de recherche français ou étrangers, des laboratoires publics ou privés.

UNIVERSITÉ PARIS-EST

ÉCOLE DOCTORALE

Thèse de doctorat

Électronique, Traitement du Signal

Tongning WU

**Etude par Simulation & Mesures d'un
système d'Exposition d'Animaux aux
Ondes Radioélectriques Induites par les
Systèmes Wi-Fi**

Thèse dirigée par

Mme Odile PICON

Mr Joe WIART

Soutenue le 20 février 2009

Jury:

Mme Odile PICON	Professeur à l'Université Paris-Est	Directrice de thèse
Mr Joe WIART	Ingénieur Expert Senior à Orange Labs	Co-Directeur
Mr Marc HELIER	Professeur à l'UPMC	Rapporteur
Mr Raphaël GILLARD	Professeur à l'IETR	Rapporteur
Mr Bernard VEYRET	Directeur de Recherche CNRS	Examinateur
Mr David LAUTRU	Maître de Conférences à UPMC	Examinateur

Remerciements

Ce travail de thèse a été réalisé au sein d'Orange Labs, dans URD, Interaction Ondes Personnes (IOP), en collaboration avec le Laboratoire « Electronique Systemes de Communications et Microsystemes », Université Paris-Est.

Je tiens à exprimer toute ma reconnaissance à Mme. Odile Picon, ma directrice de thèse qui m'a accordé toute sa confiance pendant les années où j'ai eu la chance d'être sous sa direction. Ses qualités humaines et son esprit critique sont des valeurs que j'ai appréciées en travaillant avec elle, et qui font que je lui témoigne un profond respect.

Je remercie très chaleureusement M. Joe Wiart, mon responsable de FT pour de multiples raisons, et en particulier pour m'avoir offert l'opportunité de travailler sur un sujet de thèse passionnant, pour m'avoir apporté un soutien sans faille durant trois années. J'ai beaucoup apprécié la qualité de son encadrement, et le haut niveau de son raisonnement scientifique qui m'a permis de faire progresser mes recherches.

Je me permets d'exprimer toute ma gratitude à M. Man-fai Wong et à M. Azzedine Gati pour l'efficace dont ils ont fait preuve lorsque je les ai sollicités et aussi pour leur disponibilité. Leurs aides m'ont toujours encouragé.

Je tiens à exprimer ma profonde reconnaissance aux membres de jury: Merci à M. Marc Hélier et M. Raphaël Gillard d'avoir accepté le rôle de rapporteur et leurs efforts pour évaluer ma thèse. Merci à M. Bernard Veyret pour sa coopération et son accueil chaleureux dans les missions à Bordeaux. Merci à M. David Lautru qui me fait honneur de sa présence dans le jury.

Je voudrais passer mes vifs remerciements aux doctorants: Jessica et Hanae pour le même bureau que l'on a partagé durant les 3 ans et pour leurs encouragements; à Aimad et à Thierry pour vos amitiés. Ces expériences seront vraiment un trésor dans ma mémoire quelque soit l'endroit où je serai. J'espère que vous aurez un bon avenir dans votre carrière ainsi que pour la thèse, et qu'on pourra se revoir de temps en temps.

Je tiens à faire mes remerciements grandioses à Hamid pour son aide énorme au quotidien, à Abdel pour sa compagnie dans plusieurs missions à Brest et à Bordeaux, Je tiens à faire tous mes remerciements à Thierry, Emmanuelle, Tristan, Suzette et Wei pour leurs disponibilités tous au long de ma thèse. Je voudrais aussi remercier Guillaume, Yahya, Aline, Fadila, Albert, Fabrice, Emmanuel, Thibault, Youmni et Amazir qui sont déjà partis de notre équipe.

Je voudrais remercier l'équipe de ESYCOM à Université Paris-Est et au groupe BioE IMS à Bordeaux, spécialement à Mme. Isabelle Lagroye.

Je voudrais aussi associer mes remerciements à M. Philippe COUSIN et M. Daniel CHALONS pour vos amitiés.

En fin, je tiens à exprimer ma gratitude à toute ma famille, amis, qui m'ont entouré pendant tous les 3 années.

Résumé : Ce travail de thèse consiste en la conception et l'analyse d'un système d'exposition des animaux *in vivo* avec les signaux Wi-Fi dans une chambre réverbérante (CR).

Notre époque est marquée par la pénétration des systèmes sans fils dans toute la société. Ils sont plus en plus répandus et utilisés pour les télécommunications et l'information. En majeure partie, ils occupent les fréquences de 300 kHz à 10 GHz. Ce domaine de fréquences est alors appelé radiofréquences (RF). Les questions du public sur effets biologiques en radiofréquences (RF) sont nombreuses et ont induit beaucoup de recherches. Basés sur ces résultats de recherche et les bases de données, la Commission Internationale pour la Protection contre les Rayonnements Non-ionisants (ICNIRP) et l'American National Standards Institute (ANSI) ont publié leur restrictions sur expositions électromagnétiques du public et des travailleurs (*Guide pour l'établissement de limites d'exposition aux champs électriques, magnétiques et électromagnétiques* et *Safety Levels with Respect to Human Exposure to Radiofrequency Electromagnetic Fields, 300 kHz to 10 GHz*).

L'Organisation Mondiale de la Santé (OMS) a aussi lancé son "International EMF Project" afin que bien comprendre les effets associés aux expositions du champ électromagnétique. Leurs résultats sont actuellement disponibles sur le site internet www.who.int/emf/. L'OMS conclut les résultats sur l'exposition aux RF avec la mention que aucun effet sanitaire positif n'a été trouvé avec les normes de l'ICNIRP. Donc le guide de l'INCIRP est autorisé et adopté par la majorité des pays et les organisations mondiales. En Etats-Unis, les restrictions d'ANSI sont adoptées pour contrôler l'exposition au champ électromagnétique. Les deux normes sont en train de converger.

Néanmoins, tout en faisant respecter les normes d'exposition sur les nouveaux environnements et sur les nouvelles techniques apparues journallement, l'OMS continue toujours de solliciter des recherches pour enrichir et compléter les bases de données. L'un des ses intérêts souligne l'évaluation des effets des expositions concernant les signaux Wi-Fi qui sont en train de pénétrer dans tous les coins de notre vie quotidienne.

L'exposition de champ électromagnétique est évaluée par l'indice de débit d'absorption spécifique (DAS ou SAR en anglais). L'ICNIRP a proposé ses restrictions de base avec

la notion de DAS corps entier. La population générale (grand public) et les travailleurs sont protégés par différentes restrictions de base et donc différents niveaux de référence. Elle ne considère pas la variabilité de la population (par exemple, différentes formes, variables paramètres physique et physiologique induits par vieillissement). Les études récentes ont démontré la variation importante du DAS corps entier chez les enfants et les adultes introduit par la même onde plane incidente. Cela nous révèle que même dans des configurations d'exposition similaires, les jeunes sont peut-être soumis à un DAS corps entier plus élevé que les adultes. Le risque est prévu pour les enfants. L'OMS a donc appelé les recherches en focalisant les effets sanitaires d'exposition sur les jeunes personnes par les expériences avec animaux. Dans ce cadre, un projet pour exposer les jeunes rats pendant la période de croissance (depuis l'embryon jusqu'à 35 jours après la naissance) était proposé par les biologistes. Un système d'exposition qui peut fournir une puissance constante ainsi que la dosimétrie pour déterminer la répartition de la puissance chez les animaux font partie des grandes lignes de ce projet. Ce système est destiné à fournir au minimum 4 W/kg (DAS corps entier) pour les rats pesant $1,5\text{ kg}$. Rat Wistar est choisi comme animal d'expérimentation. Dans le système mis au point dans ce travail, les rats ont la possibilité de se déplacer avec un volume suffisamment large à ne pas perturber leurs activités quotidiennes.

Si l'on analyse les buts de ce système, on pourra déduire les besoins suivants:

Le système doit,

- (1) être capable d'exposer les $1,5\text{ kg}$ d'animaux avec 4 W/kg DAS corps entier par les vrais signaux Wi-Fi
- (2) permettre le déplacement libre des animaux dans le système
- (3) fournir l'exposition uniforme quel que soit le mouvement des animaux
- (4) pouvoir émettre les signaux de Wi-Fi constants et consécutifs durant 2-3 heures

Pour satisfaire ces critères, on a divisé les travaux prévus en trois parties : l'émission des signaux Wi-Fi, le bilan de puissance et la conception du système.

Les spécificités des signaux Wi-Fi sont étudiées selon la norme IEEE 802.11. Les puissances émises par les systèmes Wi-Fi sont faibles. La Puissance Isotrope Rayonnée Equivalente, ou PIRE (égale à la puissance d'entrée pondérée par le gain de l'antenne)

de ces systèmes est inférieure à 100 mW pour les stations et points d'accès de la norme 802.11b (2,4 GHz). Cette valeur est en fait l'émission maximale. Pour atteindre ou plutôt approcher cette valeur, il faut maximiser temps d'occupation du canal. Un logiciel est appliqué pour forcer le maximum d'émission de la carte Wi-Fi qui est installée sur un PC de communication. Ce logiciel est capable de produire plusieurs paquets consécutifs à pleine puissance avec un temps minimal d'attente.

Le bilan de puissance est estimé par les études sur les signaux de Wi-Fi et le critère sur la puissance absorbée par les animaux. En théorie, le DAS corps entier à 4 W/kg pour 1,5 kg des rats demande 6 W de puissance émise par le système d'alimentation en supposant une parfaite efficacité du système (100% absorbée par les animaux sans la perte vers le système).

La chaîne de puissance incidente comprend un générateur de signaux, les câbles et l'amplificateur. Le générateur commercial de signaux est capable de sortir une puissance de l'ordre de 20 dBm. L'amplificateur doit être rajouté dans cette chaîne pour augmenter les signaux aux différents niveaux dépendant de sa capacité et du besoin. Ici, nous devons considérer le budget financière pour ce projet car l'amplificateur avec fortes sortie est très cher. Nous avons donc deux choix lorsqu'on décide de cette chaîne de mesure, soit un amplificateur avec la puissance sortie plus forte (qui est aussi très cher et n'est pas favorable par ce projet), soit un amplificateur avec une puissance de sortie modérée. Le dernier choix exige que le système ait une efficacité élevée. La puissance absorbée par le système est plus faible. Sinon, les animaux seront sous-exposés. On a choisi un amplificateur de 50 W. Suivant l'estimation, ce système d'exposition doit atteindre au minimum 60 % d'efficacité.

En recherchant dans les études précédentes, il y a 4 systèmes enregistrés pour l'expérience d'expositions *in vivo*. Ce sont la chambre réverbérante (CR), la chambre anéchoïque (CA), la cellule TEM et le guide d'onde rayonné. La CR et la CA sont capables d'opérer les expériences sans restriction. Pour les deux candidates, le CR est plus économique par rapport au coût de construction. Du coup, elle peut produire le niveau de champ plus élevé que le CA pour une puissance incidente donnée et le même volume d'expérience. La cellule TEM et le guide d'onde rayonné sont cités pour les recherches d'exposition restreinte. Ces deux choix ne peuvent fournir que de très petits espaces de test dans le système. Notre projet demande les espaces pour 4 adultes et 12

petits rats. C'est extrêmement difficile à fabriquer pour les deux méthodes. Après avoir comparé les avantages et inconvénients des différents systèmes, la CR a été choisie comme système d'exposition.

Le schéma de puissance incidente est montré dans Figure 1.

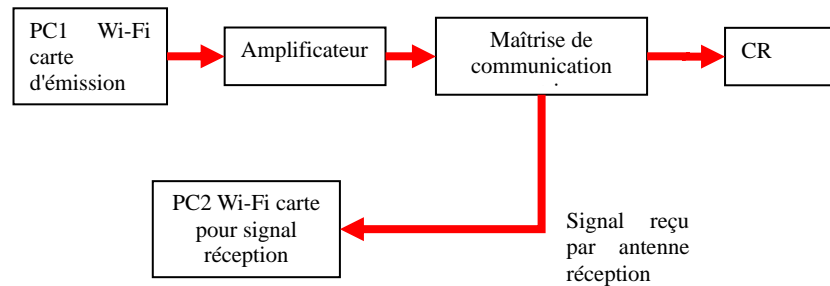


Figure 1 Schéma de puissance incidente de ce système

La CR inclut en théorie une cage métallique. La distribution du champ dans la cage peut être modifiée de façon considérable par une variation de la fréquence de fonctionnement ou par la rotation d'un brasseur (s'il y en a plusieurs, nous devons prendre en compte toutes les combinaisons) de modes. L'uniformité statistique de l'espérance est alors constatée à partir du prélèvement d'un nombre suffisant de positions de la rotation des brasseurs ou d'échantillons de fréquence.

La norme CEI EN 61000-4-21 *compatibilité électromagnétique (CEM) – Partie 4-21: Techniques d'essai et de mesure-Méthodes d'essai en chambre réverbérante* est une norme de Compatibilité Electromagnétique décrivant les techniques d'essai et de mesure en CR. Cette norme présente les procédures à suivre pour opérer les mesures sur l'immunité électromagnétique, les émissions et les boucliers électromagnétiques d'équipements électriques et électroniques. Elle introduit des paramètres très importants, par exemple, Q (facteur de qualité), CCF (facteur d'étalon), l'uniformité du champ et les fréquences des modes. Ces paramètres servent à évaluer la performance de la CR. Elle présente aussi les caractéristiques minimales à vérifier pour les CR afin de procéder à des tests du champ électromagnétique. Malgré tout, cette norme n'est pas éditée pour les expériences sur les animaux et certains paramètres ne conviennent pas directement pour ces expériences. Nous avons donc emprunté les théories ainsi que les

méthodes citées par la norme comme référence pour développer un système d'exposition des animaux. Nous allons discuter en détail les paramètres.

Parmi eux, un important paramètre de la CR est le facteur de qualité (Q). Cette notion est relative à la capacité à emmagasiner de l'énergie électromagnétique dans la CR. L'amplitude de champ dépend largement à ce facteur de qualité. Généralement, on le définit comme étant le rapport entre l'énergie moyenne emmagasinée et l'énergie dissipée par unité de temps. Elle est calculable et mesurable selon les équations ((1) et (2)) de la norme EN 61000-4-21.

$$Q = \frac{3V}{2\mu_r\delta_s A} \left[\frac{1}{1 + \frac{3\lambda}{16} \left(\frac{1}{l} + \frac{1}{w} + \frac{1}{h} \right)} \right] \quad (1)$$

ou,

V : Volume de la CR

μ_r : Permittivité relative de la cage

δ_s : Épaisseur de peau de la CR

λ : Longueur onde dans la CR

A : La surface de la CR

l , w et h : Trois dimension de la CR

$$Q = \frac{16\pi^2 V}{\lambda^3} \frac{P_{RX}}{P_{TX}} \quad (2)$$

P_{RX} est la puissance reçue par l'antenne de réception

P_{TX} est la puissance transmise par l'antenne émettrice

On pourra mesurer le Q avec l'équation (2). Cette valeur de Q est ensuite retournée dans (1), les propriétés électriques de la cage sont calculées. Il faut faire attention sur cette valeur calculée de Q parce qu'elle ne représente pas le Q réel. Dans la CR, la fuite de la cage, l'absorption des parois et les pertes dans les appareils de mesure diminuent le Q mesuré. Lorsqu'on utilise ce Q, les propriétés électriques (conductivité, si l'on précise) sont inférieures à la valeur réelle. Avec cette approche, on a sous-estimé la conductivité et le Q. Ces deux paramètres servent à caractériser la distribution du champ dans la CR et à construire le modèle d'exposition dans l'étude suivante. Donc l'on doit prendre en

compte cet effet et évaluer ces valeurs mesurées-calculées avant leur utilisation pour déterminer la performance de la CR.

Généralement, nous devons décider quatre paramètres pour la conception de la CR qui sont les formes, les tailles, les matériaux, les méthodes d'excitation et la méthode de brassage de la CR.

La forme de la CR est discutée comme régulière ou irrégulière citée par les études précédentes. La CR avec des formes régulières prévaut dans les cas où l'homogénéité du champ est la considération prioritaire car cette configuration peut produire un espace uniforme plus grand pour les champs. On choisit un volume irrégulier si l'on demande beaucoup de modes électromagnétiques. Dans notre cas d'exposition uniforme, une CR cubique est de préférence.

La taille de la CR est déterminée par simulation. Un cube de liquide équivalent conforme à la norme de CEI 62209 (*Exposition humaine aux champs radio fréquence produits par les dispositifs de communications sans fils tenus à la main ou portés près du corps - Modèles du corps humain, instrumentation et procédures - Partie 2 : Procédure pour la détermination du débit d'absorption spécifique produit par les dispositifs de communications sans fils utilisés très près du corps humain (plage de fréquence de 30 MHz à 6 GHz)*) est placé dans la CR. Il bouge librement tous les 5 cm dans un volume de $40\text{cm} \times 40\text{cm} \times 40\text{cm}$ qui se situe dans au milieu de la CR. Une antenne dipôle est installée à 4 cm de distance des parois. Le s_{11} de l'antenne est noté en fonction des différentes positions de ce cube. L'écart type du s_{11} est calculé pour la CR avec les différentes dimensions de $60\text{cm} \times 60\text{cm} \times 60\text{cm}$, $80\text{cm} \times 80\text{cm} \times 80\text{cm}$, $100\text{cm} \times 100\text{cm} \times 100\text{cm}$ et $120\text{cm} \times 120\text{cm} \times 120\text{cm}$. En conclusion, une cage de $120\text{cm} \times 120\text{cm} \times 120\text{cm}$ introduit 0,59 dB d'écart type. Afin d'assurer une bonne performance, une plus grande cage cubique de $150\text{cm} \times 150\text{cm} \times 150\text{cm}$ est choisie (Figure 2).

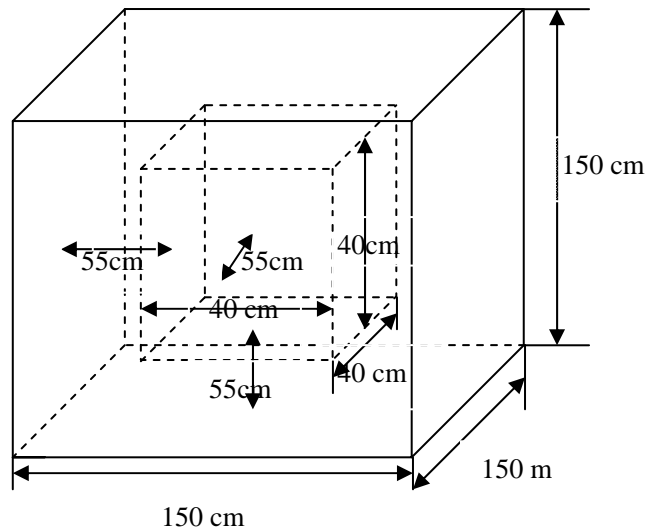


Figure 2 Dimensions de la CR

Comme nous l'avons dit dans le principe de la CR, la première fonction de brassage est de produire nombreux modes dans la cage. Lors que la densité de modes est suffisamment élevée, la CR peut entrer en résonance quelque soit la fréquence d'excitation. Une seconde propriété du brassage de modes est le fait qu'il rende le champ statistiquement isotrope et homogène sur une rotation de brasseur. Ceci signifie que sur une rotation de brasseur, la valeur maximale du champ électromagnétique est quasiment identique en tous points de la CR et suivant toutes les directions. C'est à dire que, si l'on a besoin d'un champ homogène, on doit concentrer les recherches sur la partie du brassage.

La méthode de brassage est constituée deux approches. La méthode mécanique et électronique.

Le brassage mécanique inclut de pâles métalliques fixées sur un axe pivotant. En changeant l'angle du brasseur, on applique une modification sur les conditions aux limites qui permet de décaler les fréquences d'apparition des modes de résonance. Ceci est la méthode répandue et plus simple. Un autre moyen est de changer directement les dimensions de la CR (ou couverture de la CR) temporellement sans la rotation de brasseur. Ce moyen est difficile à réaliser pour une performance satisfaisante (la fuite de la puissance à cause de fabrication est importante).

La rotation du brasseur et les accessoires mécaniques occupent un certain volume dans la CR. Ces volumes deviennent inutiles. La fonction des appareils mécaniques donnent

aussi les bruits qui vont perturber les activités des rats. Donc tous les efforts tendent à supprimer la présence du brasseur pour garder un volume suffisant pour l'expérience. Nous pouvons évoquer la méthode du brassage électronique ou sa modification. Le brassage électronique est constitué de deux méthodes: brassage de la phase et brassage de la fréquence. Les deux méthodes ont été appliquées pour éviter les brasseurs solides. Néanmoins, elles ne conviennent pas à notre expérience d'exposition seulement en fréquence Wi-Fi. Nous devons chercher une autre méthode pour remplacer les pâles du brasseur.

Cette nouvelle méthode d'excitation comprend l'installation de 6 antennes identiques de dipôle sur les parois de la cage. Leurs positions ne sont pas complètement centralisées. Trois coins de la cage sont occupés par des morceaux métalliques et équipés avec un petit brasseur (diamètre: 300 mm). Ces 6 antennes fonctionnent aléatoirement pour avoir des ondes venant de toutes les directions. La performance de la CR est validée par la mesure. Cette configuration permet d'éviter une grande taille du brasseur de la chambre réalisée (Figure 3).

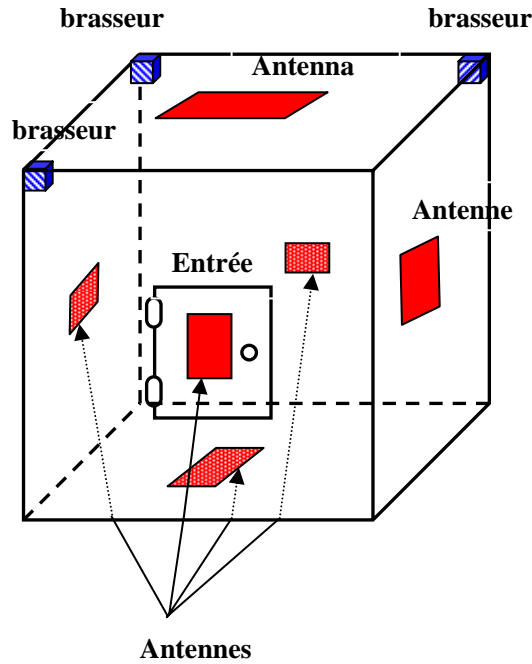


Figure 3 Schéma d'excitation et brassage

Comme nous l'avons dit brièvement, la couverture (je ne comprends pas) de la cage influence le Q. Le Q est l'indice de performance de réverbération. Il décide aussi de l'efficacité du système. L'étude déclare que des matériaux présentant une haute conductivité électronique n'améliorent pas la performance de l'homogénéité des champs. Cela produit un niveau de champ plus élevé dans la CR. L'aluminium est un métal commun avec une conductivité plus grande que le fer. Les matériaux en aluminium avec les trous (diamètre 1mm) sont choisis pour fabriquer la CR. Cette conception permet d'échanger de l'air pour la CR et donc la respiration des animaux. Il n'y a pas d'équipement supplémentaire pour cette fonction. On peut gagner cet espace pour le test et éviter les bruits des rotations des pâles.

Un banc de test plastique est placé dans le milieu de la cage. Ce banc a deux étages. Sur chaque étage, deux boîtes plastiques servent comme espace de déplacement pour les rats. Le banc de test et les 4 boîtes sont électromagnétiquement transparents.

La CR réalisée est montrée dans Figure 4

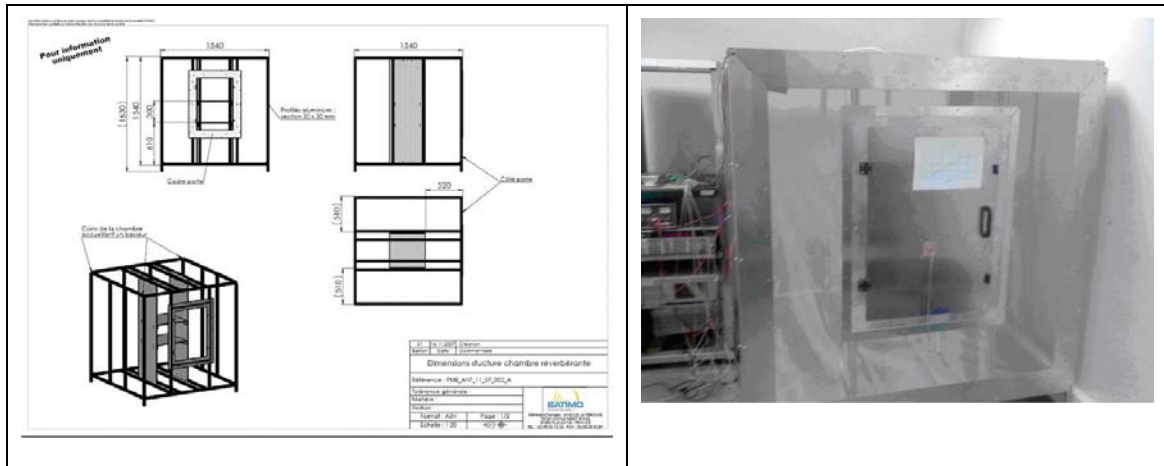


Figure 4 Réalisation de la CR

Lors que l'on discute la caractérisation de la répartition de puissance dans ce système, nous avons deux outils. Ce sont les mesures et les simulations.

Il y a des études pour déterminer la puissance absorbée par les animaux seulement par la mesure. Cette méthode tout d'abord estime les pertes sur ce système d'exposition. Quand la puissance entrée dans ce système est donnée, il nous suffit d'un simple calcul pour la puissance absorbée chez les animaux.

$$P_{abs} = P_{inc} - P_{diss} \quad (3)$$

P_{abs} La puissance absorbée pour les animaux

P_{inc} La puissance incidente dans le système

P_{diss} La puissance dissipée vers le système

Le défaut de cette méthode est l'impossibilité d'estimer précisément les pertes pour un système compliqué comme la CR. L'homogénéité, Q et le niveau de champ sont les mesures caractérisant la CR. Leurs procédures de mesure sont bien établies par la norme. Mais avec tous ces types de mesure, nous ne pouvons pas intervenir à l'intérieur des animaux et savoir directement la puissance dissipée dans leurs corps. En revanche, nous n'avons pas d'autre moyen non-envahissant et précis pour mesurer la puissance absorbée par les rats. Déterminer la puissance absorbée uniquement par les mesures est impossible.

Il y a aussi des publications sur la distribution de puissance utilisant uniquement la simulation. Dans ce cas, lorsque tous les paramètres concrets environnent

d'exposition seraient connus, les mêmes environnements sont reproduits dans la simulation. Nous pourrions prévoir de réaliser l'évolution de ces paramètres avec le calcul.

La simulation électromagnétique emprunte la méthode numérique consistant à calculer l'évolution du champ. Pour déterminer le DAS dans les animaux, on doit choisir et appliquer une méthode numérique analysant la distribution du champ dans la CR. Les logiciels basés sur la méthode des éléments finis (MEF), la méthode de moment (MoM) et la méthode FDTD (pour finite difference time-domain) ont été déjà commercialisés. La FDTD est une méthode temporelle. Il n'est pas nécessaire d'inverser une matrice. Cette méthode est choisie pour la simulation car demandant moins de mémoire.

La simulation demande de connaître tous les paramètres d'entrée qui sont très difficiles à obtenir pour la CR (nous les avons constatés dans l'analyse de Q). De plus, les calculs électromagnétiques dans la cage réverbérante sont plus compliqués car la propagation des ondes et leurs réflexions prennent beaucoup de temps pour que les signaux soient stables. La CR fonctionne selon la théorie de réverbération. Donc elle a besoin beaucoup de temps de calcul ainsi que d'une grande mémoire pour stocker les variables temporelles et spatiales. Une simulation nous montre l'impossibilité de mener les calculs au bout. Les configurations similaires à l'expérience sur s_{11} sont utilisées. Les dimensions de la CR est $1m \times 1m \times 1m$. Trois coins de cette cage sont coupés pour éviter la symétrie. Le cube de liquide équivalent (1,5 Kg) est placé au milieu de la CR. On applique les paramètres électriques CEI. Une impulsion gaussienne est émise par l'antenne dipôle sur les parois. Il y a 27 points dans le cube et les 27 autres points dans la CR sont en dehors de ce cube. Sur les 54 points, les valeurs des composantes d'amplitude des champs électromagnétiques sont enregistrées à chaque itération de la FDTD. La méthode de filtre d'IIR (Infinite Impulse Response) est appliquée pour analyser la convergence de cette méthode. Les résultats nous montrent qu'après 200.000 itérations (5 semaines de calcul), la convergence n'a pas encore été atteinte. En résumé, Il est impossible de caractériser les champs dans la CR et la répartition de puissance chez les rats uniquement avec la FDTD classique.

On propose donc ici, d'étudier la répartition de puissance chez les rats par une méthode hybride de simulation-mesure. Cette méthode est basée sur deux hypothèses. La

première, suppose que pour la partie de simulation, la relation de DAS corps entier et le champ moyen dans la CR sont proportionnels. Plus le champ moyenné dans la CR est élevé, plus le DAS corps entier des animaux est élevé. Deuxièmement, pour la partie de mesure, la puissance incidente dans la CR induit un niveau de champ moyenné dans la CR déterminé. Donc la puissance d'entrée est liée au champ moyenné dans la CR. Le niveau de champ moyenné dans la CR peut servir à la connexion entre la simulation et la mesure. La relation de puissance incidente et DAS corps entier est ainsi établie (Figure 5).

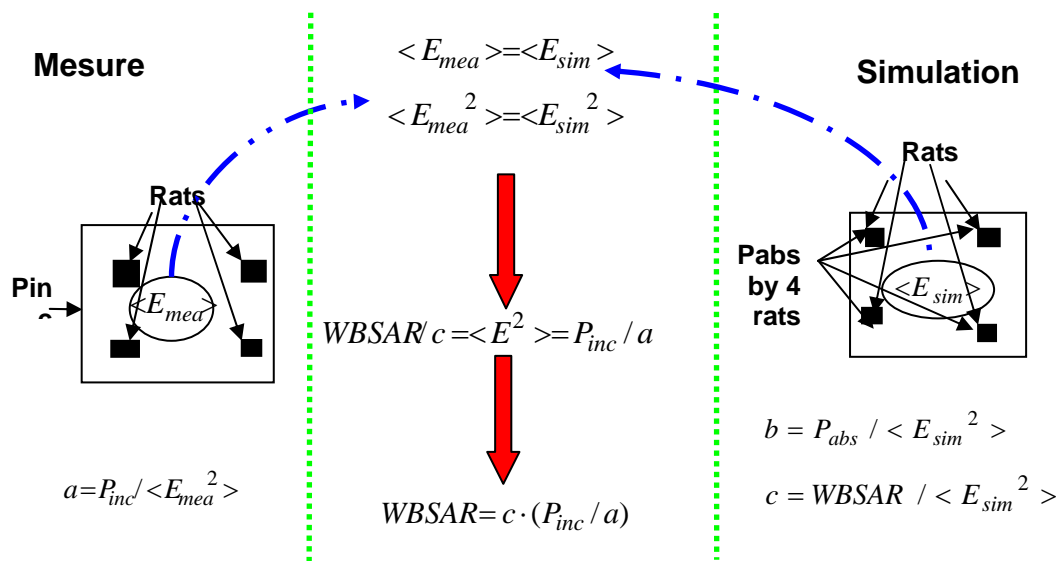


Figure 5 Schéma de simulation-mesure hybride méthode

Ou,

E_{sim} : E simulé

E_{mea} : E mesuré

P_{abs} : la puissance absorbée par les rats

P_{inc} : la puissance incidente dans le système

WBSAR: DAS corps entier

Cette méthode se base aussi sur l'hypothèse que le niveau du champ moyenné par la simulation et le niveau de champ moyenné ont le même sens. Toutes les simulations ou mesures sont faites avec une charge ou des modèles numériques d'animaux. Le niveau

du champ moyenné par la simulation est en effet la valeur moyennée spatiale. Elle est moyennée avec 10^6 points en milieu de la CR (volume sans les animaux ou chargé). Par comparaison, la valeur de mesure est obtenue suivant le moyennage sur 26 points en milieu de CR (volume sans les liquides équivalents). Sur chaque point de mesure, la valeur est moyennée en au minimum 2 minutes (60 rotations des brasseurs). Cette valeur est alors une valeur moyennée temporellement et spatialement (si les 26 points représentent bien le niveau du champ moyenné dans la CR).

Dans la simulation, le modèle numérique est fabriqué par Brooks AirForce avec 36 différents tissus ou organes. La résolution du modèle est 0,827 mm. Le poids réel est 374 g.

Ayant constaté les mémoires et temps demandés par les calculs de la FDTD, nous avons cherché une approche pour réduire les ressources de calcul. Les études sur la distribution du champ ont vérifié que si facteur de qualité (Q) de la CR est supérieur à 100, la distribution du champ suit une statistique de Rayleigh. Dans la CR construite, on a lancé les opérations sur la mesure de Q. Suivant la norme de CEI 61000-4-21 et selon (2), un Q de l'ordre de 1000 est obtenu. Quand nous nous rappelons notre discussion précédente sur la valeur mesurée de Q, cette valeur en fait sous-estime la réverbérance dans la CR. Ce Q n'est pas utile à déduire les propriétés conductrices exactes de la cage, mais il nous permet de connaître la performance de la CR. Surtout, la distribution de champ dans la CR est validée comme suivant une statistique de Rayleigh (parce que le vrai Q est sûrement supérieur à 1000). Avec cette importante conclusion, nous pouvons caractériser le champ dans la CR avec cette distribution statistique.

La boîte de Huyghens est utilisée pour émettre les champs électromagnétiques à rayonner vers les animaux. La boîte de Huyghens évite la réalisation des parois avec des valeurs exactes des propriétés conductrices, des antennes et de tous les accessoires de la CR. Cette simplification permet de réduire les calculs énormément: les calculs FDTD concentrent dans un volume de $40\text{cm} \times 40\text{cm} \times 40\text{cm}$ au lieu de un volume de $1.5\text{m} \times 1.5\text{m} \times 1.5\text{m}$. De plus, il n'est pas nécessaire de mettre des PML autour du volume de calcul. C'est-à-dire, cette méthode utilise moins que 1% de ressources de calcul que la méthode FDTD.

Il y a quatre paramètres à déterminer pour construire la boîte de Huyghens. Ce sont l'amplitude des ondes planes (sur chaque point de cette boîte de Huyghens, de nombreuses ondes planes sont effectivement émises), le nombre de rayons (les ondes planes) sur un point et leurs phases et directions de propagation.

La distribution Rayleigh impose que les phases et directions de propagations des ondes planes sont aléatoires. Aucune contrainte n'existe sur l'amplitude des ondes planes et le nombre de rayons dans les simulations. Nous devons discuter ces paramètres par les résultats de simulation.

Quand on parle d'amplitude des ondes, nous avons deux possibilités, soit une valeur fixe, soit les valeurs aléatoires. Si nous choisissons la valeur fixe, nous pouvons prendre l'amplitude à 1 dans les simulations. Le nombre de rayons en un point de la boîte de Huyghens varie alors de 15, 40, 100, 200, 300 à 400. Pour chaque valeur, on étudie les deux possibilités sur l'amplitude (1 et aléatoire). 20 simulations sont lancées pour chaque condition. Les résultats sont moyennés sur ces 20 simulations. Le rapport de DAS corps entier sur E carré moyenné est calculé. On peut conclure qu'à partir de 200 rayons, ce rapport commence à converger à une valeur de l'ordre de 7.8×10^6 . L'écart type pour les 20 simulations diminue avec l'accroissement du nombre de rayons. A partir de 200 rayons, cette variation est très faible (moins que 5 %). La réalisation des rayons aléatoires (phase, amplitude et directions de propagation) prend du temps. Le temps augmente rapidement avec le nombre de rayons. Donc, on a choisi 200 rayons pour les expériences d'exposition des rats. L'amplitude aléatoire ou fixe ne change pas les résultats. Considérant la vraie condition sur la CR (multi-réflexions avec la perte), nous avons choisi l'amplitude aléatoire. On cherche une valeur moyennée sur les simulations avec différentes rayons.

Ces configurations sont adoptées pour exposer les animaux dans la CR. Pour simplifier la situation et tester le système d'exposition, les premières simulations portent sur 4 rats placés sur les deux étages du banc de test. Chaque rat pèse 375 g. Ils ne bougent pas. Le but de cette simulation est de vérifier si la puissance incidente de la CR est suffisante pour 4W kg de DAS corps entier chez les animaux dans notre système d'exposition (Figure 6). Par les résultats de 20 simulations, un rapport de DAS corps entier et champ électronique carré moyenné est obtenu comme 7.6×10^6 . De l'autre côté, nous avons mesuré le champ dans la CR et la puissance incidente. Le ratio de puissance incidente

sur le champ électrique au carré moyenné est obtenu. Avec les deux ratios, le lien entre la puissance incidente et le DAS corps entier chez les animaux de 1.500 g est déterminé. Avec cette étude, on peut estimer que pour avoir 6 W de puissance absorbée, 9 W puissance incidente dans la CR est nécessaire qui est supportable pour notre chaîne comme puissance d'entrée.

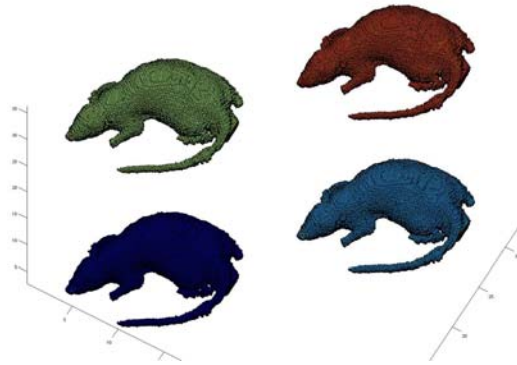


Figure 6 Configuration pour les premières simulations

Une autre méthode de simulation est aussi appliquée pour vérifier le résultat. La similarité pour les deux méthodes est que toutes les deux utilisent la boîte de Huyghens pour imposer les champs de l'exposition. On n'utilise alors que 12 ondes planes au lieu d'ondes planes aléatoires. Dans cette méthode les 12 ondes planes avec ont une phase et une direction choisies et une amplitude fixe (Expliquer comment sont choisies les directions). On en déduit que les autres ondes planes contribuent très faiblement sur le DAS corps entier. Cette méthode de rayons fixes nous mène au résultat similaire à la méthode avec les rayons aléatoire. 8.1×10^6 . 5% de différence est trouvé entre les deux méthodes. Donc notre méthode de simulation est validée.

Si l'on compare les deux méthodes, on trouve que la première méthode (avec les rayons aléatoires) peut donner le résultat plus vite que la deuxième méthode. On a comparé le résultat sur le rapport moyenné en fonction de différents nombres de simulations. 6-7 simulations nous donnent le résultat très semblable au résultat moyenné sur les 20 simulations (200 rayons). Le temps de calcul pour une simulation par n'importe méthode est identique (elles appliquent la même boîte de Huyghens et le même volume de calcul). Donc la première méthode (les ondes aléatoires) prévaut en face de deuxième méthode.

Pour préciser l'influence de maillage. Les mêmes simulations sont lancées avec le maillage de 1 mm et 2 mm. Avec la méthode des ondes aléatoires, il y a 5% de différence sur DAS corps entier entre les deux configurations. Donc le maillage de FDTD ne change pas beaucoup de résultats.

Il faut toujours prendre en compte les spécialités d'expérience *in vivo*. Les animaux doivent être capable de se déplacer dans un volume de $40\text{cm} \times 40\text{cm} \times 40\text{cm}$. Le système doit garantir que soi-même si les animaux bougent, le DAS corps entier reste le même ou change très peu. De plus, le but de ce projet est d'étudier l'exposition pendant la période de croissance de jeunes animaux. Donc des modèles numériques très différents sont réalisés et appliqués pour déterminer l'évolution de DAS corps entier. Nous avons deux choix pour le modèle numérique, soit le modèle proportionnellement réduit depuis le modèle d'adulte, soit le modèle modifié suite aux résultats de mesure sur les animaux dans expérience.

Plusieurs recherches sur l'homme ont montré que le modèle proportionnellement réduit ne convient pas pour les jeunes qui ne sont pas en fait la simple diminution d'un adulte. La technique de morphologie est appliquée pour modifier le modèle. Inspiré par cette méthode, on a utilisé le même moyen. D'après le modèle proportionnellement réduit de celui d'adulte, la mesure sur les tailles d'animaux en fonction de l'âge est effectuée pour obtenir les informations permettant de modifier le modèle réduit. Ces paramètres sont:

- (1) poids
- (2) longueur de la tête
- (3) longueur du corps
- (4) largeur du corps
- (5) longueur de la queue

Les modèles sont créés pour le rat de 4 jours, 6 jours, 13 jours, 16 jours, 23 jours et 30 jours après sa naissance. Les modèles d'embryon sont fabriqués par des sphères de différents diamètres avec une couche de liquide amniotique. Le modèle de nouveau né (4 heures après la naissance) est réalisé par un cylindre.

Le comportement des animaux dépend à l'âge. Les petits animaux préfèrent vivre ensemble avec leur mère. Ils disposent de la capacité de bouger dans la boîte plastique et de s'éloigner de leurs copains (Figure 7).

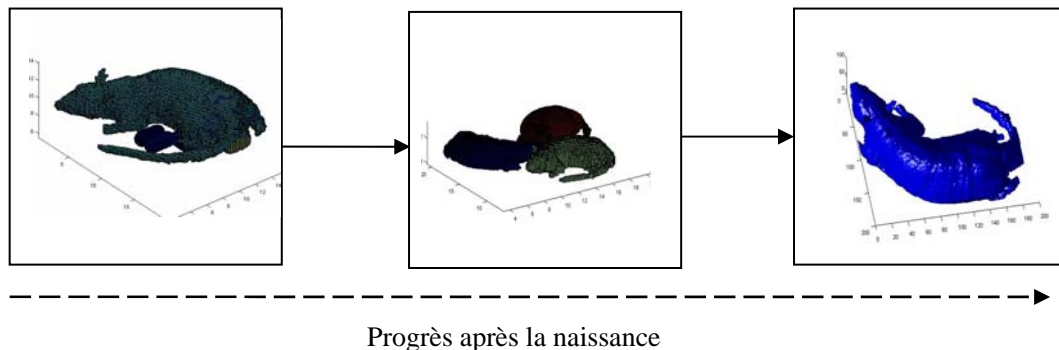


Figure 7 Progrès après la naissance

Donc le DAS corps entier sera très varié sur différentes périodes d'exposition. Pour bien simuler toutes les configurations, une camera est installée dans la CR. Elle enregistre les activités des animaux. Par les informations vidéo, on peut trouver des configurations standards. La configuration standard est définie par celle qui correspond au comportement le plus fréquent (petits rats en groupe avec ou sans la mère), donc à un niveau de champ moyenné imposé par une puissance incidente constante (parfaite uniformité), les mêmes propriétés conductrices, le même poids, etc. Dans ce cas, un DAS corps entier est calculé. Cette valeur est effectivement une valeur de référence. Nous pouvons ajuster ces paramètres pour les cas "extrêmes". Ces cas extrêmes peuvent donner un domaine de variation du DAS corps entier. C'est-à-dire, une marge de variation du DAS corps entier est obtenue pour chaque paramètre. Celui-ci nous amène à deux limites pour les valeurs variables (propriétés électriques, poids, posture, etc.). Ensuite, tous les cas extrêmes pour ces paramètres seront combinés. Cela permet d'obtenir le résultat complet pour toute la période d'exposition.

Avec cette approche, nous pouvons montrer l'évolution de DAS corps entier en fonction de l'âge. La variabilité des résultats doit être prise en compte. Les analyses des variations se classent dans 3 parties. Ce sont la partie de simulation, la partie de mesure et la partie de l'interface entre la simulation et la mesure.

Les variations de la partie de simulation sont:

- l'uniformité du champ dans le volume de test

- la proximité des rats
- variation entre les poids des rats sous exposition
- variation des propriétés électriques des rats sous exposition
- variation de la posture

L'uniformité de la CR est mesurée selon la norme CEI 61000-4-21, 4 bouteilles de liquide équivalente (CEI 62209) de 375 g sont utilisées pour charger la CR. L'uniformité de la CR est 1,2 dB.

La position des rats contribue à la majorité de la variation. Chaque jour d'exposition, la caméra enregistre les activités des rats. Pour les simulations, il faut réaliser toutes les configurations que l'on a constatées. La plus fréquente configuration est prise comme une référence. Les autres configurations possibles sont utilisées pour les marges de variation.

Notre simulation applique le modèle homogène. Sur toutes les simulations que nous avons lancées, nous avons trouvé que pour les configurations où les rats sont proches, le DAS corps entier est plus faible. C'est explicable car pour les modèles homogènes, il n'y a pas de tissus ou organe plus absorbant. L'absorption dépend de la surface de la peau. Quand la masse est fixe, plus la surface de la peau est grande, plus le DAS corps entier est élevé. Si les rats sont très proches ou se touchent, la surface de peau sous exposition diminue (caché par les autres rats). Dans le cas extrême, un groupe qui se compose de trois petits rats est sous le ventre de sa mère est une configuration très courante. Le petit rat en milieu du groupe a la surface minimale d'absorption. Il est estimé d'avoir le DAS corps entier minimal. Cette hypothèse est validée par toutes les simulations. Si un rat est couvert au maximum par les autres petits rats et sa mère, ce rat est le moins exposé. Au contraire, nous pouvons aussi déterminer le DAS corps entier par la configuration d'un seul rat s'éloignant des autres rats.

Après avoir discuté chaque paramètre, on a aussi étudié leur indépendance pour combiner les résultats. Ce résultat a donné l'histogramme d'exposition. Ce ne sont pas les erreurs de système. Au contraire, ils font partie du résultat. On prévoit donc que le résultat sur DAS corps entier présente des fluctuations car l'objet d'exposition a un comportement changeant. Notre tâche est d'évaluer cette fluctuation qui sera utilisée par les biologistes pour analyser les effets sanitaires.

Les incertitudes de mesure sont inévitables. Nous pouvons les réduire par l'amélioration des appareils et la technique de mesure. Nous avons obtenu une incertitude de mesure de 29%.

La méthode hybride comprend deux types de travaux. En intégrant les résultats de méthodes complètement différentes, nous devons analyser les différences induites par les non-convergences. Ces différences sont évitables et compensables si les simulations reconstruisent bien l'environnement d'expérience ou de mesure.

Sur nos recherches, quatre non-convergences sont trouvées. Elles sont:

- (1) La non-convergence de propriétés diélectriques des liquides dans les simulations et les mesures.
- (2) Perturbation de la présence de la sonde de mesure
- (3) E moyenné mesuré et simulé
- (4) L'homogénéité du champ

Elles sont étudiées d'une part par les simulations. D'autre part, nous avons aussi trouvé un schéma pour mesurer le E dans la CR. Ce schéma nous permet d'obtenir le champ moyenné dans la CR avec le nombre minimal de points.

Ayant calculé les variations provenant des trois parties, nous pouvons combiner les variations pour le résultat définitif.

Cette étude pourra être utilisée afin d'évaluer des résultats d'une exposition des animaux à long terme. Elle pourra aussi servir à caractériser le champ dans des environnements domestiques et urbains.

Nous sommes actuellement dans une société qui se préoccupe de la caractérisation de l'exposition des personnes au champ électromagnétique. Les environnements urbains présentent des multi-réflexions. Les ondes s'étendent très lentement avec plusieurs réflexions. Pendant les réflexions, l'exposition provenant de toutes les directions est produite. Si l'on rajoute les effets des points d'accès qui ont déjà pénétré partout dans ces environnements, l'exposition du champ électromagnétique est comparable à la situation de la CR. Nous pouvons l'utiliser pour analyser ce type d'exposition.

Nous avons introduit une procédure basée sur une méthode hybridant la mesure et la simulation qui pourra être utilisée pour des applications similaires. Il est nécessaire de connaître la distribution du champ électromagnétique. Cette distribution est peut-être associée à une distribution statistique connue (Gaussien, Rayleigh, Racié etc.). La distribution statistique est appliquée pour reconstruire les environnements d'exposition autour d'objets sous test. On a montré qu'il n'est pas nécessaire de réaliser les détails du système (qui est plus complexe et sans doute impossible à obtenir). On pourra aussi réduire le volume de calcul.

Le résultat définitif associe les recherches sur la variabilité des résultats. Les variations proviennent de plusieurs parties. On peut éliminer et réduire quelques variations avec l'étude concernant les détails de simulations et mesure. Les variations des résultats seraient peut-être très importantes. Mais elles représentent la vraie condition d'exposition.

Mots clés : *in vivo* exposition, Wi-Fi, DAS corps entier, chambre réverbérante, statistique Rayleigh, simulation, mesure, variabilité

Index

1. General introduction	1
1.1. Electromagnetic field and Wi-Fi environmental exposure	1
1.2. Health concern to EMF exposure	3
1.3. Guideline for EM field exposure-ICNIRP and IEEE standard	4
1.3.1 Basic restriction	5
1.3.2 Special Absorption Rate	5
1.3.3 From basic restriction to Reference levels	6
1.4. Purpose of the thesis	7
2. Animal <i>in vivo</i> EMF exposure system.....	10
2.1. Objectives and requirement for animal Wi-Fi <i>in vivo</i> EMF exposure project	10
2.1.1 Wi-Fi signal characterization	11
2.1.1.1 Duty cycles	11
2.1.1.2 Transmission rate	12
2.1.1.3 Numbers of subscriber	12
2.1.1.4 Conclusion	12
2.1.2 Power budget	13
2.1.3 E field uniformity	13
2.1.4 Ventilation method of the system	13
2.1.5 Container and its size	14
2.2. Comparison for available animal <i>in vivo</i> EMF exposure system	14
2.3. Option for exposure system	17
2.4. Conclusion	17
3. Reverberation Chamber theory	19
3.1. Origin and development of the Reverberation Chamber	19
3.2. Principle of the RC and parameter option	19
3.2.1 Perfect metallic cavity	19
3.2.2 Shape and dimension of the chamber	20
3.2.2.1 Size of the cavity	20
3.2.2.2 Shape of the cavity	21
3.2.3 Stirrers and paddles	21
3.2.4 Quality factor	24
3.2.5 Difference between the theory and the measurement for Q	26
3.3. Conclusion for parameter option of RC	27
4. Numerical methods	28
4.1. Option for numerical methods	28
4.2. Principle of the FDTD method	29
4.3. Limit of the FDTD method for RC	30
4.3.1 CFL limit and numerical dispersion	30
4.3.2 Limit in application to simulation of the RC	30
4.3.3 Simulation on testing the FDTD calculation time for RC application	31
4.3.3.1 Purpose of the trial simulation	31
4.3.3.2 Configuration of the trial simulation	31
4.3.3.3 Statistical results of the temporal E	33
4.4. Conclusion	35
5. Design and realization of RC	37
5.1. Shape of RC	37
5.2. Dimension of the RC	37
5.3. Power excitation and stirring layout	41
5.3.1 Consideration for the stirrers	41
5.3.2 Ventilation of RC	43
5.4. Assemblage of RC	44
6. Proposition of an hybrid approach to characterize the field in RC ...	47
6.1. Measurement and simulation methods	47
6.1.1 Available measurement and simulation methods in RC	47

6.1.2 Available methods in deciding the animal power absorption	48
6.1.2.1 Pure measurement method	48
6.1.2.2 Pure simulation method	48
6.1.3.3 Simulation-measurement alternative method	49
6.2. Simulation-measurement hybrid method principle	49
6.2.1 Inspiration of the method	49
6.2.1.1 Limit of the available characterization methods for RC	49
6.2.1.2 Concept of the simulation-measurement hybrid method	50
6.2.2 Simulation part	53
6.2.2.1 Field distribution model in RC	53
6.2.2.2 Discussion of the parameters in Random Multiple Plane Waves Method (RMPWM)	54
6.2.2.3 Deterministic Multiple Plane Wave Method (DMPWM)	56
6.2.3 Measurement in the loaded RC	57
6.3. Simulations with animals models and results	60
6.4. SAR assessment for tissue/organ specified SAR	65
6.5. Conclusion	65
7. WBSAR assessment.....	67
7.1. Objective	67
7.2. Rat models in simulation and measurement	67
7.2.1 Numerical model of different ages	67
7.2.1.1 Realization of the scaled models	68
7.2.1.2 Modification for the scaled numerical models	69
7.2.2 Positions of the loads in measurement	74
7.2.3 Dielectric parameters for the small rat models	77
7.2.4 Resonance length of the rat's model	79
7.3. WBSAR vs. single rat of different ages	81
7.4. WBSAR vs. rats group	82
7.5. WBSAR vs. most frequent occurred animal configurations	84
8. Exposure result and variation analysis	96
8.1. Objective	96
8.2. Assessment of variation for the simulation results	96
8.2.1 Objective	96
8.2.2 Parameters in determining the results of simulation variation	97
8.2.2.1 Field variation	97
8.2.2.2 Interference with the nearby animals (proximity of peers)	98
8.2.2.3 Difference of weight	99
8.2.2.4 Difference in posture	99
8.2.2.5 Difference in dielectric properties	100
8.2.2.6 Discussion and combination for the variation components	100
8.3. Uncertainty from measurement part	103
8.3.1 Principle of measurement uncertainty	103
8.3.2 $\langle E \rangle$ field strength measurement	104
8.3.3 Equivalent liquid dielectric measurement	105
8.3.4 Conclusion	105
8.4. Variation assessment for measurement-simulation interface	106
8.4.1 Tissue equivalent liquid and measurement sham mismatch	106
8.4.2 Perturbation of the measurement probe to field in RC	107
8.4.3 Measured $\langle E \rangle$ and simulated $\langle E \rangle$	108
8.4.4 Field homogeneity	112
8.4.5 Conclusion	112
8.5. Conclusion for the result	112
8.6. Discussion for the result	114
9. Conclusion	116
Annex I FDTD method	121
AI.1 Maxwell function and Yee's function	121
AI.2 Total field/scattered field technique	124

AI.3 Huygens principle in FDTD	126
AI.4 Non-uniform and sub-grids method in FDTD.....	126
Annex II Uncertainty evaluation principle.....	129
Reference	131

1. General introduction

1.1. Electromagnetic field and Wi-Fi environmental exposure

Once born, we are inevitable plunged into the electromagnetic field (EMF) exposure.

Figure 1.1 shows the main sources of the radiation.

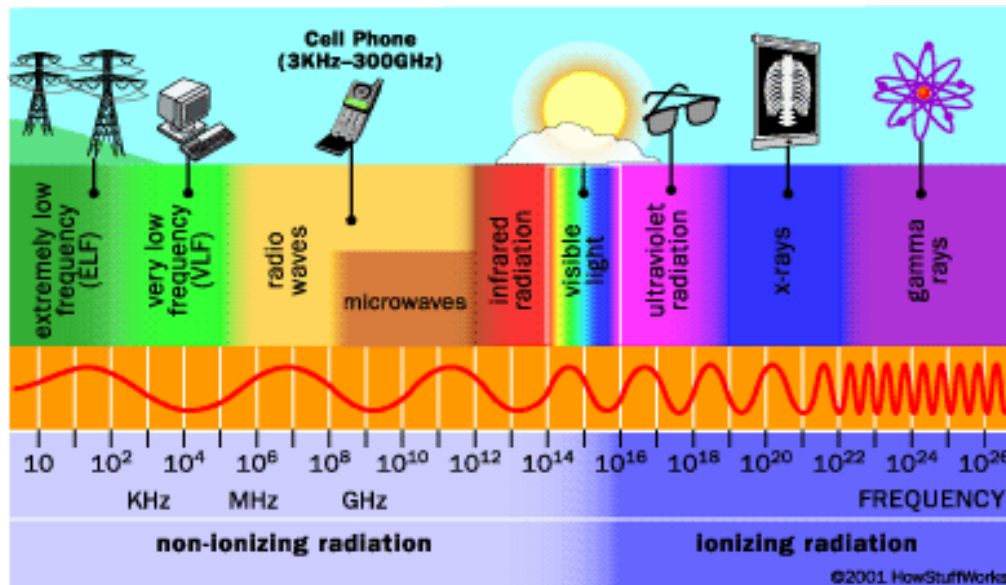


Figure 1.1 EMF frequency spectrums*

*: [HowStuffWorks](http://www.astrosurf.com/luxorion/Radio/spectrum-radiation.png) [Online] (<http://www.astrosurf.com/luxorion/Radio/spectrum-radiation.png>)

Nowadays, integrated with computer-based information systems to process, store and transmit information, EMF emitters are widely used in daily lives. Numerous instruments exist and will surely appear in our environments. By means of either unintentional leakage or intentional transmission, EMF exposures are escalated to one omnipresent state in term of frequency spectrum. Their frequencies are mainly concentrated from 300 kHz to 300 GHz. They are usually called as Radio Frequency (RF) (Figure 1.2).

General introduction

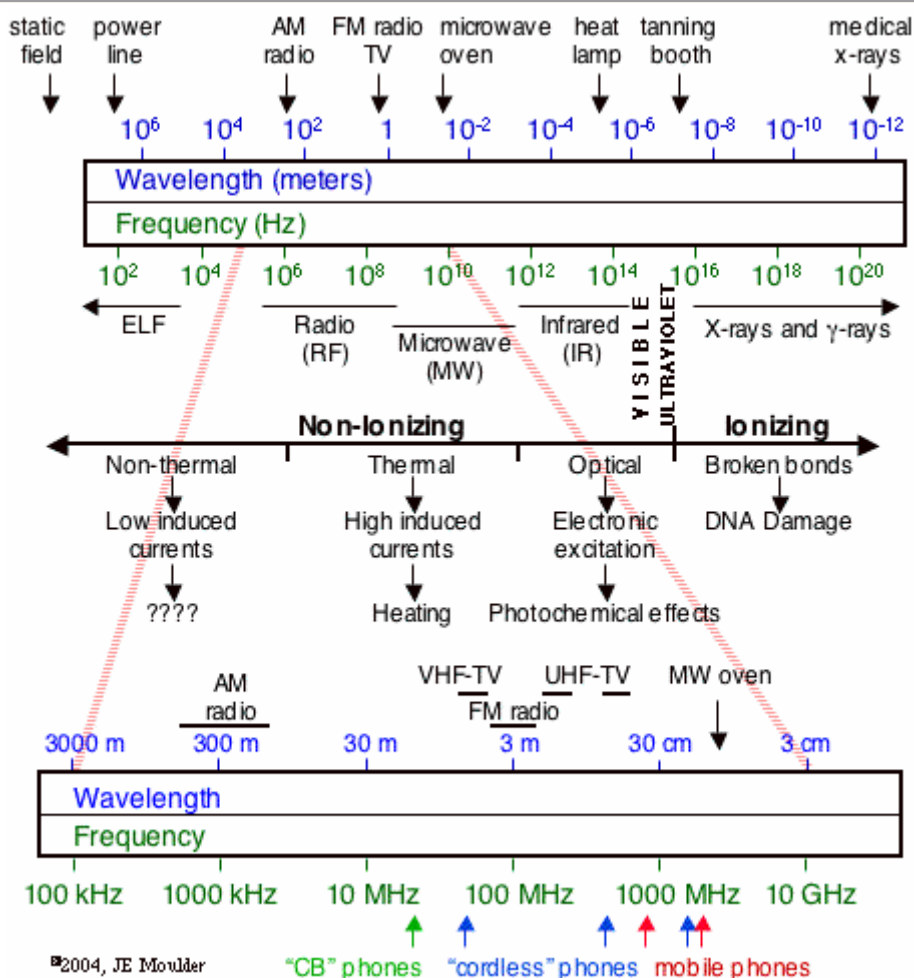


Figure 1.2 Spectrum of RF*

* ElectricHuman Online (http://huntersofthecloud.com/electric_human.htm)

Emergence of the EMF emitters permits the mobility of the communication systems such as the mobile phones. Profiting from its convenience, subscriber number have been marked as a remarkable increase in the recent decades. Mobile phone subscriber has been booming in the entire world. For the past 5 years, they are almost tripled.

Other wireless networks that allow high-speed internet access and services, such as Wi-Fi [1], become increasingly common in homes, offices, and many public areas (airports, schools, residential and urban areas...). Wi-Fi network adapters are built into mobile phones, laptops, PDA, MP3, etc... It could be witnessed for even dramatically increase in near future.



Figure 1.3 Hot spots in Paris*

* Online (<http://blog.brassero.net/2007/06/11/du-wifi-gratuit-partout-dans-paris/>)

1.2. Health concern to EMF exposure

Explosion and prevalence of RF enabled devices is a double-edged sword. There is always a public concern about the potential health effect to human beings accompanied with the convenience that it brings by extensive and rapid growth of such devices. As consequence, research institutes or organizations have been asked for risk evaluation. Numerous research results have been published during the past several decades.

However, there are some uncertainties in the experiment configurations, thus the results can not necessarily lead to one conclusive decision. It is also need to point out that isolated and individual experiment is hard to give one definitive and conclusive results. One comprehensive database built on weighting all the current available information will help to explain the EMF health effect. So mechanism of the EMF to human body should be studied in full details by rigorous theoretical and experimental ways as well as statistic analysis of the results to avoid any potential detrimental effect.

International Commission on Non-Ionizing Radiation Protection (ICNIRP) has dedicated to available reports about the RF's health effects. With the accumulated

General introduction

evidences, it has published the guideline [2] to protect the people (public and professional worker) against the RF health effect.

World Health Organization (WHO), through its International EMF Project, has identified research needs and is coordinating a world-wide program of EMF studies to allow a better understanding of any health risk associated with EMF exposure. Particular emphasis is placed on possible health consequences of low-level EMF. Information about the EMF Project and EMF effects is provided in a series of fact sheets, which is available at its website www.who.int/emf/. Some data sheets are also published in [3], [4], [5], [6], [7] and [8]. Upon studying the experimental results on the RF health effect, it has claimed not to find any health effect below protection level of ICNIRP.

In Europe, the European Scientific Committee on Toxicity, Ecotoxicity and the Environment (SCTEE) has endorsed the protection level recommended by ICNIRP. The latter has also been endorsed in France through a decree (May 2002).

By now, several reports have been published concerning the Wi-Fi exposure. There is no established or consistent evidence to date that Wi-Fi and WLANs adversely affect the health of general population. ' *The signals are very low power, typically 0.1 watt in both the computer and the access point and the results so far show exposure are well within ICNIRP guidelines* ' –Great Britain Health Protection Agency (HPA). Nevertheless there is a need of research and WHO continues recommend investigations.

1.3. Guideline for EM field exposure-ICNIRP and IEEE standard

International bodies such as ICNIRP or IEEE have established limits to provide protection of occupational and public populations. Based on the literature and known effects with safety margin, exposure guidelines have been developed. "*Guidelines for Limiting Exposure to Time-varying Electric, Magnetic, and Electromagnetic Fields (up to 300 GHz)*" has been published by ICNIRP [2] and "*Standard for Safety Levels with Respect to Human Exposure to Radio Frequency Electromagnetic Fields, 3 kHz to 300 GHz*" by IEEE [9]. Most of nations have endorsed these international standards to protect their citizens against adverse levels of RF fields.

General introduction

1.3.1 Basic restriction

ICNIRP guidelines define Basic Restriction exposure limits. In the RF domain they provide a limit for the maximum local and whole body absorbed power. Table 1.1 summarizes local and whole body exposure limits.

	Public	Worker
Whole body averaged SAR	0.08 W/kg	0.4 W/kg
Local SAR head and body averaged over 10 g mass	2 W/kg	10 W/kg
Local SAR averaged over 10 g mass	4 W/kg	20 W/kg

Table 1.1 Limits by ICNIRP

1.3.2 Special Absorption Rate

The basic restrictions represent the maximum acceptable Special Absorption Rate (SAR) expressed in watt per kilogram. From the mathematics point of view, SAR is the time derivative of energy.

With dW is the energy and dm is the mass, it can be expressed as:

$$SAR = \frac{d}{dt} \left(\frac{dW}{dm} \right) = \frac{d}{dt} \left(\frac{dW}{\rho dV} \right) \quad (1.1)$$

The SAR can also be linked to the conductivity σ , the mass density ρ and the electric field strength through the formula 1.2

$$SAR = \sigma \frac{|E|^2}{\rho} \quad (1.2)$$

In such case,

$|E|$: RMS (root mean square) of the electric amplitude (V/m)

σ : Tissue conductivity (S/m)

1.3.3 From basic restriction to Reference levels

Since SAR is complicated to be assessed with its definition function (1.1), ICNIRP has also provided the derived reference level to evaluate the conformity of the exposure to the basic restriction.

Compliance to the reference level (expressed in v/m, a/m or w²/m) is deemed to guaranty the conformity with the basic restriction. Figure 1.4 shows the E reference level from ICNIRP guideline.

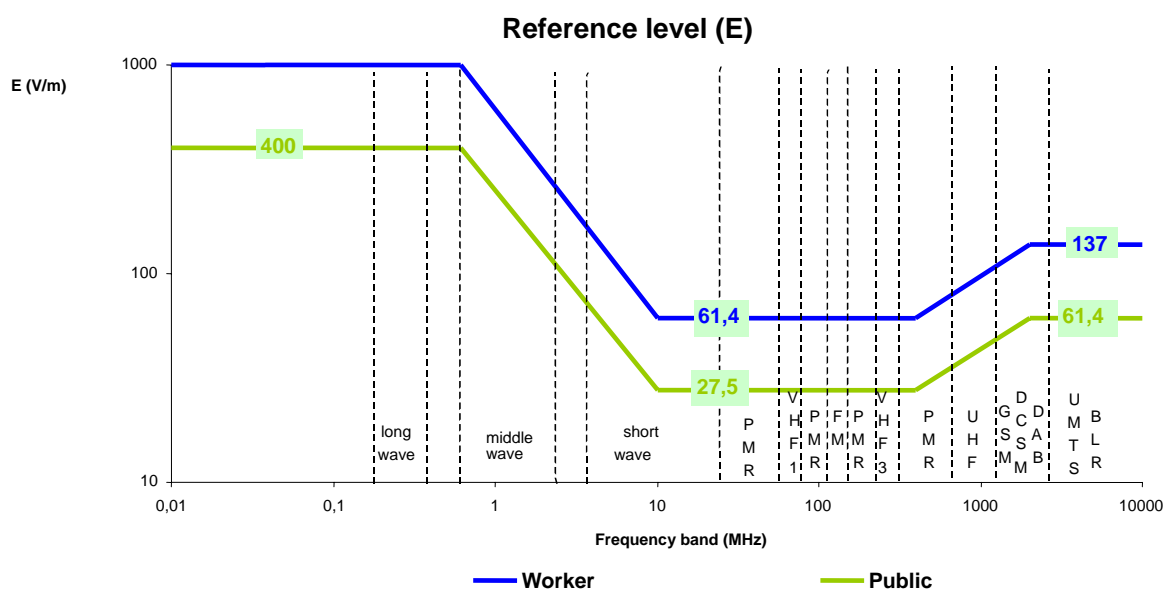
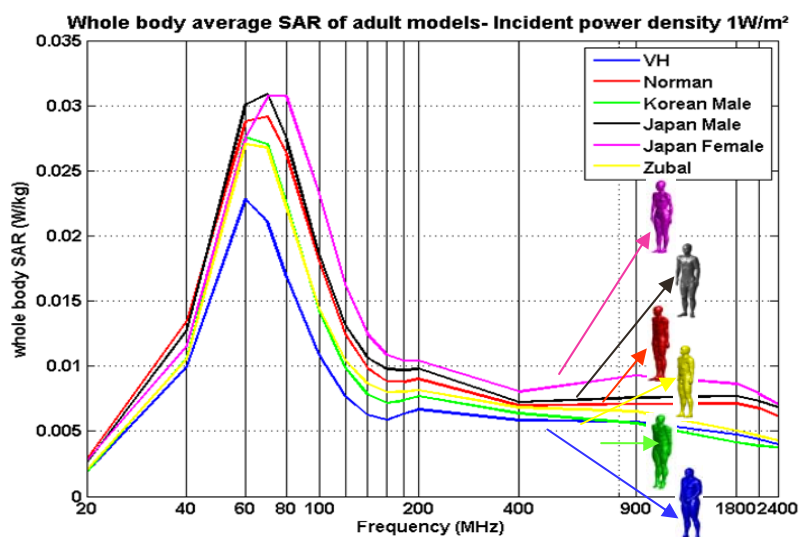


Fig.1.4 Reference level from ICNIRP guideline

Study ([10]) shows that whole body absorption depends on morphology and frequencies. The maximum absorption occurs a frequency resonances close to 100 MHz. Figure 1.5 ([10]) shows the absorption level for different phantoms at the same incident power density.



To well protect people, one reference levels taking into account frequency dependence and the special radiated population should be defined.

1.4.Purpose and organisation of the thesis

Upon review of the current background for RF products' tendency and the public concern, WHO is always calling for researches data on exposure assessment of Wi-Fi emitters, which have different frequencies, modulations, operational methods or communication products. In particular, WHO recommends researches for children exposure issue. On 9-10, June, 2004, WHO held the workshop in Istanbul on children sensitivity to EMFs and has recommended children EMF exposure health in its priorities.

Since exposure experiments with human being is not always feasible due to ethical constraints, animals or cultures studies are used to perform investigations

In this context, many laboratories have carried and are performing researches with animals, tissues and cell cultures. Among these studies, to assess the impact of exposure and the exposure uncertainty requires to develop an applicable method in determining comprehensively and precisely the dosimetric information for radiated target. It includes, the design of one exposure system with stable, sustainable and controllable incident EM power, characterization for the exposure pattern which exists in the real environment and integrate it in the experiment, determine the power distribution in the exposure volume and the dosimetric information of exposure in the

General introduction

radiated samples (either *in vivo* or *in vitro*). It should also analyze the possible result variation range of the exposure experiment.

In this thesis, we present one project on designing an animal *in vivo* Wi-Fi exposure system that can be used with free of movement for animals. Researches for field distribution and the exposure variation are also included in the study. The thesis is organized as:

Part 2 describes the requirement of the project. Based on the detailed analysis for the criteria, several candidate exposure systems are proposed. Advantages and disadvantages of each one are discussed in order to select the appropriate system.

Part 3 focus on the principle of reverberation chamber which has been chosen as the exposure system. Its theory has been presented with emphasis on size, shape, stirrers and quality factor (Q). Several studies have been discussed to decide the relevant parameters for the exposure system. Q factor is analyzed to demonstrate the importance of evaluating one reverberation system and the difference between the measured and theoretical values.

Part 4 introduces and compares several available numerical methods for simulating one reverberation chamber. Finite-Difference Time-Domain (FDTD) method is accepted as the method to analyse the power absorption in the animal body. Limit of FDTD in simulation of reverberation chamber is given by one trial example. Other approaches should be researched to character the power absorption by animals.

Part 5 shows the construction and realization specification of the exposure system.

Part 6 generalizes several available methods to characterize the power absorption for the animal exposure experiment. One simulation-measurement hybrid method is conceived and elaborated. Simulation part (which provides the ratio of averaged E in reverberation chamber as well as the power absorption in the animals) is linked with the measurement part (which provides the net incident power to the system and the averaged E in reverberation chamber). Several parameters of the method are chosen by simulations. Q is obtained by measurement. It guaranties the application of the distribution of field in reverberation chamber. Another different simulation method is also performed to consolidate the results.

General introduction

Part 7 and part 8 focus on the whole body averaged SAR vs. different animal configurations. Results about long-term exposure are presented. Result variation is discussed by analyzing the distinctive variation sources which could be classed as from simulation part, measurement part and simulation-measurement interface part. Several propositions aiming to reduce variation of the results are also proposed.

The paper is concluded with Part 9 with potential amelioration and perspective of the researches.

2. Animal *in vivo* EMF exposure system

The systems which can provide stable EMF exposure play an important role in either *in vivo* or *in vitro* exposure experiments. They permit evaluation of possible risks for RF exposure using well-studied systems under strictly controlled conditions. Exposure system must be well designed in line with the biological objectives, the exposure should be completely characterized, the uncertainty must be evaluated and the environmental parameters shall be recorded during the experiment (pressure, humidity...) For *in vivo*, *in vitro* or tissue experiments, there are numerous published studies designated for exposure system. To realize and to betterment the exposure system are always big challenges for one successful exposure experiment.

2.1.Objectives and requirement for animal Wi-Fi *in vivo* EMF exposure project

IMS (Laboratoire de l'Intégration du Matériau au Système, <http://www.ims-bordeaux.eu/spip.php?article75>) has proposed one animal *in vivo* project on long term Wi-Fi exposure for the tumor, nerves health effect from embryo to adolescent period.

Preliminary plan about the exposure system would be decided with the analysis for requirement based on each component of these criteria.

The system should be able to deliver 0.08 W/kg, 0.4 W/kg and 4 W/kg whole body averaged SAR (WBSAR, defined as the total absorbed power averaging over the entire mass) to rats which will weight up to 1.5 Kg. The type of signal is a real Wi-Fi signal operating at 2450 MHz. Rats should have the ability to move freely in the exposure system (thus, it is actually one non-restrained experiment). Duration of the exposure should be 2-3 hours for each day and it would last for several months. Exposure experiments would be repeated for several generations to accumulate the statistical sufficient data. The system is preferred to be compatible for other animal experiments (e.g., mouse).

Wistar (Figure 2.1) rats are chosen as the experimental animals.



Figure 2.1 Wistar rat

Wistar rats are very suitable for exposure experiment. They are marked by their calm character. Wistar rats can easily adapt to the environments so that they are less likely to be anxious in the confined experimental space and much tolerable to the noise or the function of the machines. By their well adaptive characters, they are usually chosen as the experimental animals in several experiments.

2.1.1 Wi-Fi signal characterization

The first version of the Wi-Fi standard 802.11 [1] was published in 1997. The standard was completed by two extensions as "a" and "b" in 1999. Three layers of physical layer (PHY) and one layer of media access control (MAC) are defined.

The 802.11a and 802.11b have defined one OFDM (orthogonal Frequency Division Multiplexing) physical layer for 5 GHz frequency with transmission rate as maximum as 54 Mbit/s and one FHSS (Frequency Hopping Spread Spectrum) PHY layer. In this exposure experiment, 802.11b has been chosen.

802.11b standard also prescribes the maximum power (EIRP) for both the stations and the hot spots should not be higher than 100 mW. Practically, the emission power is less than 100 mW. Actual power level can be influenced by channel occupation time and duty cycle, transmission rate and number of users.

2.1.1.1 Duty cycles

One important character of Wi-Fi signals is time channel occupancy (TCO). Power of the frame is constant and is inferior to the 802.11 standard. However, the average power in the channel can vary greatly due to TCO. The effective transmission time corresponds to the TCO and is determined by the mechanism of random backoff (Figure 2.2), which is used to decide the priority of access to the medium. Simply, in case of multiple senders occupying the same channel, they have to wait a surplus long

time to avoid any potential transmission collision. During this time, they keep idle with no emission. In order to maximize the power, the backoff time should be minimized. So in this exposure experiment, multiple sender condition is replaced by one sender- one receiver mode.

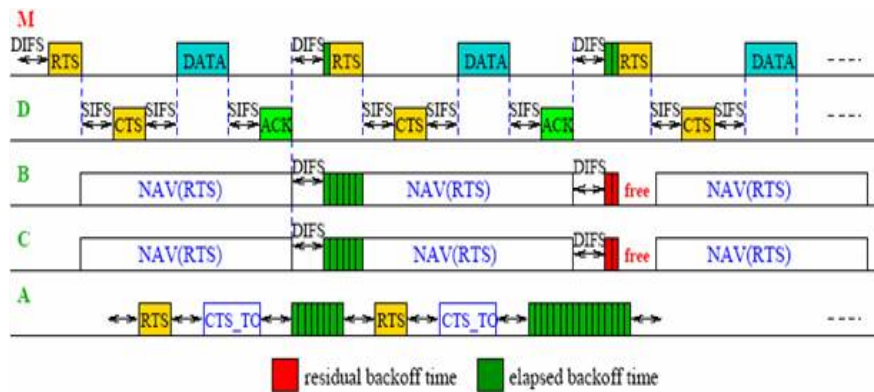


Figure 2.2 Backoff time mechanism of Wi-Fi

2.1.1.2 Transmission rate

Transmission rate depends to transmission environment. In 802.11 standard, the maximum rate can be up to 54 Mbps. The real rate is the average rate in the whole transmission period. Considering the signalization, synchronization, preamble and the backoff time, the average transmission rate is much lower than the nominal rate.

For maximization the averaged power, the throughput rate for one frame should be minimized.

2.1.1.3 Numbers of subscriber

One access point can connect with several users. They all transmit within one channel. The access point communicates with one user at one time, while others keep idle. So the number of the users has no effect on the exposure amplitude if the access point is considered as the exposure source. Transmission rate for the access point is always the same while the transmission rate for each users changes.

2.1.1.4 Conclusion

Wi-Fi communication can be influenced by several factors. These factors directly change the power of the emitter. In order to achieve the controllable and sustainable power emission, the software which imitates the Wi-Fi communication should be utilized. To avoid the problem of switch between different subscribers, point to point

communication would be applied in the experiment. The software should be equipped with the option as continuous maximum emission.

2.1.2 Power budget

The biologists' requirements were to be capable to have a WBSAR up to 4 W/kg. If a maximum of 4 W/kg SAR needs to be obtained in 1.5 Kg animal body, the total absorbed power in animal of about 6 watts and the system has, at minimum (exposure efficiency 100%) to radiate 6 W (38 dBm)

Current commercial WI-Fi signal simulator can generate about 20 dBm signals. Considering Wi-Fi occupancy and the cable loss, actual transmitted power to the amplifier can be less than 15 dBm. There are two possible methods to achieve desired radiation power: either by one powerful but expensive amplifier or by one moderate amplifier with an efficient exposure system. After weighting over the instrument cost and the realistic need, the exposure system should maintain over 60% efficiency in term of animal absorbed power to net incident power of the system.

2.1.3 E field uniformity

Animal *in vivo* exposure experiment has always the concern about field uniformity. If the animal under exposure has the possibility to move around in non-uniform exposure volume, the situation will be extremely complicated. In the entire exposure volume, the E field strength should be homogeneous in order to keep one stable and known exposure dose for the experimental target. Even if in the exposure volume, where the field level is not perfectly uniform, it should be within acceptable deviation. The E field uniformity is one major uncertainty sources for the results. It is actually the most important factors for the system design. Lots of work would be expected toward the performance of uniform exposure.

2.1.4 Ventilation method of the system

In order not to disturb the normal living rhythm of the animals, exposure system can be, if necessary, furnished with the ventilation system. If such systems were to be used, researchers have to take care of possible impact on the exposure system and its effects on animal behaviors.

2.1.5 Container and its size

Among the available researches, there are various configurations for the containers. They can be mainly classified as two types: either by totally confined or by one partially confined container with a bit larger volume.

This exposure experiment aims to reproduce the animal living environment which less likely disturbs compartments of the rats from the gestation period to the adolescent period. Container should not be of the type of completely confined and the volume should allow the movement of one adult female rat weighting about 250 g with three small rats of 120 g in total.

By observation of the compartment for the rats and their actual size, EM transparent plastic containers with the volume of 20cm×40cm×25cm (length/width/height) are manufactured (Figure 2.3). Straw tissues are piled in the plastic containers for rats to construct their nests.

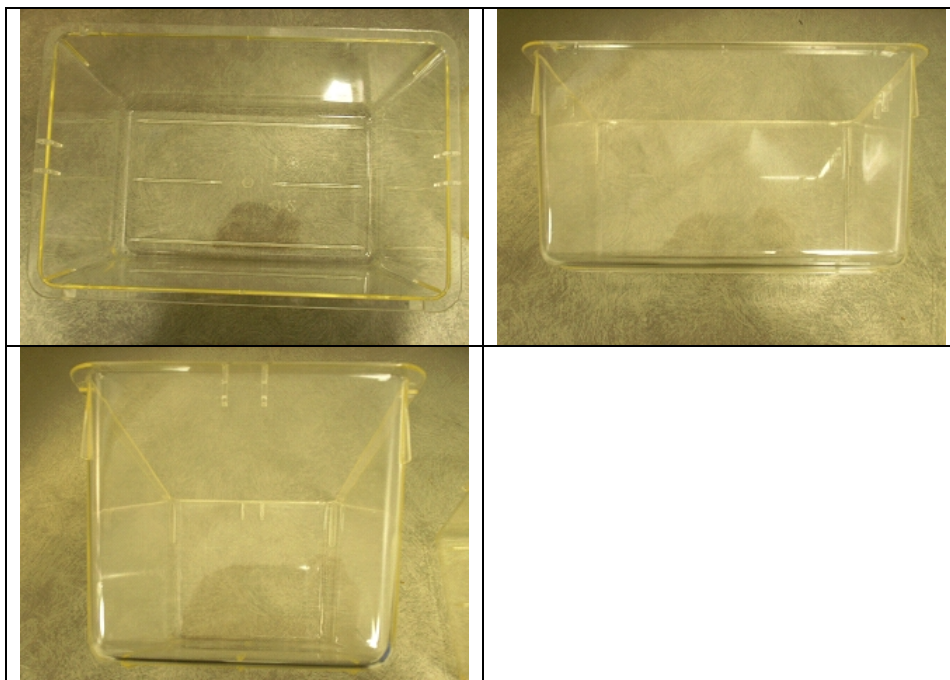


Figure 2.3 Container for animals

2.2. Comparison for available animal *in vivo* EMF exposure system

From literatures and available reports, four kinds of system setups for animal *in vivo* EMF exposure experiments exist.

Animal in vivo EMF exposure system

They are (1) Reverberation Chamber (RC), (2) Anechoic Chamber (AC), (3) TEM Cell and (4) Radial Waveguide. Relevant exposure experiment with the respective four systems can be referred to [11], [12], [13], [14], [15], [16] and [17]. Configurations for 4 different systems are shown in Figure 2.4.

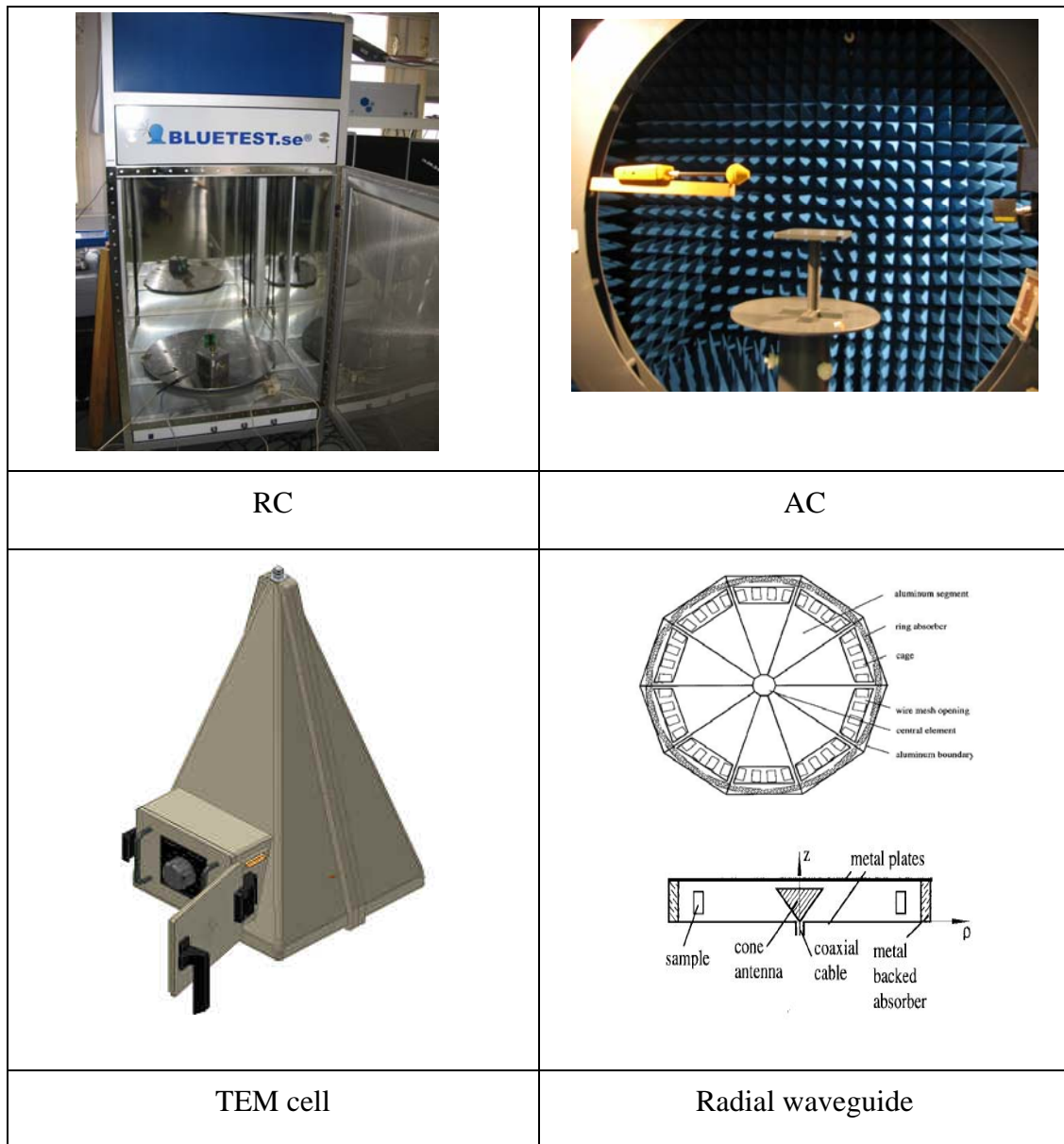


Figure 2.4 Four major systems for animal exposure experiments

Their specialties are listed in Table 2.1 for comparison.

Animal in vivo EMF exposure system

	RC	AC	Tem cell	Waveguide
Space occupation	Middle	Largest	Small	Small
Exposure Type	Whole body	whole body	whole body	Local/whole body
quantity of load	Several hundreds depending on amplifier	Several hundreds depending on amplifier	Several or Dozens	Several hundreds depending on amplifier
Animal movement	Could be partial free	Could be partial free	Confined	Confined
Input Power	Medium	Highest	Low	Low
Cost	Middle	Highest	Low	Low
Efficiency	Middle	Highest	Low	Low
Working zone	Large	Middle	Small	Small

Table 2.1 Comparison for RC/AC/TEM cell/Waveguide as whole body exposure setup

2.3. Option for exposure system

According to discussion about the current available animal exposure system, we have already one comprehensive view on advantage for respective system.

Since the exposure system is designed for non-restrained animals, radiated waveguide and TEM cell are the least appropriate. They have less usable exposure space in the system. Animals are preferred to be fixed in the systems. Movement and different position may change the desired exposure pattern and thus exposure dose is unpredictable.

AC can support non-restrained animals exposure of as many as hundreds of rats. It can also achieve the highest efficiency among all the candidate systems. There are three disadvantages which compromise the application of AC. First, construction budget of AC is much higher than that of RC with the similar size. Second, it occupies much more space than RC if the working volume is the same. Third, it needs additional equipment such as turntable to generate omni-direction and uniform whole body exposure.

Comparatively, RC has medium exposure efficiency. It takes some comprehensive advantages over all the other systems. It is suitable for non-restrained experiments and its space efficiency is better than AC. That is to say, working volume is the biggest if the dimension is fixed. This is a very favorable factor. It means that animals have the ability to move in a much bigger space and live in less crowded environment which helps to alleviate the stress of animals in long term experiments. RC can generate omni-direction exposure without additional supplementary equipment in the working volume. The structure of the system is very compact. Also, less expenditure is the strong point of RC.

In all, RC prevails in animal *in vivo* non-restrained Wi-Fi exposure experiment. We chose it as the exposure system for this project.

2.4. Conclusion

This part has presented the requirements of this project. Upon the requirement analysis, one preliminary but comprehensive view of the exposure system is established. Several key factors and elements of the experiment should be considered in the design and fabrication. Non-restrained experiment, homogeneous exposure, stable and sustainable

Animal in vivo EMF exposure system

Wi-Fi signal emission and system efficiency are of the most importance for the project. As consequence, four candidate systems are proposed. Their advantages and disadvantages are discussed and compared. Fitting with requirement of the project, RC is chosen as the most appropriate option.

Following parts (3, 4 and 5) will deliberate the technical details of RC and the realization of the system by means of analytical and numerical tools.

3. Reverberation Chamber theory

3.1. Origin and development of the Reverberation Chamber

Concept of the RC appears in the 1940's and many applications have emerged since 1960s. It has gradually stepped into the electromagnetic field research domain and becomes one powerful experimental tool with the proposition of H.A. Mendus [18]. Researchers have developed wide scope for RC including susceptibility test and immunity test as well as emission test. In the past 20 years, application of RC has experienced one drastically increase. It has demonstrated its advantages as concluded by [19], [20]. Some current research aspects and methodologies by means of RC are concluded in [21].

In 2003, the first edition of the European standard on RC test is published as Electromagnetic compatibility (EMC)-Part 4-21: Testing and measurement techniques-RC test methods [22]. It is the comprehensive document comprising both mode-tuned and mode-stirred procedures. This standard streamlines a measurement procedure for immunity tests, emission tests, shielding effectiveness measurement as well as calibration processes.

3.2. Principle of the RC and parameter option

3.2.1 Perfect metallic cavity

RC generally takes shape of one perfect metallic cavity. By this means, structure of the RC is much like a micro-oven. It depends on multiple reflections from the metallic wall to 'cook' the objects in the center.

In perfect metallic cavity, the distribution of the EM field is standing wave points. Once it reaches the stable state, the maxima and minima will not change with time and position (Figure 3.1). The maxima and the minima differ sharply.

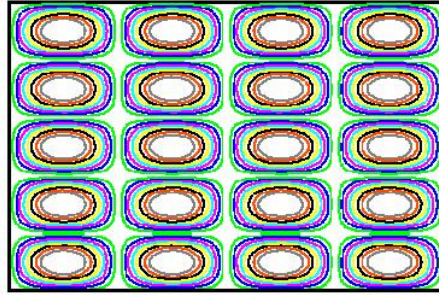


Figure 3.2 Typical standing wave pattern in the metallic cavity

Perfect metallic cavity is very important to maintain higher field strength in the working zone, which is the advantage over the anechoic chamber. However, the practical wall of the cavity could never be perfect. Many aspects make the wall as lossy materials. The field distribution in the cavity can thus be attenuated and distorted.

3.2.2 Shape and dimension of the chamber

On design of the RC, the construction of the cavity is always the first step. Two aspects are on consideration. One is the dimension of the cavity; the other is the shape of the cavity.

3.2.2.1 Size of the cavity

Size of the RC depends on the operational frequency and the actual needs. By IEC standard [22], mode frequency $F_{l,m,n}$ in MHz is calculated as:

$$F_{l,m,n} = 150 \left(\left(\frac{l}{L} \right)^2 + \left(\frac{m}{W} \right)^2 + \left(\frac{n}{H} \right)^2 \right)^{0.5} \quad (3.1)$$

l,m and n are the mode indices,

L,W,and H are dimensions of RC in meters.

Working frequency sets limits for the minimization of RC.

It [22] also rules the distance between emission antenna and RC wall should be:

- at least $\lambda/4$ (with λ taken at the lowest frequency used for a particular case
- or,
- at least 1 m (for the lower frequency)

Reverberation Chamber theory

Exact distance should be determined by simulation with animal phantom. It also plays one important role in deciding RC dimension.

3.2.2.2 Shape of the cavity

Shape of the cavity can be completely different. Either Spherical, cubic or rectangular shape has been already applied in commercial use.

There is no definitive decision on option of the optimal shape but at least two points are observed: first, an irregular shape cavity can generate much more regularly spaced (in frequency) modes, and may give better performance at low frequencies; second, a regular shape generates more uniform space for internal waves. Both of the two approaches have some studies to support their claims ([23], [24] and [25]).

In experiments for animal *in vivo* Wi-Fi exposure, animals are designed to move freely in the system. Enough space with uniform field distribution is much appreciated for non-restrained experiment. Irregular shape cavity helps to generate much more spaced modes and thus ameliorate the performance of RC at low frequency. For non-restrained experiment, large uniformly field distribution space prevails over the need for more modes. On the other hand, other designs such as excitation layout can help to ameliorate the modes occurrence in RC. So, RC with regular shape is adopted.

3.2.3 Stirrers and paddles

Upon the previous discussion about the shape and size of the cavity, one metallic enclosure with fixed standing wave points is available but it is not enough to be called as RC. Additional methods must be added to make the maxima and minima move temporally and spatially in the cavity. It is usually realised by mechanical stirrers or paddles. The role of the stirrer is to sufficiently generating the modes in the cavity by varying the boundary condition and thus creating a multi-mode cavity. It leads to completely random variations of the field values, which enables the cavity to behave with the uniform E strength feature. With this character, one metallic cavity can be called as RC.

Movement of the stirrers or paddlers brings us two panoramas in the cavity: spatially, at any time point, the maxima and minima could appear and they could vary sharply. Temporally, at any specific position, within one sufficient period, the averaged field

Reverberation Chamber theory

strength is of the similar level - higher field strength as well as the uniform field strength can be guaranteed.

Traditionally, the most common types of the stirrers are the continuous mode stirrers and the step by step stirrers [22]. They often take shape comparable to $\frac{1}{4}$ length of the RC. Rotations of the significant size stirrers aim to efficiently change the boundary condition in RC.

Existence of electrical large size stirrers is not always advantageous in many circumstances. They may stuff the test space. Existence of the large size stirrers also introduces some mechanical elements in the test volume, which will disturb EMF distribution. Aiming to eliminate the mechanic large size stirrers, several studies are available for substitution for stirrers. Some of the propositions are concluded as follows:

- *Moving walls*

One possibility to replace the mechanical stirrer inside the RC is to change the field distribution by random movement of the RC. It was proposed by Leferink *et al.* [26]. The method is realized by Kouveliotis *et al.* [27]. The cavity is covered by the flexible electromagnetically conducting cloth. Different modes are stirred by random movement of the walls. Small motors with drive fixtures move the cloth sufficiently so that the field is changed and certain of field uniformity is achieved within the enclosure [28]. When the enclosure wall is vibrated, the boundary conditions are significantly varied and consequently the basic RC's properties are obtained (Figure 3.2).

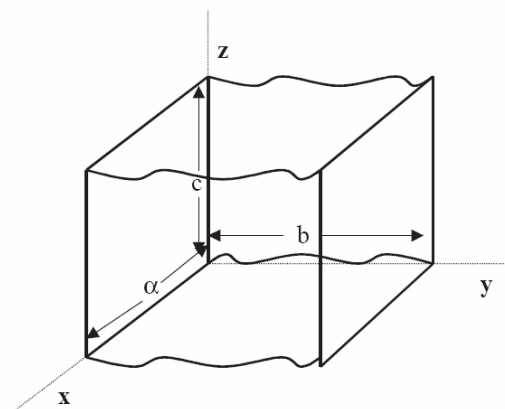


Figure 3.2- Schema of the Vibrating intrinsic RC

Reverberation Chamber theory

This approach removes the stirrers from the RC's interior surface and therefore, much larger test volume is obtained. It was successfully applied to build up portable and detachable RC. However, it does not get rid of mechanical problems completely. By supplementary accessories on the enclosure, shielding performance is not satisfactory.

- *Electronic stirring*

Principle of the electric stirring is the same as the mechanical stirring. Instead of altering the mechanical boundary of the cavity, it changes the excitation type. Different sources utilize multiple excitation phases, different orientations or less correlative signal type, the name of this type of stirring comes from this way. By different excitations, consequently, different boundary conditions appear in RC. One remark is that, by economizing the test space for large size stirrers, there is extra need for additional antennas and cabling as well as signal modulators or couplers.

In the domain of the electric stirring, the most popular modulation methods are frequency and noisy stirring. This method is utilized by Hill *et al* in 1994 ([29], [30]). Principle of the electrical stirrer is the same as the mechanic stirrer. Both of them target to alter resonance frequencies of the cavity modes.

There already exists two-dimensional analysis in [29]. This technique had been applied earlier in realistic, three-dimensional RC [30]. The underlying principle of “frequency stirring” is to acknowledge that the change of the resonance frequencies of the cavity modes by a rotating mechanical stirrer has some similarity to the frequency modulation of the source [31]. Instead of changing the frequency “monochromatically” by standard frequency modulation, another proposed method uses additive white Gaussian noise (AWGN) which is mixed with a periodically changing centre frequency [30]. This approach claims that the field uniformity is increased compared to pure frequency modulation, while the test results also shows that one band width is necessary for RC to achieve well uniformity in the test volume. Electronic stirring can further be classified as multiple sources and phases stirring and multiple sources alternative emission stirring.

Multiple sources and phase stirring

Instead of frequency stirring (which is inappropriate for our 2450 MHz fixed frequency exposure experiment), the usage of multiple source antennas is advantageous for

Reverberation Chamber theory

single-frequency, high-power excitation cases because they eliminate the need for combining high-power signals through external RF components. In [29] it was investigated whether multiple sources alone (without any stirring) would lead to sufficient field uniformity: it concludes that the improvement in field uniformity is rather marginal, and nevertheless a mechanical stirring device is needed. It was found to be true even if the sources were incoherent or varied in phase (so called “phase stirring”) [32].

Multiple sources alternative emission stirring

If some modification could be made on the multiple sources stirring schema, another type of the stirring method could be obtained:

Multiple antennas emit alternatively. At any time point, only one single antenna works. Antennas are installed on the different surface of the cavity wall. To avoid any symmetric configuration, the antennas are not put exactly in the central wall. Alternative source emission is much easier to be achieved and controlled than emission of different phases. This design is adopted in the project. Further detailed modifications are also to be added in the design. Theoretically, with the switch of the different antennas, much more modes would be produced in RC.

3.2.4 Quality factor

Quality factor (Q) is a useful parameter indicating the efficiency of RC to store energy as well as the mean field strength induced by the input power. A high Q indicates that an RC has low losses and is therefore very efficient in storing energy. For concern of the mean field strength in the animal exposure, the Q should be sufficiently high in order to generate the desired field strength. In addition, it sheds lights on estimation of chamber shielding effectiveness (SE) and the RC time constant.

Analytical approach for definition of the Q based on the time-averaged stored energy W_s and the energy dissipated during one period W_d within the resonator.

$$Q = 2\pi \frac{W_s}{W_d} \tag{3.2}$$

$$Q = \omega \frac{W_s}{P_d} \tag{3.3}$$

Where P_d being the dissipated power. w_s can be computed from

Reverberation Chamber theory

$$W_s = \frac{1}{2} \iiint_V \vec{D} \cdot \vec{E} dv = \frac{1}{2} \epsilon \iiint_V |\vec{E}|^2 dv \quad (3.4)$$

Replacing (3.4) into (3.3), we get

$$Q = \frac{\omega \epsilon}{2 P_m} \iiint_V |\vec{E}|^2 dv \quad (3.5)$$

Equation 3.5 is not a rather practical estimation of the Q due to the difficulties in determining the spatial E strength at the vicinity of the RC where field strength varies greatly and contribute much to the total energy partition in RC. It should be defined by other approach.

Q involves directly with the loss of the cavity. Several loss sources, such as aperture leakage, Joule heating by enclosure, disturbing by the cabling in the RC, assemblage of the materials (welding, piecing up, bolts etc), accessory system (ventilation, illumination system [33]), influence the Q. Simply and approximately, Q can be calculated by (3.6) [33]:

$$Q = \frac{3V}{2\mu_r \delta_s A} \frac{1}{\left[1 + \frac{3\lambda}{16} \left(\frac{1}{l} + \frac{1}{w} + \frac{1}{h} \right) \right]} \quad (3.6)$$

Where,

V : RC volume

μ_r : Relative permittivity of the RC enclosure

δ_s : Skin depth of the RC enclosure

λ : Wave length in RC

A : Internal surface of the RC

l , w and h : dimensions of the RC

In this equation, all loss other than the Joule heating on the RC internal enclosure (metallic wall) is overlooked. On contrary, if Q is already known for one RC, the conductivity can be deduced by aid of (3.6). In this approach, the conductivity is a *nominal conductivity*. So the lossy contributions (leakage, loss by the measurement system, dissipation by cables, etc.) are thought to origin from the enclosure conductivity if we want to calculate the conductivity with the known Q.

Reverberation Chamber theory

High conductivity of the enclosure will also bring much higher averaged E strength in the cavity. It is verified by [34], that aluminum enclosure cavity can produce much higher averaged field strength (and higher Q) than the iron one while the uniformity result is not confirmed. It inspires the researchers that if the high E field strength (High efficiency) is desired, the most obvious option is to apply high conductivity material as the cavity wall.

So, aluminum has been chosen as the enclosure materials for RC of our experiment.

3.2.5 Difference between the theory and the measurement for Q

By [22], Q from measurement is defined by (3.7):

$$Q = \frac{16\pi^2 V}{\lambda^3} \frac{P_{RX}}{P_{TX}} \quad (3.7)$$

P_{RX} is power received by receiver antenna

P_{TX} is power transmitted by emission antenna

Q is obtained with the average of each movement position of the stirrers.

However, there always exist some differences between the measurement and the theoretical results. It is not mainly due to the measurement errors but to the weak field strength level and the energy dissipation on load of the measurement equipments. Weak field strength can lead to very unstable readout. Dissipated energy on measurement system is hard to be qualified. When measuring within the high E field system, loss on the measurement can change the results insignificantly. By comparison, in RC measurement, the readout is usually at the order of several V/m. The result of Q will be changed by loss on the measurement and reception system. One solution to partly compensate the disadvantage is the small size receiving antenna (such as dipole) [33].

How to interpret the measurement value Q and the divergence between the measurement Q and the analytical Q to evaluate RC? It is the key problem in verifying RC features.

One feasible and meaningful way to treat the measured Q likes a conservative estimation. Since the dissipation on the measurement load will lower the actual Q, actual RC will always have higher Q than the readout from measurement. With the measured Q (which is inferior to the actual theoretical Q), when conductivity is obtained from (3.6), it is inferior to the effectual conductivity of the RC. The purpose of

the conservative estimation is to predict the reverberation performance in RC. Simply, reverberation performance in RC will be implicitly much better than measurement results. With application of the conservation value, when the measured (and lower) Q is demonstrated to be in compliance with some criteria, performance and field strength in the real RC will be guaranteed.

3.3. Conclusion for parameter option of RC

In this part, development of each components of RC is reviewed. From the analysis of each parameter and the prerequisites of the exposure experiment, RC with regular shape, small size stirrers, multiple source alternative excitation layout and aluminium enclosure is proposed. Size of RC is discussed with the available standard recommendation and will be determined in the followed part. Q factor is also studied in this part. The difference between the measurement and the theoretical estimation is analysed. Conservative interpretation Q from the measurement is also discussed. It would serve to the following Q estimation for the experimental RC.

4. Numerical methods

4.1. Option for numerical methods

Since current popular measurements are still invasive to the animals, numerical methods are fundamental to evaluate the field or power distribution in the biological tissues.

Several completely different methods have been applied in *in vivo* or *in vitro* exposure experiments. Some are based on EMF integral equations such as Method of Moment (MoM) [35]; others are based on differential equations such as Finite-Difference Time-Domain method [36] and finite element method (FEM) [37]. All of them have already had some commercial solvers such as FEKO [38], HFSS [39] and CST [40].

MoM is essentially the method of weighted residuals, which can be used for solving differential and integral equations. The fundamental concept employs orthogonal expansions and the linear algebra to reduce the integral equation to a simultaneous linear equation system. It begins with deriving the currents on each segment, or the strength of each moment, by using Green's function. Then one can calculate the charges at points of the structure. Usually, it approximates the surface by wire-grid approximations. It has been successfully applied to wide variety of EM problems such as radiation due to thin-wire elements and arrays, scattering problems and the analysis of microstrip and lossy structures. Integral methods (e.g. MoM) use a surface mesh, and the numbers of unknowns increase with the square of the linear meshing density. For a dense matrix calculated with an iterative solver, the memory and solution time costs increase with square of the unknowns, which is $O(n^4)$. In small animal exposure analysis, fine resolution should be applied. The matrix is expected to be very dense. Computation task for MoM could be very heavy.

FEM has its original in the field of structure analysis. FEM is a more versatile and powerful numerical technique for handling problem involving complex geometries and inhomogeneous media than MoM and FDTD. It divides the entire domain into several sub-domains (elements). An element is described by its vertices and one point on each edge. These points are called as nodes. FEM mesh is constituted by nodes and elements.

Approximation is made on the nodes of the elements, which is sufficient to approximate the fields at any points. FEM is an accurate method. Main limitation of this method in bioelectromagnetism is the matrix inversion which FEM requires. Since bioelectromagnetic problems associate with large heterogeneous problems, the number of unknown is often of several millions (e.g., about 30 millions for a head and a phone). In such configuration, the matrix inversion is still a big problem which limits the application of FEM in bioelectromagnetism.

FDTD is a time-domain method. It belongs to mesh-based differential time-domain numerical methods. The time-dependent Maxwell's equations (in form of Partial Differential Function, PDF) are discretized using central-difference approximations to the spatial and temporal partial derivatives. With this approach, no matrix inversion is required. The resulting finite-difference equations are solved by either software or hardware in a leapfrog manner ([41], Annex I): the electric field vector components in a volume of space are solved at a given instant in time; then the magnetic field vector components in the same spatial volume are solved at the next instant in time; and the process is repeated over and over again until the desired electromagnetic field behavior is fully evolved.

After the analysis, FDTD is chosen as the numerical method to characterize the power distribution in experiments.

4.2.Principle of the FDTD method

Finite-difference time-domain method is a popular computational electrodynamics modelling technique ([36], Annex I). It is relatively easy to be understand and easy to be interpreted into software.

Because FDTD is solved by propagation of the fields forward in the time domain, the electromagnetic time response of the medium must be modelled explicitly. For an arbitrary response, this involves a computationally expensive time convolution, although in most cases the time response of the medium can be adequately and simply modeled using either the recursive convolution technique, the auxiliary differential equation technique, or the Z-transform technique.

4.3.Limit of the FDTD method for RC

4.3.1 CFL limit and numerical dispersion

In FDTD method, the time increment Δt , and the spatial increments (Δx , Δy and Δz) are not independent. They should satisfy certain relationship so as to avoid the instability and numerical dispersion.

$$\Delta t \leq \frac{1}{v \sqrt{\frac{1}{(\Delta x)^2} + \frac{1}{(\Delta y)^2} + \frac{1}{(\Delta z)^2}}} \quad \text{is the FDTD numerical stable condition}$$

(Courant-Fredrich-Lewy criteria, CFL [36]). Δt is the time update step.

Interpreting Maxwell functions with finite differential method would introduce numerical dispersion. That is to say, propagation speed in the medium will change with the frequency. It depends on the propagation direction of waves in the lattice as well as the discretization level. Follow condition [36] should be satisfied when choosing the dimension of the cells.

$$\frac{\lambda_{\min}}{10} \geq \text{Max}(\Delta x, \Delta y, \Delta z) \quad (4.1)$$

λ_{\min} is the minimal wavelength

Much higher frequency, much dense discretization should be expected to avoid numerical dispersion.

4.3.2 Limit in application to simulation of the RC

EM simulations with RC by means of FDTD are always a contentious topic. Several papers have been provided ([42], [43], [44] and [45]). The difficulties in the simulations are:

- ✓ Difficulties in deciding the dielectric parameters of RC enclosure
- ✓ Endless simulation times

The dilemma in dielectric parameters of the enclosure lies in two aspects:

On the one hand, it is nearly impossible to find the exact value for the FDTD inputs. Although the theoretical dielectric parameters for enclosure could be found in many documents, the manufacture of the RC often lowers the theoretical values to some

unpredictable level. By measurement, the dielectric parameters could be studied but nevertheless the exact value can not be obtained ([46], [47]).

On the other hand, less the loss on the RC enclosure (thus much lower conductivity value for the enclosure), the constant time for the EM waves in RC is longer and the waves in RC tend to experience much more times of reflections. Researchers have many propositions such as modification of the dielectric properties for the air in RC to seek one fast stable state [42]. But the cavity that has an enclosure conductivity of just 100 S/m can less likely be called as RC. The significant loss by the air during propagation of wave in the cavity can not guarantee the idea of sufficient reflections-principle of RC.

Progress of the computation technology may be marked as magnificent and astounding. Breakthrough in the hardware and algorithm permit the computation in much finer grids and much bigger volume. Current computation technology is very powerful, however not enough powerful to solve the problem. With the extremely dense discretization of RC model, computation task could also be seemingly endless. The difficulties also exist in the simulation of temporal variation of boundary condition. One example can show us the limits of application of FDTD to RC.

4.3.3 Simulation on testing the FDTD calculation time for RC application

4.3.3.1 Purpose of the trial simulation

One trial simulation has been designed to estimate the expenditure of the FDTD application to RC. Since rotation of the stirrers is just the matter of the planning and the computation with matrix, one RC without stirrers is applied in the research.

Simulation time and resource are not the exact values for RC which would be put into use but it is enough to estimate the minimum time and memory cost.

4.3.3.2 Configuration of the trial simulation

Configurations of the simulation are specified below:

Computation volume: $1m \times 1m \times 1m$

Resolution of FDTD cell: 2 mm

Absorption boundary: PML [36] with 8 layers

Cavity dielectric parameters: conductivity = $5000S/m$ and relative permittivity = 1 (for

reference, conductivity of ideal aluminum metal is $36.7 \times 10^6 S/m$, which means cavity enclosure in the simulation has much loss than true RC.)

Load: 1.5 liters IEC 2450 MHz human head equivalent liquid ([48]) is placed in the centre of RC.

FDTD time step: 3.66×10^{-12} second

Operational frequency: 2.45GHz

Among four top corners of the RC, three are filled with metallic cubes to avoid potential symmetric field distribution in the cavity (Figure 4.3)

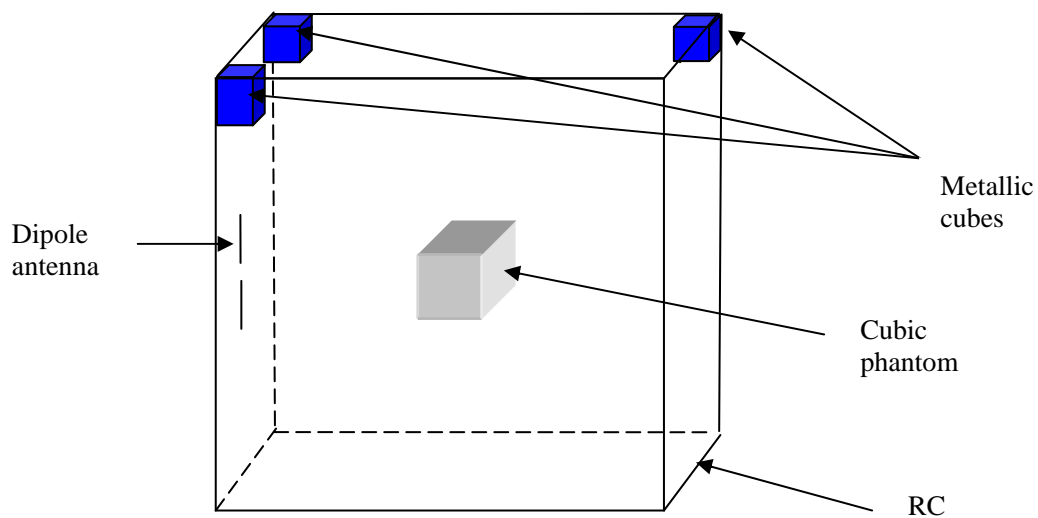


Figure 4.3 Configuration of the RC for test

One pulse excitation is launched at the gap of the dipole antenna, which is shown in Figure 4.4.

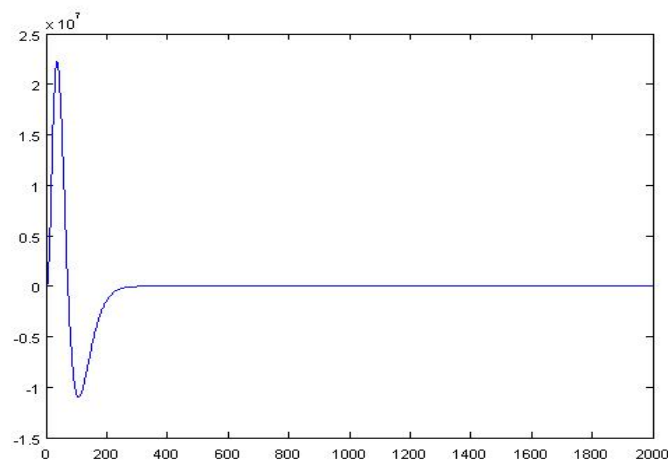


Figure 4.4 Voltage pulse excitation between the antenna gaps

4.3.3.3 Statistical results of the temporal E

Temporal evolutions of three E components on 54 points have been recorded. Half of the data are within equivalent liquid and the others are within the empty space of the RC.

By each 20000 updates, we calculate averaged value for the points inside the equivalent liquid and outside the equivalent liquid. We get Figure 4.5 and Figure 4.6:

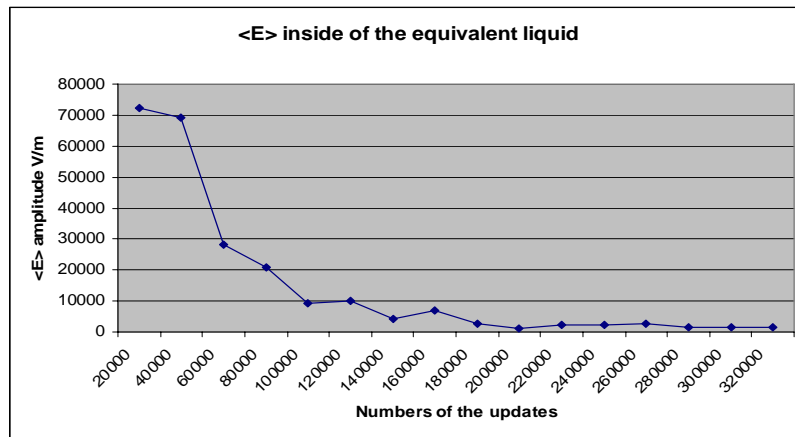


Figure 4.5 <E> for 27 points inside the equivalent liquid

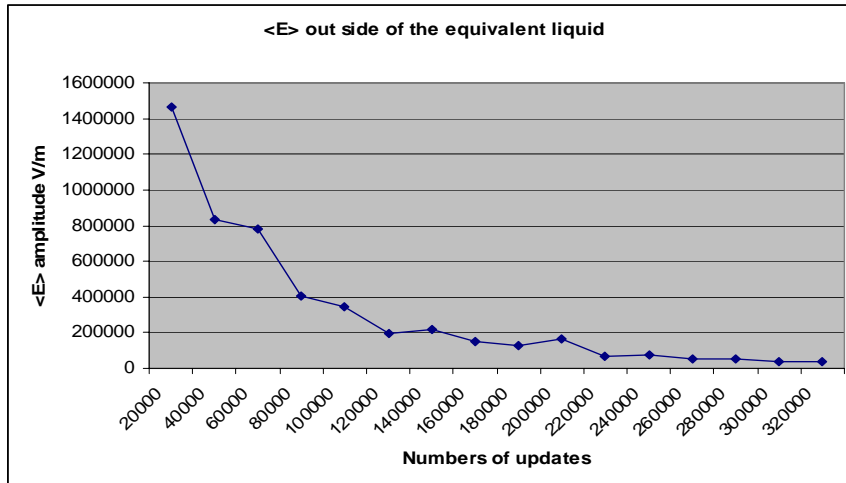


Figure 4.6 <E> for 27 points outside the equivalent liquid

Signals in RC seem stable for 3.2×10^5 time steps which take 2 months by one 2.8 GHz dual-core CPU.

Convergence of the temporal signals in the RC can be evaluated by IIR (Infinite Impulse Response) filter theory [49].

FDTD method could be interpreted as a high order digital filter with input ($x(t)$, E excitation in RC) and output ($y(t)$, E components recorded at certain position in RC) signals. This method is based on finite differential equation which can basically be written as:

$$\hat{y}(n) = \sum_{i=1}^N a_i y(n-i) + \sum_{j=0}^M b_j x(n-j) \quad (4.2)$$

By Z-transformation, we can re-write the above function as:

$$y(z) = H(z)x(z) \quad (4.3)$$

In it,

$$H(z) = \frac{b_0 + b_1 z^{-1} + \dots + b_M z^{-M}}{1 + a_1 z^{-1} + a_2 z^{-2} + \dots + a_N z^{-N}} \quad (4.4)$$

So the coefficients can be described as the zeros and poles of the transfer function in z-plane. By computational procedure of the adaptive algorithm [50], the convergence of all the coefficients can be determined.

For example, results of field components E_y for 2×10^5 time update steps at one point in RC have been recorded for IIR filter convergence evaluation. IIR filter with 400 poles and 70 zeros were used to simulate the wave propagation process in RC. For concerns of the enormous computation resources needed in the inversion of the matrix, 2×10^5 values are re-sampled by a factor of 60, thus around 3400 values are used for determination of the coefficients of transfer function. Results about the zeros and poles for one point are shown in Figure 4.7.

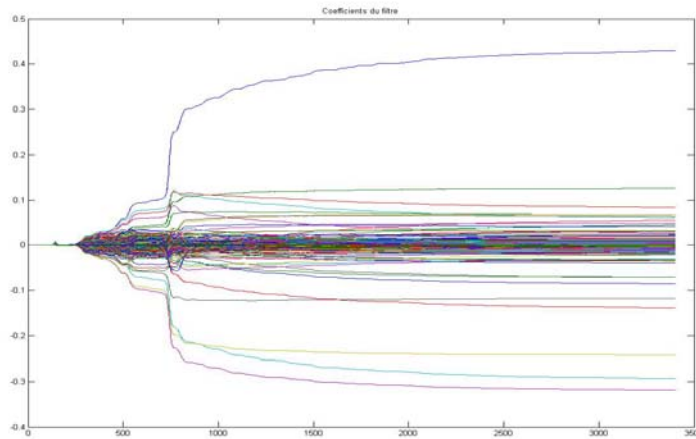


Figure 4.7 Evolution of the zeros and poles

Obviously, for 2×10^5 updates, E_y induced by the pulse excitation in the RC tends to be constant; however, neither completely absorbed by equivalent liquid nor reached the resonant state. Actually, it has already cost dual-core CPU of 2.8 GHz for 5 weeks calculation. If we repeat the simulation for the other 5 antennas, probably six months will be predicted viewing no advance for the hardware.

Even if resolving the problem of calculation resources and computation time by means of advanced hardware, we still need to face the problem to define the exact dielectric parameters of the metallic enclosure.

4.4. Conclusion

Compared with other popular numerical methods, FDTD is chosen as the numerical method for determining the power distribution in the experiment. FDTD is very powerful in solving many problems in EMF domain. However, RC is a very special case. In contrast with other instruments for wave propagation research, which deal with less reflective waves and thus have instantaneous stable time, RC depends completely on the reflective waves. The simulation method must describe the temporal evolution of the field distribution in the RC or at least in the entire test volume. Then one tedious or even endless simulation period and updates steps are expected.

As we explained in the part, several difficulties exist in the FDTD simulation for the real-size RC. The difficulties can be partly resolved with the progress of the hardware technology. However the inputs of the simulation can not be the exact as the real RC due to loss power on the load of measurement instrument.

Numerical methods

Pure FDTD method encountered some problems in analysis animal's power absorption in RC. Other alternative method which can combine simulations and measurements should be studied. This would be described in part 5.

5. Design and realization of RC

Upon previous discussion, fundamental knowledge about the concept of the experiment system has been obtained. The RC could be realized by furnishing several key parameters.

5.1. Shape of RC

Shape of the RC has been discussed in 3.2.2.2. Regular shape RC is more suitable for our experiment when larger uniform test space is needed.

Considering the dimensions of the experimental container, test zone is chosen as one cubical shape of $40\text{cm} \times 40\text{cm} \times 40\text{cm}$. A certain distance between the antennas and the test space should be allocated to avoid the coupling between the experimental animals and the emission antennas, which would be discussed in 5.2. Then cubic shape RC seems to be satisfactory for the requirement. It is displayed in Figure. 5.1.

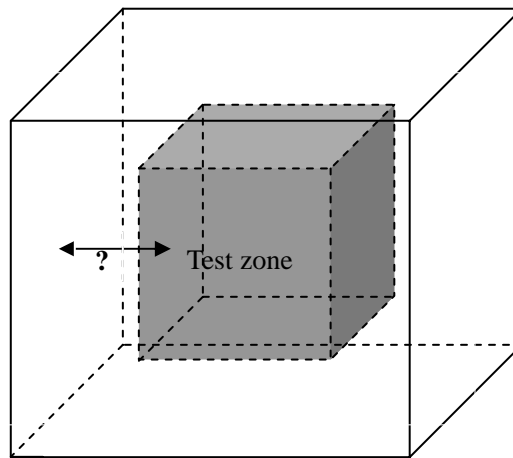


Figure 5.1 Plan of the regular shape RC

5.2. Dimension of the RC

Once the preliminary model of RC has been decided, its dimension needs to be discussed. As we have stated, besides efficiency and uniformity of the system, there is another criterion as the space requirement for each animal under exposure. Briefly, it is defined by the total exposure system volume divided by the maximum numbers of the animals in the system.

Compact dimension is advantageous because of space occupation and expenditure to build a RC. But some factors such as the interaction between the animals and the antennas need to be taken into account and they inversely prohibit the reduction of the RC dimension.

RF design dedicates with matched impedance to ensure maximum and stable power transfer. If emitter and reflector are self-influenced, current distribution on the emitter will be changed, thus the impedance is adversely changed. Emitter could not maintain the stable RF radiation.

In animal *in vivo* Wi-Fi exposure experiment, animals are allowed to move at least partly freely in the test zone. When RC is too compact, animals and the emission antenna could be sometimes very close. There is one risk that the antenna emission power would be unstable during the movement of the animals.

One of network parameters S_{11} can well present the interaction between the emission antenna and the animal under exposure. It refers to the ratio of signal that reflects from one port to the incident signal on the same port. Extent of perturbation by the approximate reflectors can alter the reflected power and change S_{11} .

Dimension of the RC has been studied by the influence of the movement of the animals to S_{11} of the emission antenna. One experiment which concerns the dimension of RC is based on the cubical metallic cavity that assumes no stirrers, no open doors, no cables connecting and no leakage from the enclosure. One half-wavelength dipole antenna is realized (Figure 5.2). The dipole antenna has one perfect reflective plane to permit the directive radiation pattern.

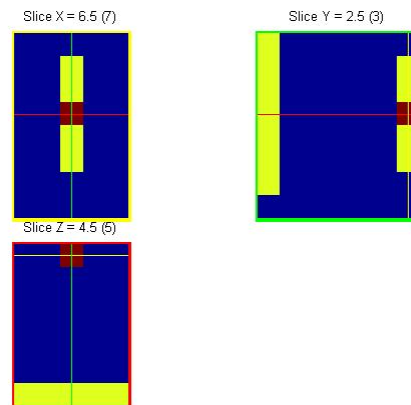


Figure 5.2 Dipole antenna numerical model

S_{11} of the antenna in free field is shown in Figure 5.3. It will be used in RC as emission antenna.

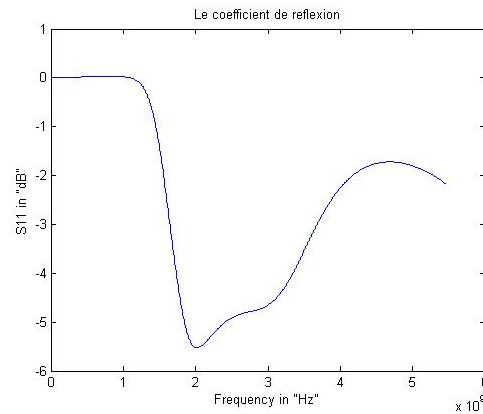


Figure 5.3 S_{11} of the simulated emission dipole antenna

Far-field radiation pattern of the antenna is shown in Figure 5.4. Obviously, existence of the metallic reflective plane changes the radiation pattern which tends to be much orientated to the central test zone instead of omni-direction.

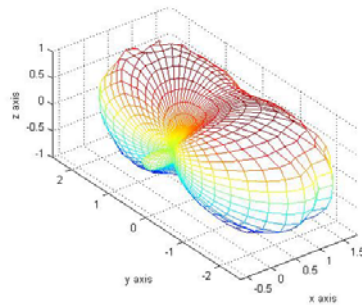


Figure 5.4 Radiation pattern of the dipole antenna

Enclosure of the wall can be deemed as flexible. It can dilate or contract at will. One dipole antenna as described above is placed in the cavity with 4 cm to the wall. Due to symmetric structure of the cavity, the effect of antenna at other sides can be equivalent by this case.

In simulation, the animal model is realized by IEC equivalent liquid. The sham has 1500 g in weight which is shown in Figure.5.6.

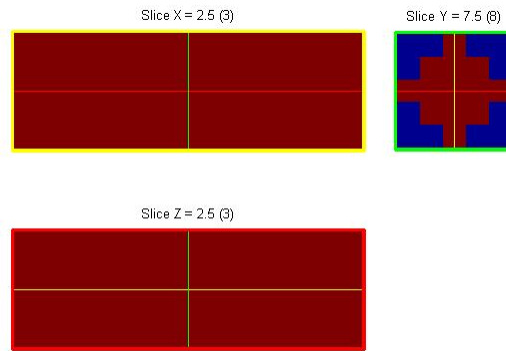


Figure 5.6 Parallelepipedic shape animal numerical model

The 1500 g equivalent liquid model can be moved in the central zone of $40\text{cm} \times 40\text{cm} \times 40\text{cm}$. It is placed on totally 26 different positions in the test zone. 26 points are uniformly distributed in the test zone. The movement of the equivalent liquid in the cavity is shown in Figure 5.7.

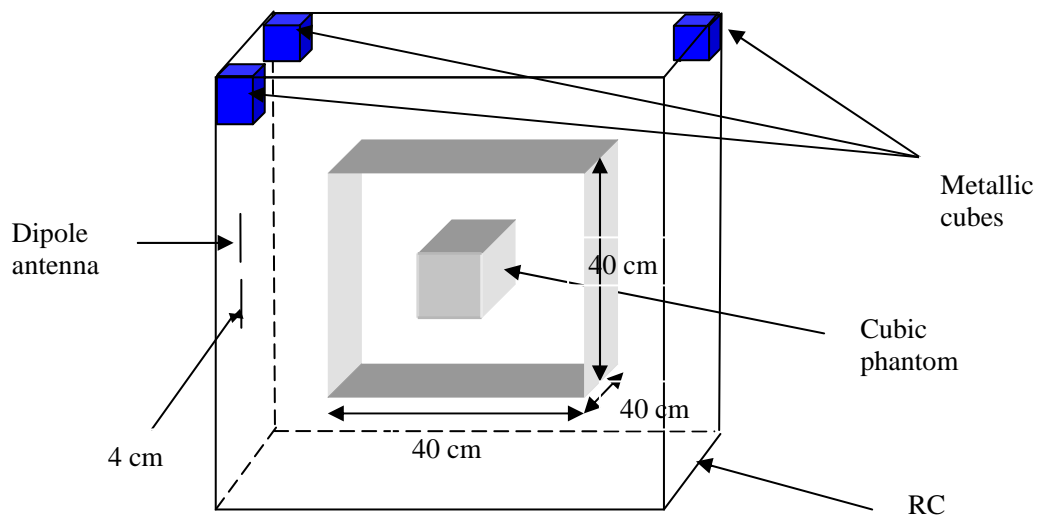


Figure.5.7 Different configurations of the equivalent liquid model in cavity

Resolution of the FDTD cell is set to $1\text{cm} \times 1\text{cm} \times 1\text{cm}$. In the simulation, no stirrers, door or leakage from the enclosure are taken into consideration. To avoid the completely symmetric field distribution in RC, three of the four top corners of the RC are filled with metals. The dimension of the RC changes from 60 cm, 80cm, 100 cm and 120 cm. For each dimension, S_{11} of the antennas is recorded for different rat's position and then variation of the S_{11} is compared. The standard deviation of S_{11} for each configuration is shown in Table. 5.1.

Design and realization of RC

Dimension of cavity	60 cm	80 cm	100 cm	120 cm
Standard deviation of s_{11}	2.47 dB	1.66 dB	1.21 dB	0.59 dB

Table 5.1 Standard deviation of the S_{11} for 26 positions

Based on the analysis, 120 cm RC has 0.59 dB as standard deviation of s_{11} when the animals sham moves in it. To assure the function of the constructed RC, some surplus margin is added to the designed RC. Dimension of the cavity is decided as $150\text{cm} \times 150\text{cm} \times 150\text{cm}$ as shown in Figure 5.8.

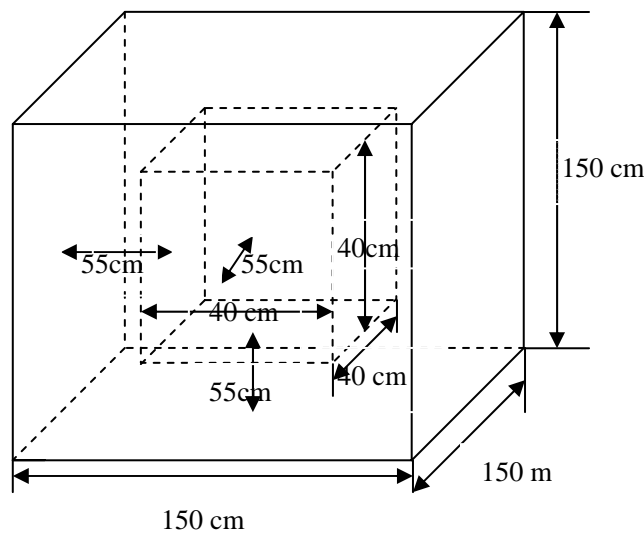


Figure.5.8 Dimension of the cavity

5.3. Power excitation and stirring layout

After dimension and the interior configuration of the cavity have been determined, accessories and the excitation systems should be added to the metallic cavity to realize one real RC.

5.3.1 Consideration for the stirrers

Existence of the large size stirrers brings up two problems to the animal exposure experiments. First, they will occupy the experimental space and second, rotation of the stirrers (both step by step and continuous) produces lots of noise in operation. The first problem is especially obvious for the small size RC. When RC dimension is not rather compact, insertion of large size stirrers as recommended by the standard [22] is better for the sufficient modes but detrimental for the small size RC of animal non-restrained exposure purpose. For the second problem, it is negative to both the large size and small

size exposure system. The noise can be minimized by better lubrication but mechanical noisy can not be completely eliminated. Chronic environmental noise has been identified as the stressor in the animal experiments [51]. By this means, any method to eliminate the noise in the animal *in vivo* exposure system is preferred in design of the animal exposure system. As stated in 3.2.3, the multiple-excitation layout can be adopted to avoid the significant size stirrers in RC as shown in Figure 5.9.

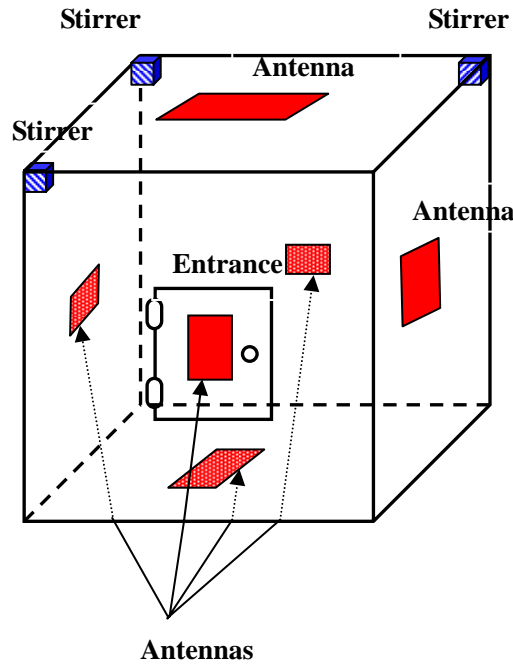


Figure 5.9 Antennas layout in RC

In the real design, six printed half wavelength dipole antennas (as shown in Figure 5.10) are installed to each interior surface of the enclosure. They keep 4 cm distance to the metallic wall.

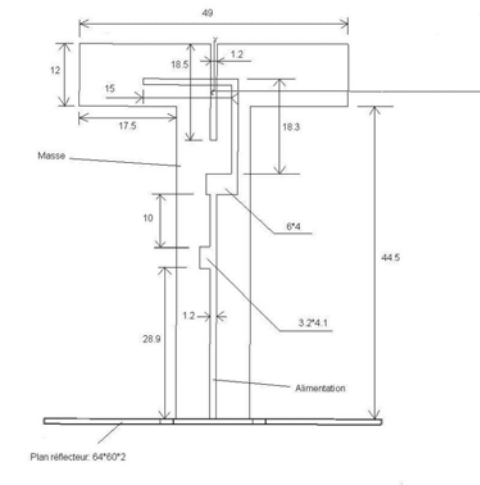


Figure 5.10 Design of the half wavelength dipole antenna (dimension in mm)

Printed dipole antenna is manufactured and installed in RC as displayed in Figure 5.11.



Figure 5.11 Realization and installation of the antenna in cavity

Three small size stirrers are placed on the top corner of the RC as shown in Figure 5.11. Stirrers are folded by aluminium materials with 1mm thick. The stirrers operate on continuous modes.

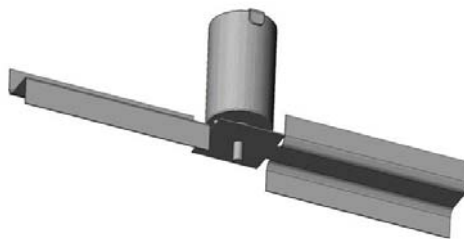


Figure 5.12 Design of the stirrer

Diameter of the stirrer is 30 cm. Minimal distance between the stirrer and its metallic support is 3 cm. Its rotation speed can be adjusted by software. The realized stirrer is displayed in Figure 5.13.



Figure 5.13 Realization of the Stirrer in RC

5.3.2 Ventilation of RC

For animal *in vivo* exposure experiment, fresh air is vital for the survival of the animals. Completely enclosed or even badly ventilated system is negative to animals: immunity

ability of the animals will be harmed [52]. Well functioned ventilation system and suitable temperature will alleviate stress of the animals under exposure. In large size RC, ventilation and air condition system is always equipped. Compared with the huge dimensions of the RC, its spatial occupation is very marginal. In the small size RC, the separate ventilation system will need piercing on metallic enclosure which will potentially lower the performance of RC.

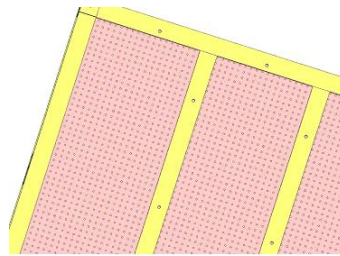


Figure 5.14 Material for the cavity enclosure

One possibility is to apply the light and aluminum wire-mesh material just as canopy-like protection materials to construct RC wall. The porous structure can assure the flux of the air without any electro-mechanic system. Commercial available aluminum gauze-net like material can have much better shielding properties. At high frequency, power can be easily attenuated as 24 dB, in other words, 1/250 of the original power.

5.4.Assemblage of RC

The cubical cage with size of 1.5 m is fabricated by aluminium frame. On the front side of the RC, one rectangular shape entrance is reserved for door of RC. The Assemblage scheme is shown in Figure 5.15.

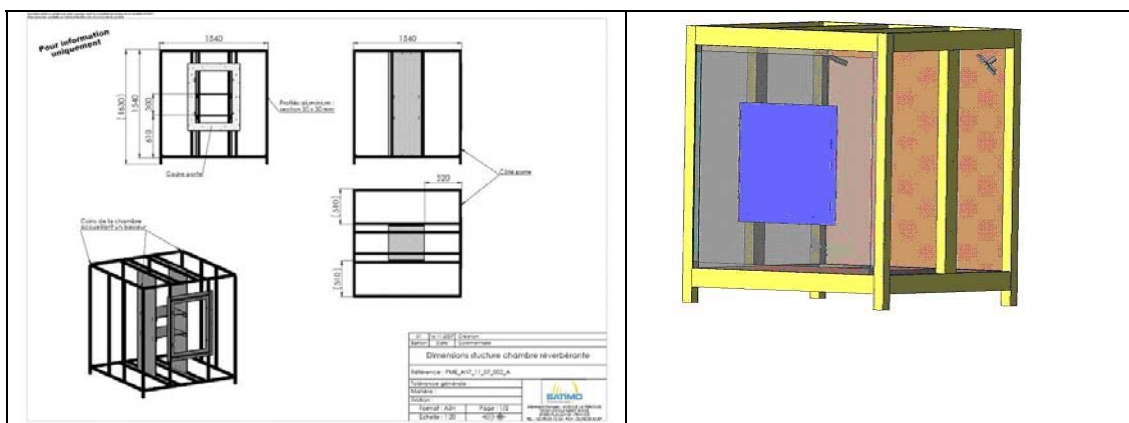


Figure 5.15 Assemblage schema of the RC

Plastic test bench is placed in the RC as shown in Figure 5.16. It has the

electromagnetic transparent property. The field will not be disturbed by the test bench.

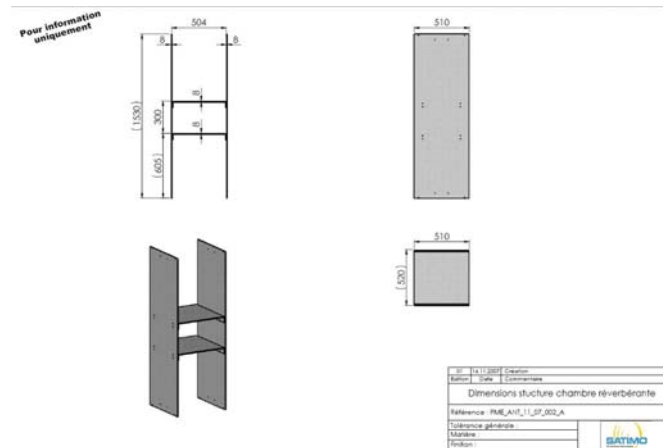


Figure 5.16 Design of the test bench of the experiment

The test bench is realised and placed in centre of RC as shown in Figure 5.17.

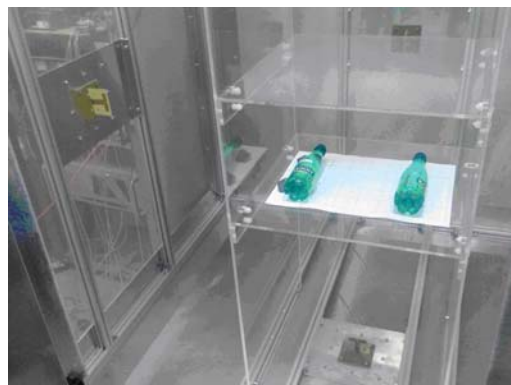


Figure 5.17 Realization of test bench in RC

EMF transparent plastic containers as mentioned in 2.1 are placed on the test bench.

Then the RC with all its accessories are ready for test if the necessary cables, amplifiers, control box, suitable PC and software can be available. RC is shown in Figure 5.18.

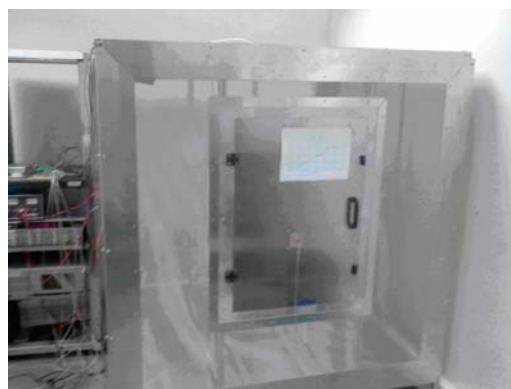


Figure 5.18 Manufactured RC

By design, the enclosure is light-permeable, so no illumination system is placed in the RC which will possibly add load to the system.

The signal generation and Wi-Fi communication system for the experiments can be described as Figure 5.19. If the system serves for continuous wave (CW) experiment, only a few modifications are need for the input system. PC1 will be replaced by the signal generator and PC2 can be definitely eliminated from the system.

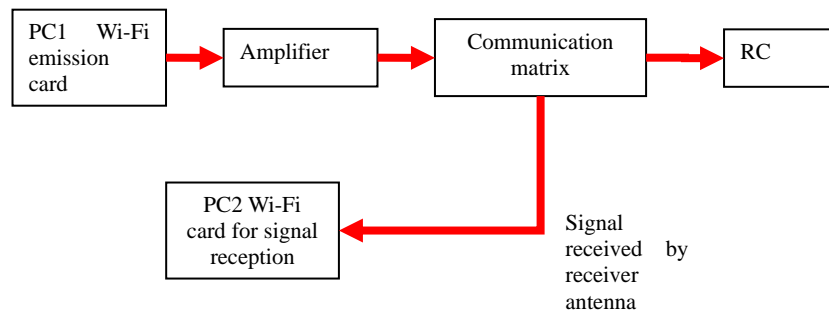


Figure 5.19 Wi-Fi signal generation chain

6. Proposition of an hybrid approach to characterize the field in RC

6.1.Measurement and simulation methods

When the entire exposure system had been designed and built, measurement and simulation tasks should be applied to characterise the system and in particular the relationship between the delivered power to the antennas and the SAR in animals.

As one exposure system, field distribution must be determined in order to recognize the radiation pattern, power partition in the system and in the radiated animals. Some parameters can be measured but precise values such as the absorbed power in animal body is hard to be exactly obtained by non-invasive measurement techniques.

Simulation would be useful tool for dosimetric assessment of the power in the animals. It can also contribute to the design of the measurement task and reduce its burden.

6.1.1 Available measurement and simulation methods in RC

In the domain of EMC and RF, measurement is the direct way to look insight into the performance of the system and validate the simulation results. For RC case, most of the experiments base on acquisition of E (field strength) or P (power) in the cavity. For example, Q, RC calibration, field uniformity measurements [22] are actually combinations and post-treatment of the E or P measurement. Tests in RC as immunity and emission test can also be deemed as the E or P measurements.

Information about E field measurement, RC calibration and Q measurement procedures can refer to [22].

EMF simulations concentrate on the evolution of the fields, current, voltage, power, etc. by means of various simulators or solvers. There are already several commercial simulators ([38], [39], [40]) based on different numerical methods.

Key issues in any simulations include acquisition of valid information from the target, selection of key characteristics and behaviours, the use of simplifying approximations

Proposition of an hybrid design and realization approach to characterize the field in RC

and assumptions within the simulation, and fidelity and validity of the simulation outcomes.

6.1.2 Available methods in deciding the animal power absorption

There are several available methods or protocols to determine the field distribution in the exposure system and the power absorption in the animals. They can be mainly classified into three branches: pure measurement, pure simulation and simulation-measurement combined method.

6.1.2.1 Pure measurement method

Pure measurement is proposed by Balzano *et al* ([53], by exposure experiment with TEM cell. The setup was prepared for 900MHz. Power dissipated into the animals was determined by measuring the incident power and the reflected power at the cavity incident port, and by estimating the resistive losses in the metal, the dielectric losses in the plastic and the radiated power as shown in the following equation (6.1):

$$P_{abs} = P_{inc_m} - P_{ref_m} - P_{diss_e} \quad (6.1)$$

Where,

P_{abs} : power absorbed by animals. (assessed by calculation)

P_{inc_m} : incident power (measured)

P_{ref_m} : reflective power (measured)

P_{diss_e} : dissipative and leakage power in RC (estimation)

However, partition of the power in different parts of animal's body can not be demonstrated and due to numerous different excited modes, considerable angular variation are inevitable. The variation is so substantial that it is unacceptable for the uncertainty analysis.

6.1.2.2 Pure simulation method

Pure simulation fits for many animals exposure experiment if all the input parameters (dimension of the exposure volume, modelling of the system, estimation of the dissipative and leakage power by the system, etc.) are accessible (either by experience or by measurement) and precision of the input values can be guaranteed. In fact, most of the animal exposure systems can be seen as of this type. Measurements serve to

Proposition of an hybrid design and realization approach to characterize the field in RC

provide input knowledge for the analytical values. No additional information is provided by the measurement part after the simulation starts.

6.1.3.3 Simulation-measurement alternative method

Simulation-measurement alternative method is partially similar to the pure simulation method. The method can be applied to the condition that there are multiple parameters which should be decided by measurement or measurement can only bring some approximation results to the simulation.

Simulation begins with the input of the measurement results to the simulators. Input values could be rather rough or approximate. Simulations are processed with these approximate inputs. Some referential results are generated with the simulation. It can be compared with the obtained knowledge (either by measurements or experiences). If the convergence of the simulated results and the obtained knowledge is achieved, simulation results are validated. On the contrary, modification should be made to the input values and the entire procedures are repeated.

In this method, simulations, on one hand, are aimed to give comprehensive results. On the other hand, it helps to reduce the tasks which are otherwise undertaken by measurement. Since measurement results or real condition might not be always easily accessible, with the step by step approximation method, the real condition of the system can be gradually approached.

6.2.Simulation-measurement hybrid method principle

6.2.1 Inspiration of the method

6.2.1.1 Limit of the available characterization methods for RC

Upon analysis in 4.3, FDTD simulation can not bring us the complete information about animal power absorption vs. antenna emission power within reasonable time expenditure for the dense discretized RC.

As for the measurement, we can obtain some useful information such as the quality factor Q , the E field strength or the net input power. However, the absorption power in heterogeneous animal body could not be directly and precisely acquired by non-invasive probes. For pure measurement method, it is impossible to estimate the

Proposition of an hybrid design and realization approach to characterize the field in RC

power dissipated in RC enclosure with an acceptable level because of unknown parameters for enclosure dielectric properties ([29]).

In contrast, computation time for pure simulation method is exhaustive. Furthermore, input information such as the dielectric properties is hard to be obtained precisely. The simulation results would never be valid.

Simulation-measurement alternative method can bring us with power distribution information in RC. By this way, Q in the real RC can be measured through (3.7). Then, it can be applied to (3.6) to calculate *nominal conductivity* of real RC. As we have stated in 3.2.5, this *nominal conductivity* has actually attributed all the loss to as from the effect of Joule heating on enclosure. So the *nominal conductivity* is inferior to the real enclosure conductivity. For the simulation part, entire RC is realised with test bench, container, animals and all the accessories exactly as those in the reality. Excitation signals are added alternatively to the six antennas. For each antenna random excitation, one simulation would be performed. E values are averaged in the centre of RC by all the six antennas excitation cases. Averaged simulated E is then compared with the measured E in real RC. By this way, E serves as referential results as we discussed in 6.1.3.3. If the two values are not converged, modified *nominal conductivity* will be used and simulation is repeated until the convergence state is arrived. Theoretically, power distribution in RC and rats can be approached by many tentative and repetitive simulation and measurement tasks. However, the simulation task would be enormous. It is a practical impossible mission.

Neither of the available methods alone would settle the problem once for all. We need to apply a new method to character field distribution in RC.

6.2.1.2 Concept of the simulation-measurement hybrid method

From the previous analysis, simulation-measurement alternative method has much difficulty in solving the relationship between the net incident power to RC and absorbed power by animals. Nevertheless, it is promising in giving us some useful hints as being possible to decide the power partition in the RC if only enough trials have been made on studying all the loss sources of RC. In this method, entire RC is realised as simulation model. It could be thought as the reason why all the loss sources (thus all the details of RC) could be considered for the simulator. We could have one proposition

Proposition of an hybrid design and realization approach to characterize the field in RC

that if much simpler simulation model could be conceived, the computation task might be reduced.

Power in RC will be absorbed by the animals as well as the RC enclosure. Higher is the E level in the environment, higher is the absorbed power by animals. In fact, power incident to the RC and the power absorbed by animals are proportional. Thus, E level in RC would be useful in linking the incident power and the absorbed power by animals. E distribution in the working volume is one key character of RC.

This relationship demonstrates that in experiment of RC, only EMF evolution in the working volume is the research interest. It deals directly with the power absorption of animals and thus WBSAR. If working volume is free of source, E on different points should be thought as very similar when averaged over one or several stirrer rotation periods (different antennas alternative switch on/off configurations in our design). If RC is perfect then the field strength is homogeneous over this volume, the averaged over this volume can characterise the exposure.

In this condition, there is no need to realise RC wall, additional leakage, antennas or stirrers in the simulation. Field distribution in the volume may follow some special statistic rules which would be generalised to construct the simulation model. Since central working volume is smaller than entire RC, less computation work might be expected.

For the simulation part, the ratio of WBSAR to averaged square E field amplitude ($\langle E^2 \rangle$) in the empty zone are obtainable (by measurement on sufficient points) in the

loaded RC. Then the ratio of $b = \frac{P_{abs}}{\langle E_{sim}^2 \rangle}$ (P_{abs} is the absorbed power by animals,

$\langle E_{sim}^2 \rangle$ is the spatial averaged square E field amplitude in the empty volume of the

loaded RC by simulation) or $c = \frac{WBSAR}{\langle E_{sim}^2 \rangle}$ (SEFR, Ratio of WBSAR to simulated

averaged square E Field) could be obtained.

In measurement part, net incident power and the E amplitude in the empty volume

could be measured in the loaded RC. Then the ratio of $a = \frac{P_{inc}}{\langle E_{mea}^2 \rangle}$ (P_{inc} is net

incident power to the RC which is measured by the power transmitted to the antenna

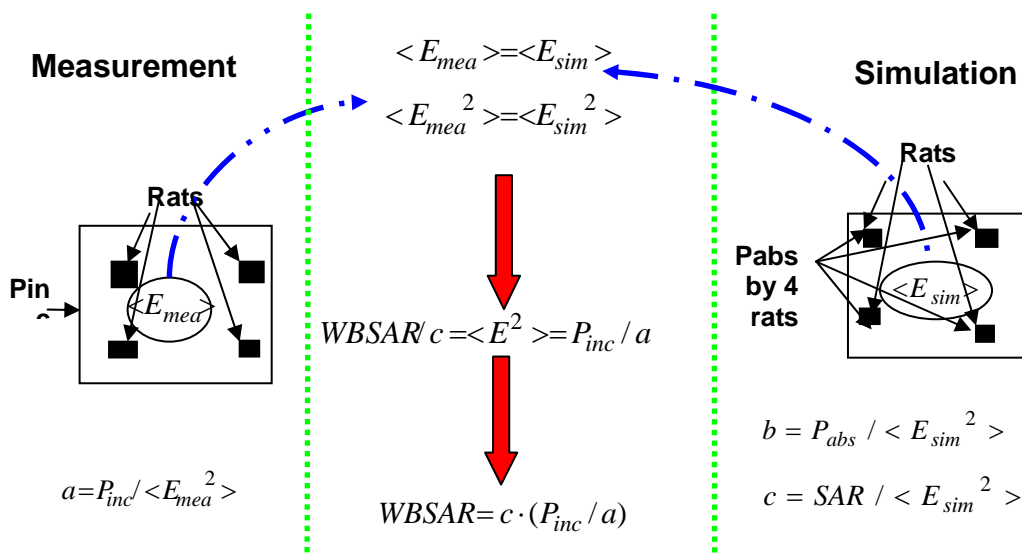
Proposition of an hybrid design and realization approach to characterize the field in RC

minus the return power from the antenna. $\langle E_{mea}^2 \rangle$ is the spatial averaged square E field amplitude in the empty volume of the loaded RC by measurement. $\langle E_{mea} \rangle$ is measured with the function of the stirrers and excitation of the antennas (exactly same as in the animal exposure experiment).

E obtained by current measurement equipment is time averaged value. In measurement with RC, all the values are averaged over several rotation of stirrers (for actual measurement, E values are acquired every 2 minutes. Rotation of stirrers is about 10 rounds/minutes). Averaged multiple measured values are based on both temporal and spatial average.

By comparison, E by simulation is instantaneous values. However, RC works on reverberation character. If less loss exists in RC, maxima and minima can move all around in RC with the rotation of stirrers and alternative function of six antennas. E amplitude on one position is the reappearance of E amplitude at an adjacent point of an earlier (or latter) time. When sufficient points could be gathered in one sufficient volume, the averaged simulated E has already taken account for the temporal and spatial process. By this means, measured $\langle E \rangle$ and simulated $\langle E \rangle$ are both temporal and spatial averaged values. They have the same physical significance.

So, the averaged square E for the measurement and simulation could be harmonised. In this point of view, $\langle E_{mea} \rangle$ and $\langle E_{sim} \rangle$ will serve as the bridge between P_{inc} and WBSAR (as well as P_{abs}), which is shown in Figure 6.1.



Proposition of an hybrid design and realization approach to characterize the field in RC

Figure 6.1 Simulation and measurement combined strategy

Esim: *E* values (RMS) obtained by simulation, *Emes*: *E* values (RMS) obtained by measurement, *Pabs*: Absorbed power by the rats, *Pinc*: net incident power to RC.

6.2.2 Simulation part

6.2.2.1 Field distribution model in RC

One important parameter in evaluating the performance of resonant system such as RC is quality factor (Q) which can be defined by measurement ([22]):

$$Q_{meas} = \left(\frac{16\pi^2 V}{\eta_{Tx} \eta_{Rx} \lambda^3} \right) \left(\frac{P_{MoyRec}}{P_{input}} \right)_{nAntennaLocation} \quad (6.5)$$

Where,

η_{Tx} and η_{Rx} : antenna efficiency factors for the Tx and Rx antenna respectively

V : chamber volume (m^3)

λ : wavelength (m) at the operation frequency

P_{MoyRec} : averaged received power from the reference antenna

P_{input} : input power deliver in the chamber

$n_{AntennaLocation}$: the numbers of antenna locations used to collect the calibration data at the frequency being evaluated

All the power information is gathered with values averaged over several stirrer rotation periods.

It is well demonstrated that field distribution in perfect RC (lossless) above Lowest Usable Frequency (LUF) conforms to Rayleigh fading model ([54], [55]). By measurement and simulation, it is also verified that field distribution in RC even with low Q (about 100) follows Rayleigh statistics ([56]).

Rayleigh fading is a statistical model for propagation environment of radio signals. It is assumed to be applicable to situations with many scatters. The signals are reflected, refracted and diffracted by the scatters so as to produce the EM waves from all the

Proposition of an hybrid design and realization approach to characterize the field in RC

directions. Rayleigh fading is most applicable when there is no dominant propagation along a sight-of-line between the transmitter and receiver.

Once the feasibility for application of Rayleigh fading model to the constructed RC is confirmed, field distribution in RC could be simulated without characterizing the cavity enclosure as well as the antennas. The excitation powers are introduced by Huygens box ([36]) of $40\text{ cm} \times 40\text{ cm} \times 40\text{ cm}$ around the rats under exposure. On each point of the Huygens box surface, a summation of EM plane waves coming from random directions with random phases at 2450 MHz can be applied by function (6.3):

$$\vec{E}(\vec{r}) = \sum_{i=1}^{nray} A_i \cdot \exp(j \cdot \vec{k}_i \cdot \vec{r} + \varphi_i) \cdot \vec{v}_i \quad (6.3)$$

Where,

$nray$: numbers of rays passing through one point

\vec{k}_i : propagation direction of the plane wave

φ_i : phase of the plane wave

\vec{v}_i : E polarization of the plane wave

A_i : Magnitude of the plane wave.

In order to satisfy Rayleigh fading model, \vec{k}_i and φ_i should be pseudo-random values. Other two parameters ($nray$ and A_i) have the possibility to keep either certain fixed values or random values.

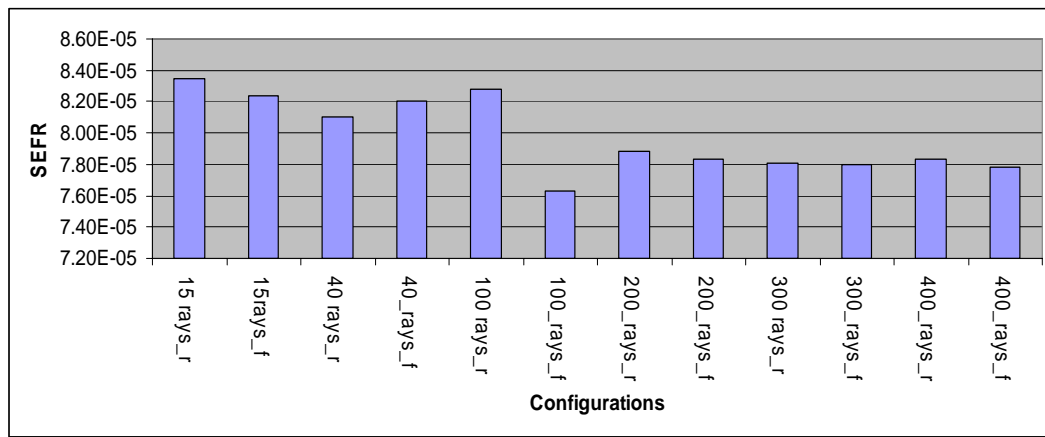
Using this approach the animals are exposed to multiple plane waves. By definition of Rayleigh statistics, the amplitudes, numbers, directions and phases of plane waves could be random. So we named this approach as Random Multiple Plane Wave Method RMPWM.

6.2.2.2 Discussion of the parameters in Random Multiple Plane Waves Method (RMPWM)

As shown in the equation to apply the EM waves to the Huygens box, two parameters need to be discussed. The first one is the number of the rays passing on one point of the Huygens box surface, the second one is the magnitude of the rays.

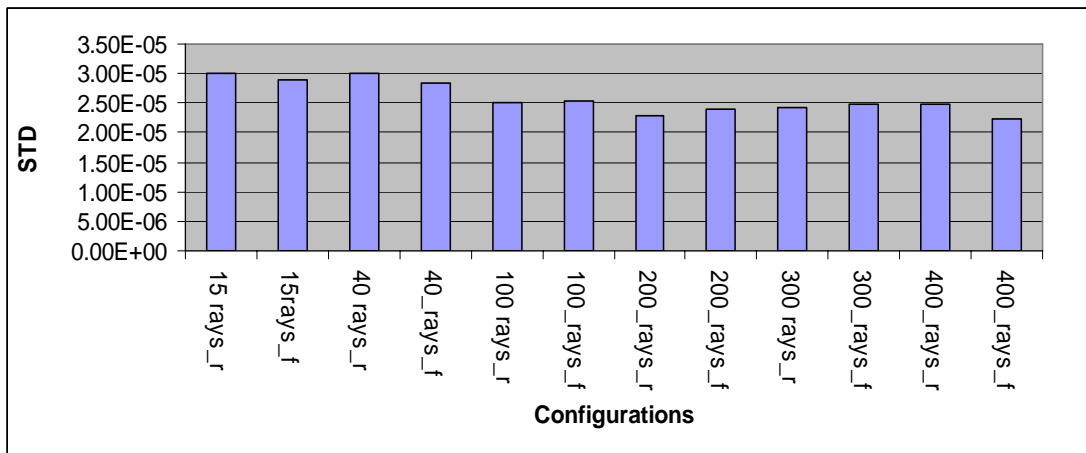
Proposition of an hybrid design and realization approach to characterize the field in RC

For fix magnitude and random magnitude cases, 20 simulations are performed for each condition in order to compare the difference between the various combined sets of the magnitudes and the numbers of the simulation to achieve the stable SEFR. The averaged results of SEFR on 20 simulations and the standard deviation are shown in Figure 6.2 and Figure 6.3. In each simulation, 3-D matrix of \vec{k}_i and φ_i are generated by pseudo-random values drawn from a uniform distribution on the unit interval. Random amplitude values are generated by the similar way.



f: fixed amplitude
r: random amplitude

Figure 6.2 SEFR for different rays/amplitudes configurations results averaged over 20 simulations



f: fixed amplitude
r: random amplitude

Figure 6.3 Standard deviation of the results

From the results of the averaged values on 20 simulations, we can see:

Proposition of an hybrid design and realization approach to characterize the field in RC

- If number of the rays is larger than 200 at each simulation, SEFR tends to converge.
- Amplitude of E field takes either random or fix will not change the result significantly.
- Generally, much more the rays applied in the single simulation, standard deviation will be less for 20 simulations.

In terms of the amplitude of the EM plane wave, there should not have any dominant ray in RC by definition of Rayleigh fading model. However, the amplitude cannot be all the same. It means that random amplitude is preferred for the RC case. On selecting the numbers of the rays on each point of the Huygens box, simulation with number of rays larger than 200 can achieve the satisfactory convergence.

If we calculate SEFR for simulation of 200 rays and compared the averaged results over 1, 2, 3...20 simulations to the averaged value of 20 simulations, we can get Figure.6.5.

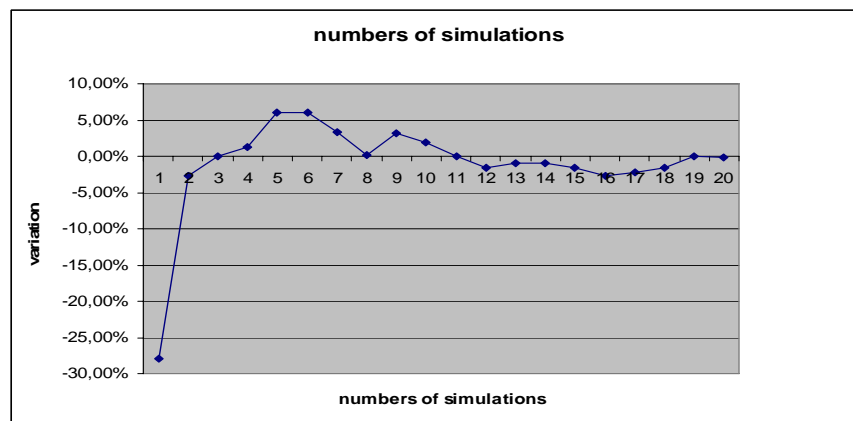


Figure.6.5 Variation of averaged different numbers of simulation results compared with the averaged 20 simulations results

We concluded that average results of 7 to 8 simulations with 200 rays will bring similar results as the averaged result of 20 simulations (within 5% difference). It provides one faster way to estimate the absorbed power in the rats on function of $\langle E^2 \rangle$ in RC for limited-time research case.

6.2.2.3 Deterministic Multiple Plane Wave Method (DMPWM)

Another approach on computing SEFR is DMPWM ([57]).

Plane waves are characterized by field vectors (E, H) and propagation direction vector (k) as described in Figure.6.6.

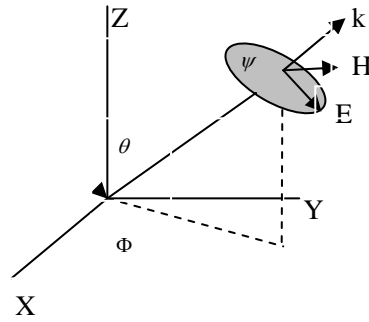


Figure 6.6 Vectors of the plane wave

According to [57], among all the plane waves, only 12 specified plane waves have the most important effects to the power absorption of the animals while other effects are negligible. Thus, averaged value over the 12 simulations is another way to determining SEFR.

Among all the plane waves, only 12 specified plane waves (with four on E polarization, four on H polarization and four on k polarization) have the most important effects to the power absorption of the animals while others' effects are negligible (Table 6.1)

Plane wave number	label	θ°	ϕ°	ψ°
E-polarization	1	90	0	0
	2	90	90	0
	3	90	180	0
	4	90	270	0
H-polarization	5	90	0	90
	6	90	90	90
	7	90	180	90
	8	90	270	90
k-polarization	9	0	0	0
	10	0	0	90
	11	180	0	0
	12	180	0	90

Table 6.1 Specified plane wave for animal exposure

6.2.3 Measurement in the loaded RC

Field intensity is measured with tri-axis probe. The antenna factor K and its uncertainties are:

Axe 1: 48.52 dB

Axe 2: 42.35 dB

Proposition of an hybrid design and realization approach to characterize the field in RC

Axe 3: 42.78 dB

RC is loaded with four 375 g IEC equivalent liquid ([48]) of 2450MHz. Measurement setups are exactly the same as for the exposition experiment (excitation of the antennas, rotation of the stirrers, etc).

Measurements have been made on both of the two stages of the plastic supporter. For each stage of the supporter, one region of $40cm \times 20cm$ has been allocated into $8 \times 5 = 40$ cells. Each cell takes the dimension of $5 \times 4 = 20cm$. The measurement probe is placed in the centre of the chosen cells.

For different configurations, totally 26 points (distance $> 5cm$ to avoid the correlation) are measured as shown in Figure.6.7.

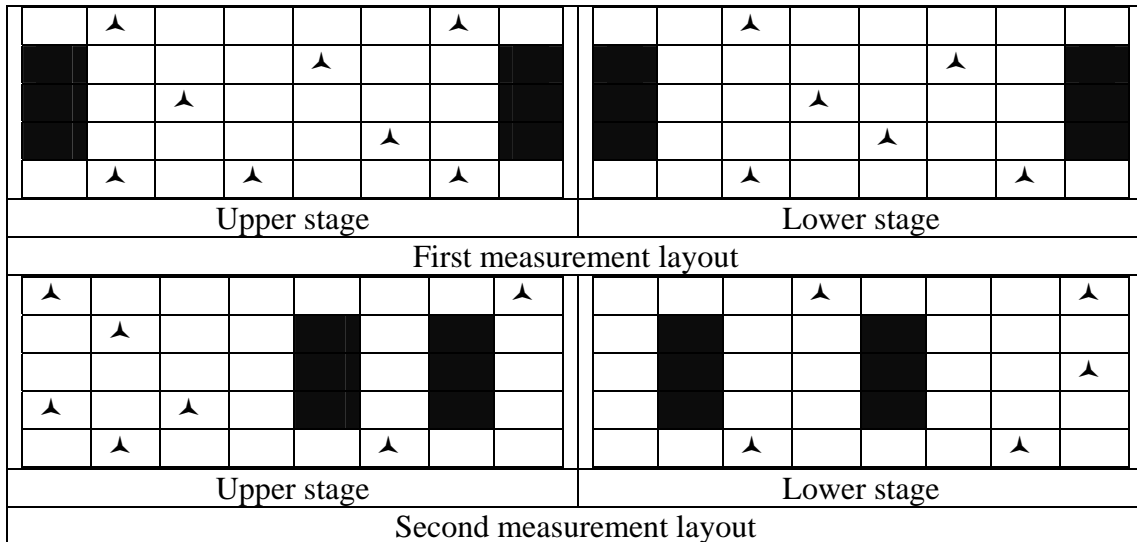


Figure.6.7 E field strength measurement points

In it, cells in black are the position of the IEC equivalent liquid, ▲ is the position of the measurement points. One real measurement layout is shown in Figure.6.8.

Proposition of an hybrid design and realization approach to characterize the field in RC

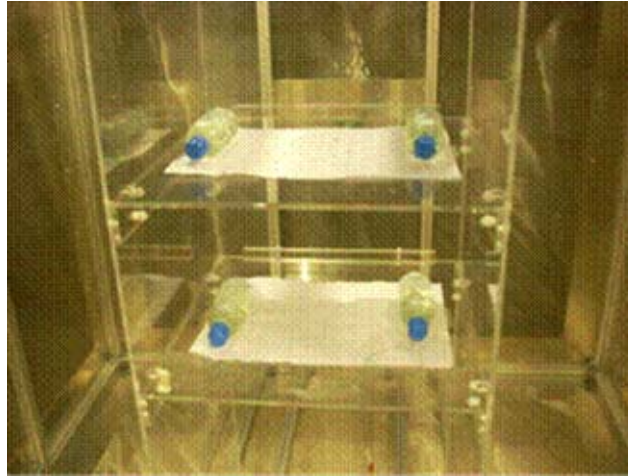


Figure 6.8 Measurement layout

Averaged E field strength is 24.5V/m with 100mW net CW input power to the antennas. Results are shown in Figure 6.9.

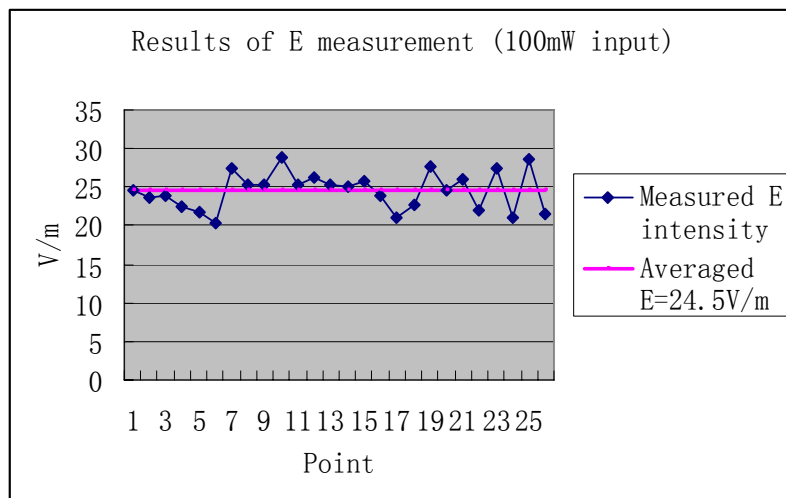


Figure 6.9 Measurement results

The E field measurement assures that the 24.5 V/m (100mW net incident power) can be

obtained in the RC. The ratio $\frac{P_{inc}}{\langle E^2 \rangle} = 1.6660 \times 10^{-4}$.

If 225 V/m is needed to guarantee 4 W/kg while body averaged SAR in the four animals, by calculation, about 8.5W is need for the incidence of the antenna. The system can achieve up to 70% efficiency.

6.3.Simulations with animals models and results

Purpose of the system is to generate homogenous exposure for 4 single/group rats with minimum WBSAR as 4 W/kg. There are two prescriptions in the experiments: sufficient dose is only one aspect, the uniform exposure should also be evaluated for different positions. The basic configuration of the experiments rules the similar WBSAR for 4 rats on various positions should be satisfied.

The digital rat model developed by Brooks Air Force Laboratory [58] (Figure 6.10) is used in this work.

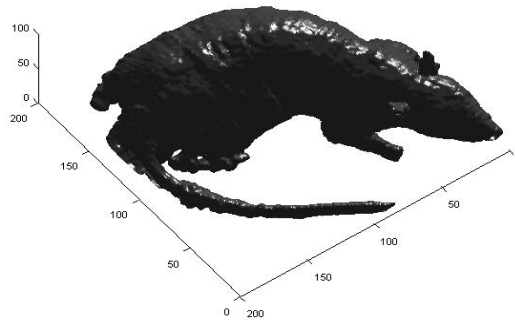


Figure 6.10 Rat numerical model

The model has resolution of 0.827mm and is composed of 36 different tissues/ organs. The weight of the rat is about 374g. So four rats weight 1496 g in total. Anatomic image of simulation model can refer to Figure 6.11.

Proposition of an hybrid design and realization approach to characterize the field in RC

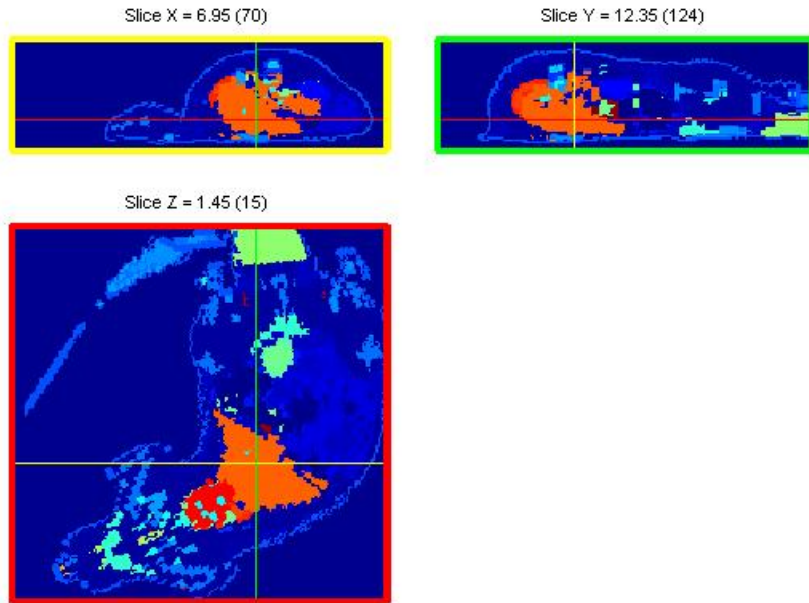
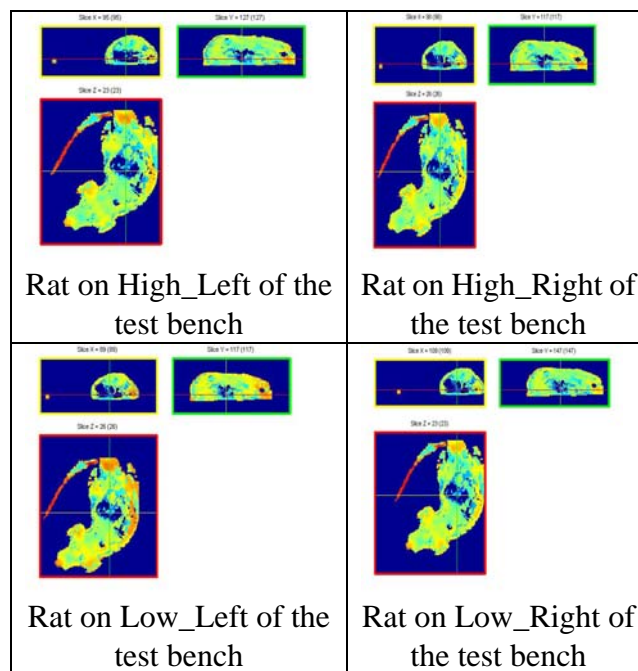


Figure 6.11 Anatomic image of the heterogeneous rat model

Power partition among 4 rats was analyzed in term of WBSAR. Simulations have been performed with RMPWM (resolution of 1mm) and DMPWM (resolution of 2mm)

Power absorption for the four rats on the different positions of the test bench is displayed by Figure 6.12 (RMPWM 2mm resolution)



Proposition of an hybrid design and realization approach to characterize the field in RC

Figure 6.12 Power distribution in the 4 rats by RMPWM

Reference $\langle E \rangle = 3.45 \text{ v/m}$, Resolution 2 mm, Different photos of rats represent 4 rats in different plastic boxes of the test bench.

Different methods of SAR have been calculated in the four rats as shown in Table 6.2.

No. of rats	1	2	3	4	Mean
WBSAR (W/Kg)	9.6e-4	9.8e-4	9.5e-4	9.8e-4	9.7e-4
$\frac{\overline{WBSAR} - \overline{WBSAR}}{\overline{WBSAR}}$	-0.7%	1.2%	1.9%	1.3%	/
SAR_peak	1.2e-2	1.4e-2	1.4e-3	1.3e-3	1.3e-3
$\frac{\overline{SAR_pk} - \overline{SAR_pk}}{\overline{SAR_pk}}$	-9.3%	6.3%	4.1%	-1.9%	/
SARMAX 1g cube	3.0e-3	3.2e-3	3.4e-3	2.8e-3	3.1e-3
$\frac{\overline{SAR_cube} - \overline{SAR_cube}}{\overline{SAR_cube}}$	-3.1%	3.4%	9.9%	-9.5%	/

Table 6.2 Variation of different SAR in 4 rats

\overline{WBSAR} , $\overline{SAR_peak}$ and $\overline{SAR_cube}$ are defined as the averaged value based on those of the 4 rats in the simulation

By comparison, the same configuration has been repeated by DMPWM as displayed in Figure 6.13 and Table 6.3.

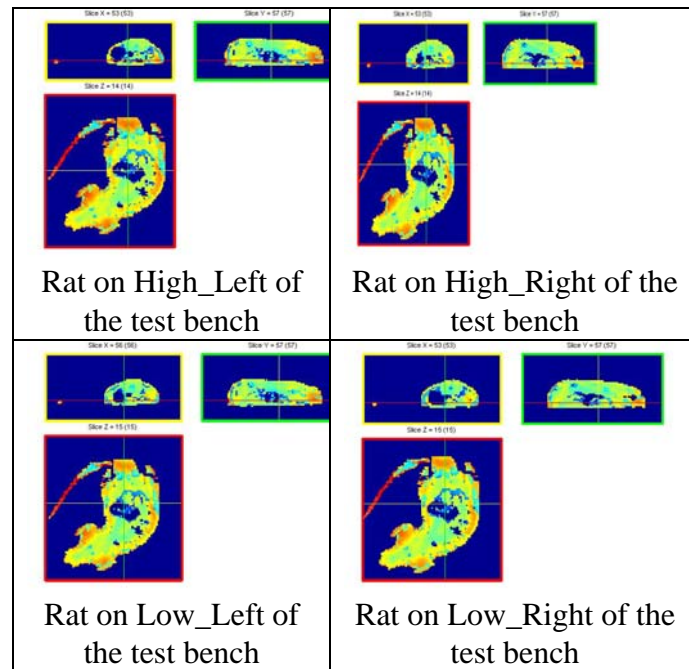


Figure.6.13 Power distribution in the 4 rats by RMPWM

Reference $\langle E \rangle = 0.963 \text{ v/m}$ Resolution 2mm Different photos of rats represent 4 rats in

Proposition of an hybrid design and realization approach to characterize the field in RC

different plastic boxes of the test bench.

No. of rats	1	2	3	4	Mean
WBSAR (W/Kg)	7.1e-5	7.7e-5	7.1e-5	7.7e-5	7.2e-5
$\frac{WBSAR - \overline{WBSAR}}{\overline{WBSAR}}$	-1.2%	6.3%	-2.2%	-2.2%	/
SAR_peak	1.1e-3	9.6e-4	1.1e-3	1.0e-3	1.0e-3
$\frac{SAR_pk - \overline{SAR_pk}}{\overline{SAR_pk}}$	4.0%	-7.6%	2.1%	0.1%	/
SARMAX 1g cube	2.7e-4	3.2e-4	3.1e-4	2.4e-4	3.1e-4
$\frac{SAR_cube - \overline{SAR_cube}}{\overline{SAR_cube}}$	-5.6%	11.9%	9.8%	-16.1%	/

Table 6.3 Different SAR by DMPWM

The same volume is re-meshed by resolution 1mm. By 20 simulations based on RMPWM, results are shown Figure 6.14 and Table 6.4.

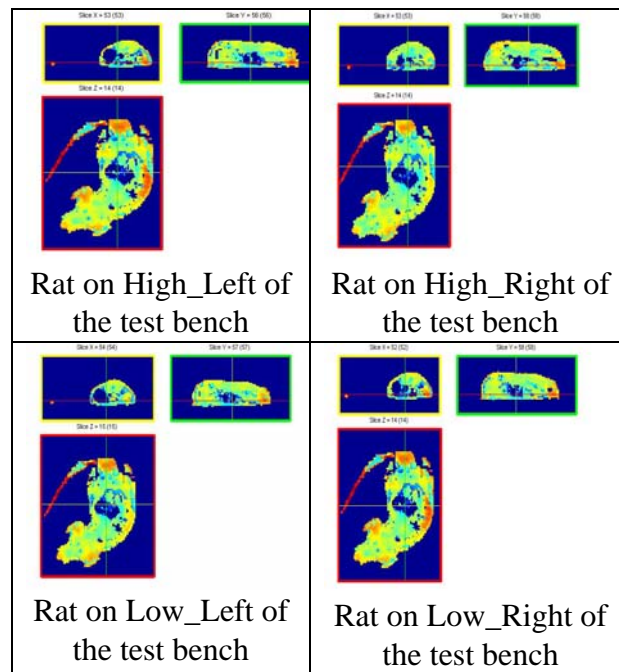


Figure.6.14 Power distribution in the 4 rats by RMPWM

Reference $\langle E \rangle = 3.376 \text{v/m}$, Resolution 1mm, Different photos of rats represent 4 rats in different plastic boxes of the test bench

Proposition of an hybrid design and realization approach to characterize the field in RC

No. of rats	1	2	3	4	Mean
WBSAR (W/Kg)	8.8e-4	8.8e-4	8.9e-4	8.6e-4	8.8e-4
$\frac{WBSAR - \overline{WBSAR}}{WBSAR}$	0.3%	0.3%	1.4%	-2.1%	/
SAR_peak	1.8e-2	2.1e-2	2.0e-2	1.5e-2	1.9e-2
$\frac{SAR_pk - \overline{SAR_pk}}{SAR_pk}$	-2.5%	13.7%	8.3%	-18.8%	/
SARMAX 1g cube	2.7e-3	3.2e-3	3.2e-3	2.4e-3	2.9e-3
$\frac{SAR_cube - \overline{SAR_cube}}{SAR_cube}$	-5.6%	11.9%	9.8%	-16.1%	/

Table 6.4 Different SAR by RMPWM (resolution: 1mm)

Absorbed power over mass (WBSAR), peak SAR and maximum SAR over 1 g cube have been calculated for all the rats in these three cases. The different SARs have been normalized by $\langle E^2 \rangle$ obtained from each simulation. Comparisons with standard deviations are shown in Figure.6.15.

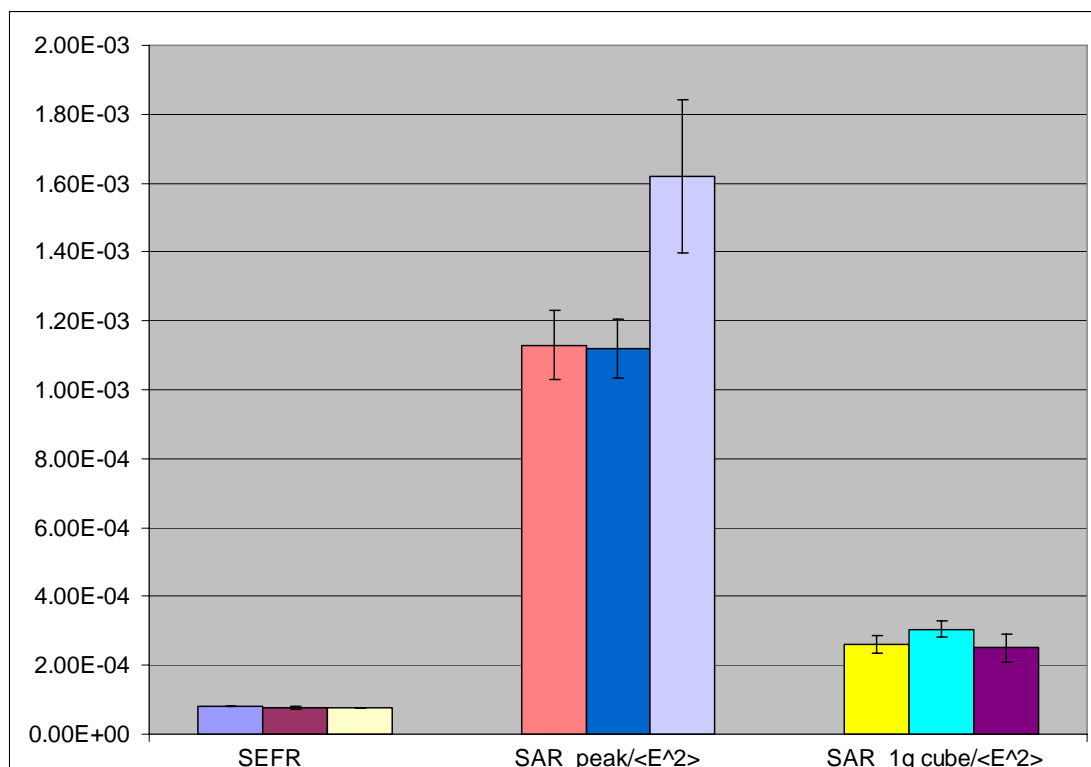


Figure 6.15 Comparison in terms of different SAR for three simulation configuration

For each SAR comparison, the first bar is from the RMPWM of 2mm resolution, the second is from DMPWM of 2mm whist the last bar is the from RMPWM of 1mm.

Proposition of an hybrid design and realization approach to characterize the field in RC

Results show, normalized WBSAR and normalized 1g cube tissue averaged SAR in all the configurations vary 4% and 10% respectively. Similar exposure result can be well observed for all the four rats in the simulation. Variation of the resolution will not influence the whole body averaged SAR. The peak SAR increases substantially when the resolution changes from 2 mm to 1 mm.

6.4.SAR assessment for tissue/organ specified SAR

By different methods of simulation, desired homogenous exposure is achieved for the rats in different positions of the test bench. The difference of WBSAR for all the rats range to maximum 4%. The peak SAR can vary up to 20% of the mean value. As estimated and proved, similar whole body averaged SAR can not necessarily assure similar specified organ/tissue power absorption. Hot spots can be well observed at the junction of the torso and the tail, the tail, acme of the head, end of the limbs and the stretch part of the torso. Power partition in both the methods with resolution of 1mm and 2 mm is very similar and no abnormal hot pots existing besides the previous stating parts. If several organs are chosen for comparison cross methods and resolution, the deviation to the whole body averaged SAR can be generalized in Figure 6.16.

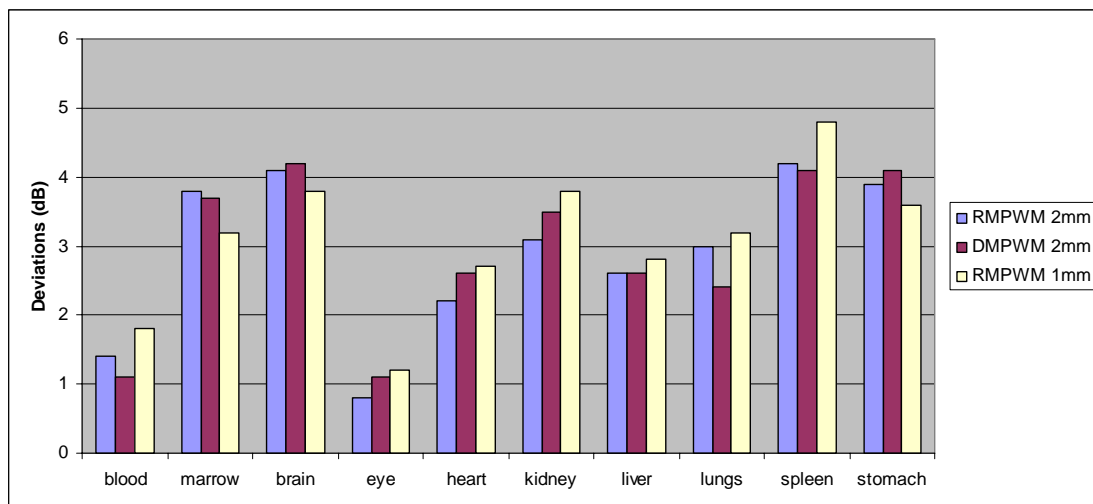


Figure 6.16 Deviation of SAR for 10 chosen organs to WBSAR

6.5.Conclusion

Neither pure simulation nor measurement method can successfully characterize field distribution in RC. Hybrid simulation and measurement is applied to the analysis of the exposure results. The relation of incident power to WBSAR is determined by $\langle E^2 \rangle$.

Proposition of an hybrid design and realization approach to characterize the field in RC

Simulation-measurement hybrid method proves that the desired target WBSAR is obtainable.

Detailed discussions about the exposure in different growth period time and configurations should be supplied in order to evaluate all the possible results. For the animal *in vivo* exposure system, variation of the result is also one of the most important aspects for animal EMF exposure assessment.

7. WBSAR assessment

7.1.Objective

Previous results have determined the relationship between the net incident power to RC and WBSAR for the given standard and simplest case (four identical adult rats in RC, no physical variation among individuals and uniform field distribution in the test volume). Nevertheless, as a long term experiment, one single rat model with the same fixed configuration can not reflect the entire exposure period.

Dielectric properties, mass and size of rats vary substantially during lifespan and the power absorption (so as WBSAR) changes with the growth of the size. Since in previous simulations, different numerical models should be used for small rat models at different ages need to be realized for simulation.

3 small rats are designed to live in the same plastic box with their mother. The mother rat would be taken out when the total weight exceed the limit for each container of 375 g. Three small rats would then live alone in the boxes. Exposure should continue for 5-6 weeks after birth. Four identical EM lossless containers are kept on the test bench during the whole experiment process.

In practical animal non-restrained experiment, rats have the ability to move, to take any postures they intend and to approach to his peers at ease. Numerous configurations will bring out different exposure possibilities. Analysis and discussions of results with some example (representative) configurations in this part will help to clarify the variation researches in part 8.

7.2.Rat models in simulation and measurement

7.2.1 Numerical model of different ages

The dielectric properties of tissues and therefore the power absorbed depend on tissues. The contour of the animals also plays an important role in power absorption and reflection (thus important to power absorption of his adjacent animals). Because of that, it is fundamental for simulation to have relevant numerical model at each exposure phase.

The simplest rat numerical models at different ages can be obtained by proportionally reduced (scaled) adult model. However, growth process can not be coarsely and proportionally minimized from the adult rat due to different development rates of each part. One feasible and simple method to construct rat numerical models is the modified model based on the reduced adult models.

7.2.1.1 Realization of the scaled models

Rat numerical models of different ages are approximately achieved by spheres with various diameters in abdomen of adult, equivalent cylinder+sphere shape homogeneous models and homogeneous/heterogeneous rat models of different sizes.

Due to limits of computation resolution as well as immature structure of the embryo and new-born phases, stratified structures and specified organs are not realized for the entire embryo and new-born periods. Instead, homogenous spheres and cylinder-spherical models are applied for these periods (Figure 7.1). For rats with length larger than 6 cm, the proportionally reduced adult models (scaled models) are realized according to different weights (Figure 7.2). Their weight roughly associates with the specific ages of rats in exposure experiment.

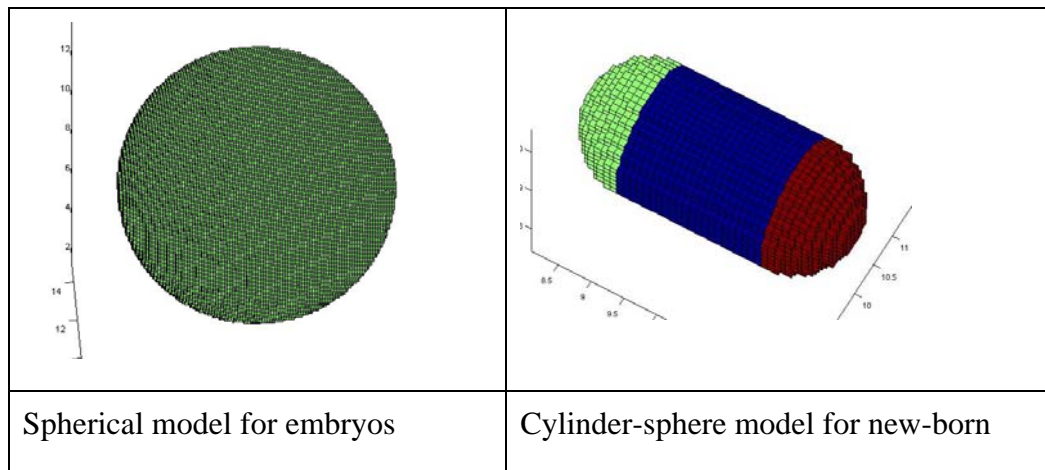
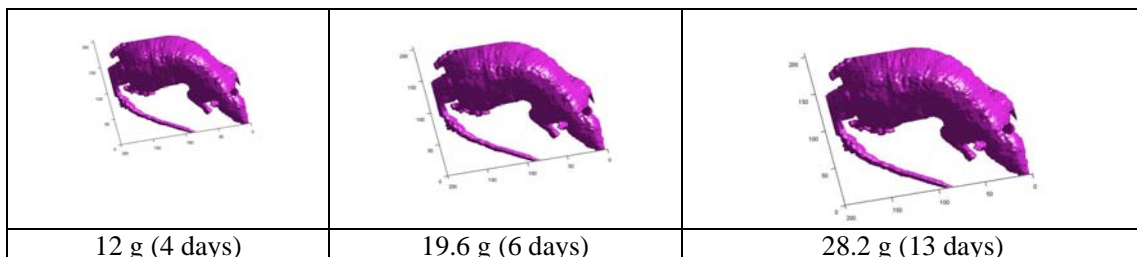


Figure.7.1 Approximate homogeneous model for embryos and new-born



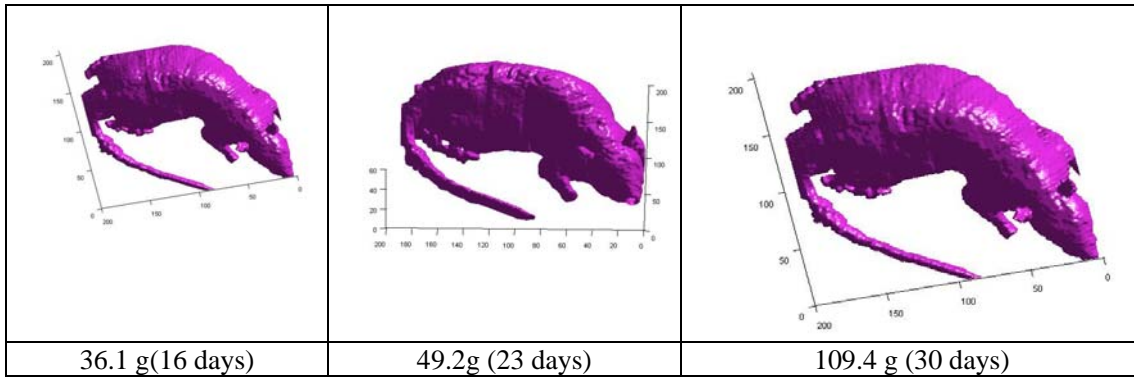


Figure 7.2 Scaled numerical models for rats at different ages

7.2.1.2 Modification for the scaled numerical models

There are two drawbacks for the scaled rat models. First, they can not well describe the rats of all the ages. Although weigh of model can be adjusted as exact the same as the animal in experiments, power absorption may change due to different sizes of the special body. Second, scaled model can not be directly linked to the time after birth if no measured information is available. Therefore, little information can be obtained for daily WBSAR evolution during the experiment.

The scaled models should be modified by measured data in order to be much similar to the animals in exposure.

Key parameters of animals are defined as:

L1: Length from the neck to the junction part of the body and the tail

L2: Length from the nose to the neck









L3: Width of the body

L4: Length of the tail

These five parameters can determine one rat model with length of the major parts as well as the width. Studies with heterogeneous rat model [57] have demonstrated that the dimensions of tail and head would play the most important roles in term of power absorption. With the five parameters (weight inclusive), these key dimensions are well presented. So the homogeneous numerical model can be well constructed. One series of rats used in exposure experiment are sacrificed and conserved by express freezing. Pictures of the rats are shown in Figure 7.3 for reference to modify numerical models.



Figure 7.3 Frozen rat sample for different ages

	
4 hours after birth	4 days after birth
	
6 days after birth	9 days after birth
	
13 days after birth	16 days after birth
	
20 days after birth	23 days after birth

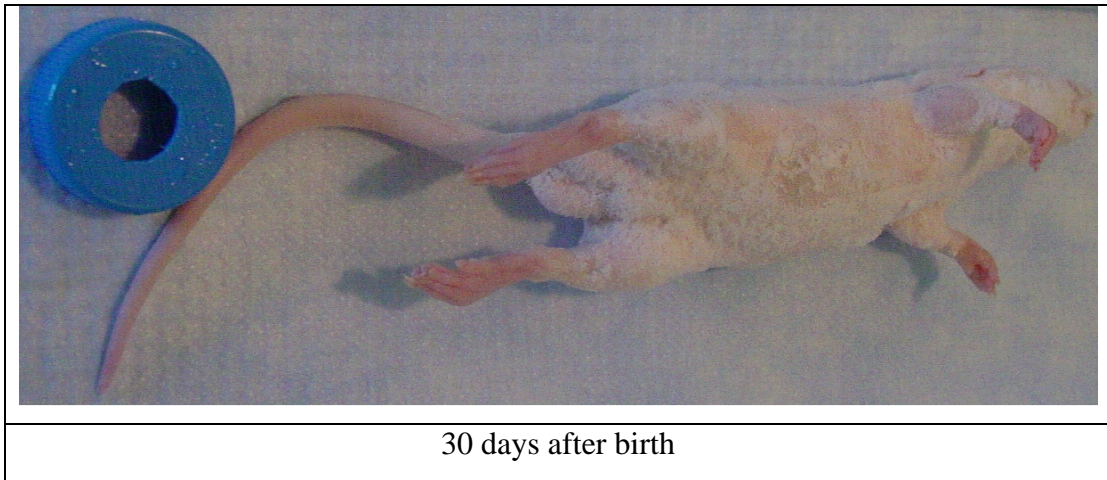


Figure 7.4 Rats for different ages

Data about the mentioned parameters are measured and displayed in Figure.7.5 and 7.6.

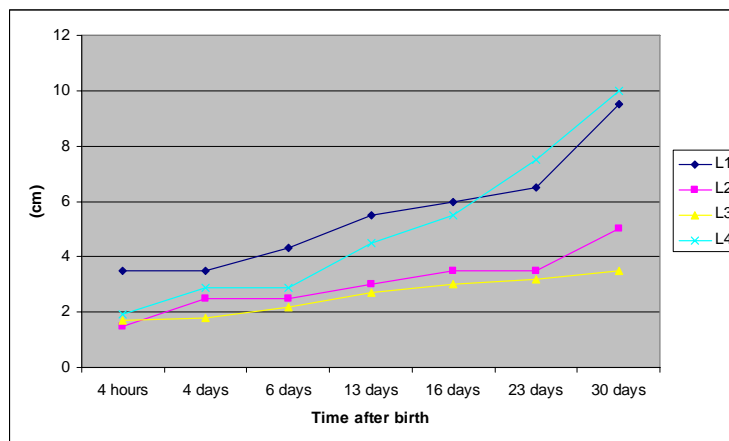


Figure.7.5 Parameters of the rat's length vs. age

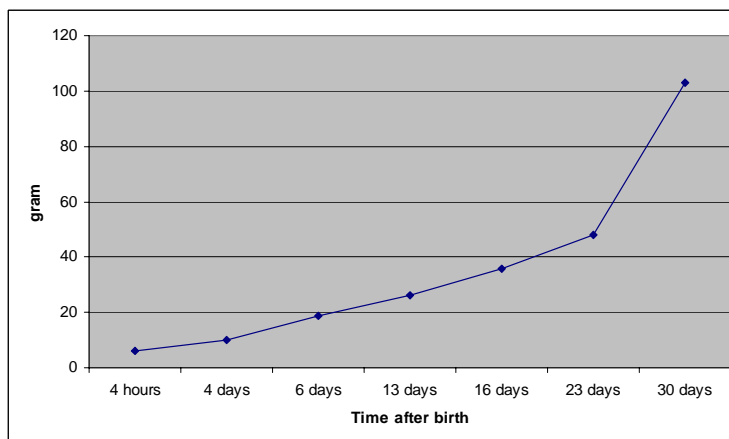


Figure 7.6 Evolution of the rat's weight

From the above information, we conclude that growth of the rat is featured by rapid growth of body after birth. Length of head after birth increase less rapid than body. Length ratio of head to body decreases. Tail increases steadily but it is always shorter than the length of the body plus head. Simply scaled models would bring to important difference with the measured data from animals, which are shown in Figure 7.7.

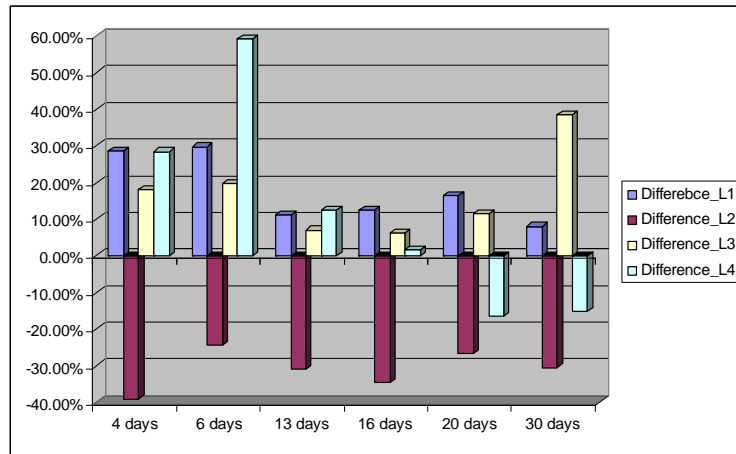


Figure 7.7 Difference between scaled model and measured data

Scaled models were adjusted (dilate or reduce proportionally) to have the same weight with the animals under measurement. Difference is calculated for example:

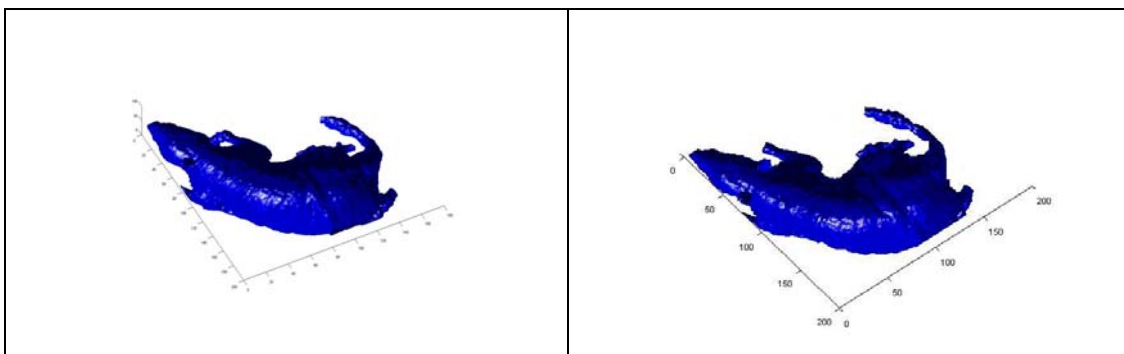
$$Difference_L1 = \frac{(L1_simp - L1_mea)}{L1_mea} \times 100\%$$

Where,

$L1_simp$: L1 value obtained from simple scaled model

$L1_mea$: L1 value obtained from measured data

Morphing technology [61] should be adopted to modify the scaled models. Results of modified scaled models are shown in Figure 7.8.



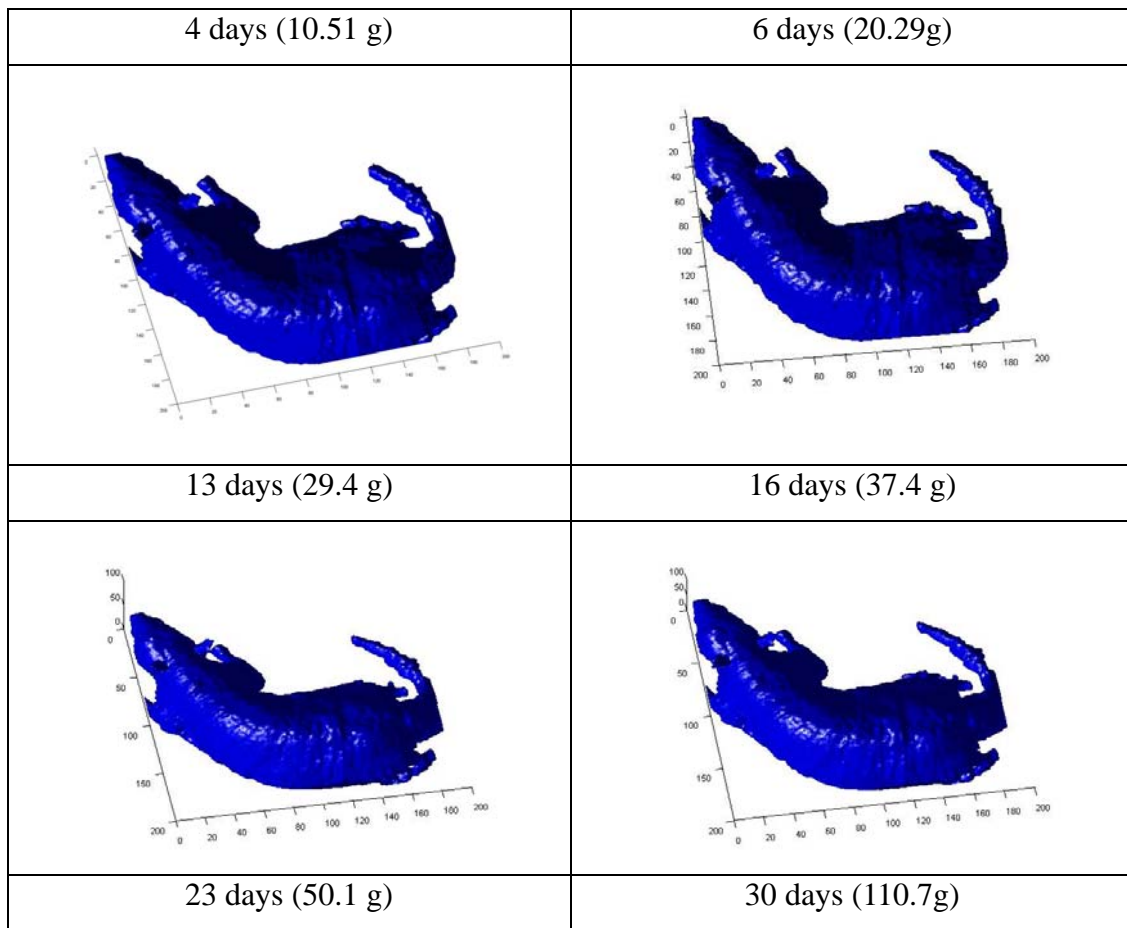


Figure 7.8 Modified numerical model of rat at different ages

Difference between the measured data and the modified models (Figure. 7.8) are shown in Figure.7.9.

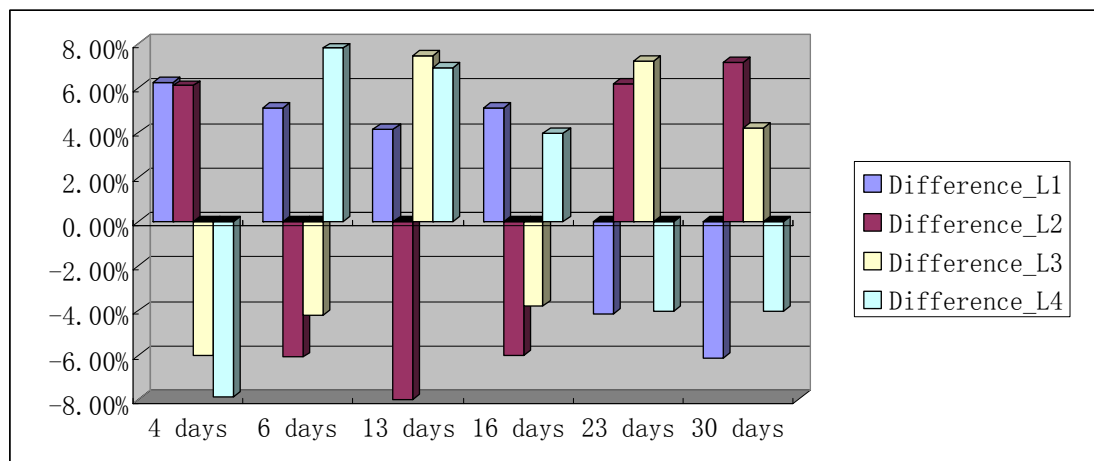


Figure.7.9 Difference between the measured data and modified data

Less than 8% difference with the measured data for all the key parameters at all development phases has been achieved by the modified models. Modified rat model can better present the animal in exposure than scaled models.

If we compare the differences between scaled model and modified scaled model in one figure, we can find the significant difference as in Figure. 7.10.

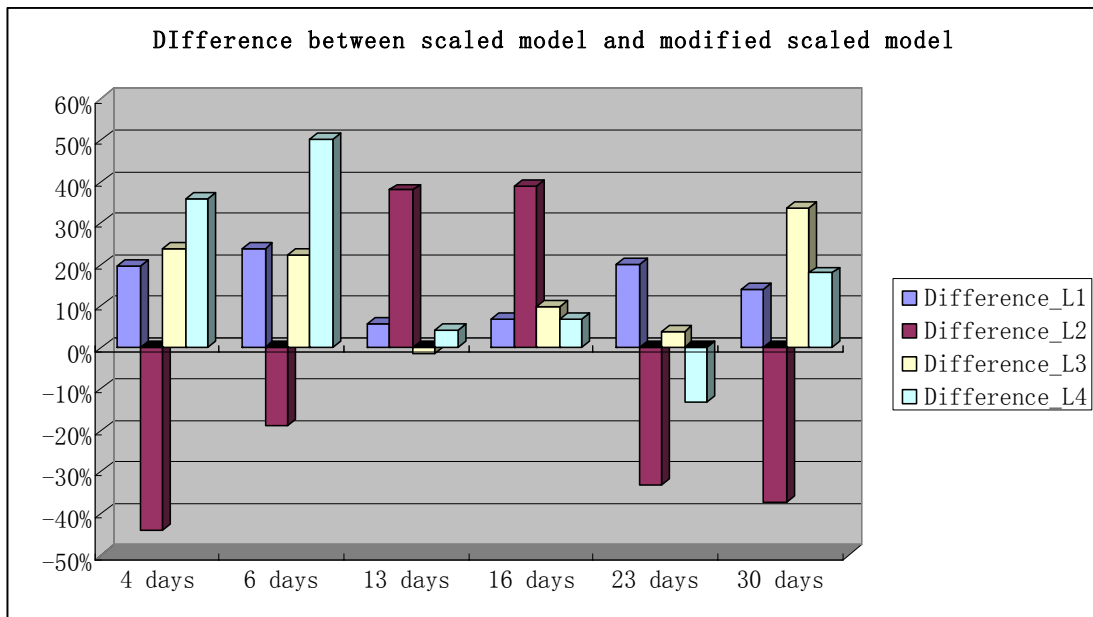


Figure.7.10 Difference between scaled model and modified scaled model for four key parameters (weight keeps the same)

7.2.2 Positions of the loads in measurement

By definition, 375 g mass is the standard weight for rats in every experimental container. In all previous measurements and simulations, the field strength in RC is characterized by 1500 g (4x375g) load. During exposure with the small rats, actual weight could be far less than 375 g (such as new-born). The insufficient weight must be compensated by IEC human tissue equivalent liquid or loads.

One ambiguity need to be clarified is the position of the loads. For example, 1000 g equivalent liquid could be placed into two 500 g bottle shams or forty bottle shams of 25 g. What is the difference between them? Where and how to place the load? Which points should be used for measurement? These questions need to be answered by measurement to see whether the insertion of the load will influence the field strength distribution in RC.

Following experiments are carried out on different configurations of loads which are displayed in Table 7.1:

- (1) E measurement with $4 \times 375g$ equivalent liquid shams without any extra load. This is also the standard configuration in the simulation when characterizing field distribution.
- (2) E measurement with $4 \times 150g$ equivalent liquid plus 3 bottles of 300 g equivalent liquid.
- (3) E measurement with $4 \times 150g$ equivalent liquid shams plus 4 bottles of 100 g equivalent liquid+ $10 \times 50g$ bottles. All the loads are put in bundles at one corner of the test bench.
- (4) E measurement with $4 \times 150g$ equivalent liquid plus 4 bottles of 100 g equivalent liquid+ $4 \times 50g$ bottles. Loads are distributed uniformly at four corners of the test bench.

Bottles	375 g	300 g	150 g	100 g	50 g	Total weight
1	4 (shams)	/	/	/	/	1.5 kg
2	/	3(shams)	4(loads)	/	/	1.5 kg
3	/	/	4(shams)	4(loads)	10(loads)	1.5 kg
4	/	/	4(shams)	4(loads)	10(loads)	1.5 kg

Table 7.2 Configuration of the different measurement

12 points on the bottom stage of the test bench are measured for the different configurations (stirrers and excitation antennas operate the same as in the exposure experiment).

At each point, E is measured with 3-axis probe connected with the spectral analyzer. All the measurement configurations are the same as for the field measurement.

For the first configuration, no load is applied. Four shams are placed on the two stages of the test bench uniformly. In the second experiment, two loads are placed

on the first stage (bottom stage) of the test bench at position LOAD_1 and LOAD_4 (refer to Figure 7.11). The other load is placed on the corner of the second stage (top stage) of test bench. In the third configuration, all the loads are place on the first stage of the test bench at position LOAD_1. For the fourth configuration, four 100 g loads are placed on first stage at position of LOAD_1 and LOAD_3 respectively. Two 50 g loads are placed on position LOAD_2 and three 50 g loads are placed on position LOAD_4. So all the other rest loads are well distributed to the corner of the test bench at second stage.

LOAD_1	X		X			X	LOAD_3
				X			
X			X				X
				X			
LOAD_2	X		X		X	X	LOAD_4

X: position to place the measurement probe

LOAD_X: position to place the loads. X=1, 2, 3, 4

Black block: position of the loads

Figure 7.11 Schema for different load configurations on the bottom stage of the test bench

Field measurement has been done on 12 points on the first stage of the test bench to see the variation as Table 7.3.

	Configuration1	Configuration2	Configuration3	Configuration4
<E> (v/m)	24.22	24.03	24.74	24.42
Standard deviation (v/m)	0.72	0.97	0.99	0.47

Table.7.3 Results of the measurement of different configuration

Results show,

- When total weight keeps the same, there is little difference between 4 standard shams without loads and 4 small shams with loads in term of $\langle E \rangle$. It means, measured $\langle E^2 \rangle$ with four 375 g standard shams is applicable to the case of small animals with loads (if only the total weight is the same).
- Much balanced layout for load will produce less standard deviation of E field. It means the field distribution is much uniform and with less measurement points, we can achieve one satisfactory $\langle E \rangle$.

7.2.3 Dielectric parameters for the small rat models

Conductivity and permittivity of rodent animals over extensive frequency domain have been studied [61]. Water content varies throughout lifetime of the animals. For example, water content in the brain of the mice can decrease about 10% from birth to the adult period. Peyman *et al.* [61] have demonstrated that the dielectric properties change with aging process of the rat. Variation of relative permittivity and conductivity has been shown for several chosen tissues as brain, skull and skin. Relative permittivity and conductivity decrease steadily with ages.

Whole body averaged relative permittivity for adult rat heterogeneous model is 40.4 with conductivity 1.7 S/m. Both these two parameters fall within $\pm 9\%$ of dielectric parameters for human head tissue equivalent liquid prescribed by IEC ([49]) at 2450MHz. If these dielectric properties are adopted as the baseline for about 70 days after birth (In fact, dielectric properties change less drastic after 30 days), the whole body averaged relative permittivity and the conductivity of the rats from 0 days to 30 days can be interpolated with the presented given tissues.

	4 hours after birth	4 days after birth	6 days after birth	13 days after birth
Relative permittivity	61	60	59	56
Conductivity	2.1	2.05	1.9	1.85
	16 days after birth	23 days after birth	30 days after birth	
Relative	54	48	Heterogeneous	

permittivity			model
Conductivity	1.8	1.78	

Table 7.4 Dielectric properties applied in the simulation

In order to verify the validity of the dielectric properties schema for the homogeneous model, two experiments have been performed.

(1) Homogeneous model vs. heterogeneous model

Homogeneous model of 30 days has been compared with the same length but heterogeneous one. Both the two models are exposed with the same RMPWM configuration. Results are compared and shown that there is 5% difference in term of WBSAR between the homogeneous and heterogeneous models of 30 days. It demonstrates that homogeneous models can be expected to well represent the heterogeneous models.

(2) Change of the dielectric properties

Gabriel *et al* 2005 ([62]) has pointed out, at 900 MHz, if homogeneous rat model is exposed with plane wave incident on an infinite half space, increase of ϵ' , σ or both of them by 15% will produce less influence on 1 g (10g) averaged SAR and peak SAR. We performed the similar simulations with RMPWM at resolution of 1 mm at 2450 MHz. Results are shown in Table 7.5.

Variation in dielectric properties	SEFR	ϵ'	σ
Standard	2.08e-4	48	1.78
$\epsilon' + 20\%$	2.00e-4	58	1.78
$\sigma + 20\%$	2.10e-4	48	2.1
$\epsilon' + 20\%$ and $\sigma + 20\%$	1.99e-4	58	2.1

Table 7.5 SEFR for different dielectric properties configurations ($\langle E \rangle = 225V/m$)

It means, actually, change of dielectric properties play an insignificant role on the SEFR (and so forth, on WBSAR if $\langle E \rangle$ is stable). Even if the dielectric properties that we applied in simulation is not the precise representation of the practical animal condition, WBSAR would be unlikely influenced.

7.2.4 Resonance length of the rat's model

Power absorption of the rats could be irregularly high if size of the model reaches the resonance length. So power absorption at resonance length should be studied to evaluate the maximum potential case. At 2450 MHz, the wavelength is around 12.2 mm. Half wavelength is about 6 cm, which falls into the range of lengths of the rat numerical model.

In order to eliminate the aspects that could influence the results, the rat model are simulated by cylinders and spheres with total length of 4 cm, 5 cm, 6 cm, 7 cm, 8 cm, 10 cm, 12 cm, 15 cm and 18 cm. Torsos of the rats can be represented by cylinder with capsules on two ends. Thus the results are helpful in analyzing the situation for real rats. The configurations of the cylinders are displayed in Figure 7.12 and Table 7.6.

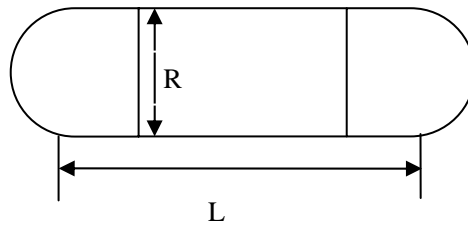


Figure 7.12 Parameters of the cylinder

Length	R (cm)	L (cm)	Surface (cm^2)	Weight (g)	Weight/surface (g/cm^2)
4cm	1	2	9.4	2.18	0.23
5.1cm	1.3	2.5	14.73	4.25	0.29
6cm	1.5	3	21.21	7.35	0.35
7.1cm	1.8	3.5	28.87	11.68	0.40
8cm	2	4	37.70	17.43	0.46
10cm	2.5	5	58.91	34.04	0.58
12cm	3	6	84.83	58.82	0.69
15.1cm	3.8	7.5	132.55	114.88	0.87
18cm	4.5	9	190.88	198.51	1.04

Table 7.6 Parameters for different cylinders

In order to standardize the results, WBSAR normalized per surface area (which represents at high frequency the ability of power absorption for unit surface) is calculated for all the cases shown in Figure.7.13:

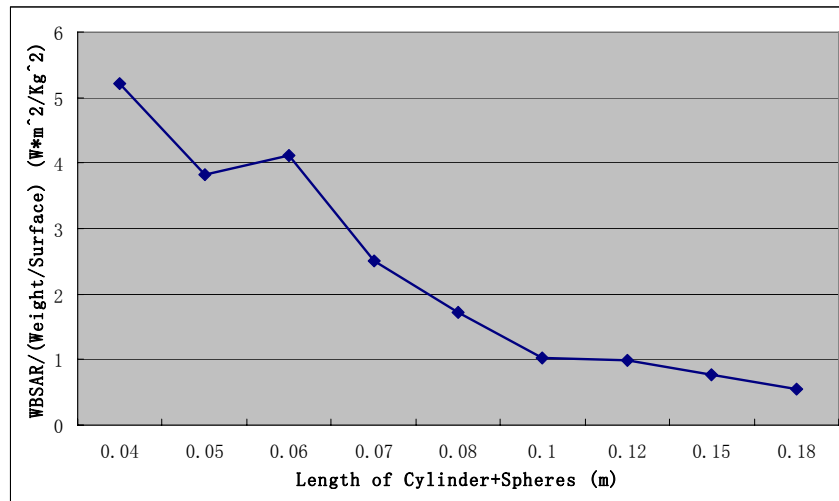


Figure 7.13 WBSAR normalized by surface area on function of the length of cylinder+spheres models

The curve shows that peak of WBSAR per surface occurs at the length of 4 cm. Power absorption per surface decrease with the dilation of the cylinder volume. One abnormal peak appears at length of 6 cm. specifically, if we calculate the ratio of WBSAR over the ratio of weight to surface (WBSAR/ (weight/surface)), we can get Figure. 7.14.

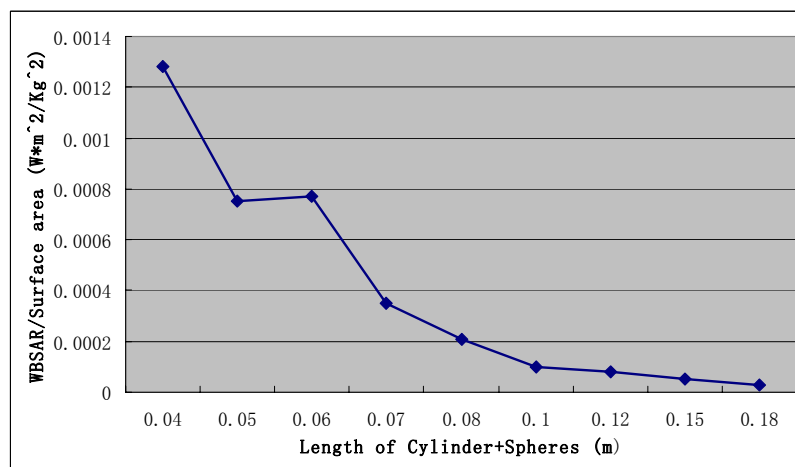


Figure 7.14 WBSAR normalized by weight to surface area on function of the length of cylinder+spheres models

It demonstrates that at the length of 6 cm, model has the capability to absorb much power. In growth period of rats, 6 cm length corresponds to about 4th day after birth. The maximum per surface power absorption might be expected at this point. This result would help us to explain and predict some maximum absorption cases in the following researches.

7.3.WBSAR vs. single rat of different ages

With all the above preparations, WBSAR for the simplest configuration-single small rat could be determined.

From results of measurement in the real loaded RC, $\langle E \rangle = 220-230$ v/m is obtained. Different numerical rat models should be placed in the same environment to evaluate results of exposure.

If the above modified scaled models are radiated with 225 V/m E field in the RC, the achieved WBSAR are listed in Figure 7.15 ($\langle E \rangle = 225$ V/m).

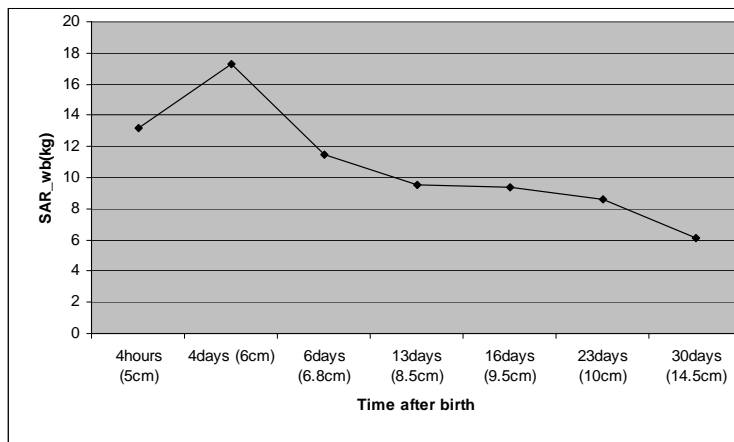


Figure 7.15 WBSAR at $\langle E \rangle = 225$ V/m on function of the length of rats

Similarly, if 4 W/kg WBSAR is desired for the entire modified model, one curve can be observed in Figure 7.16.

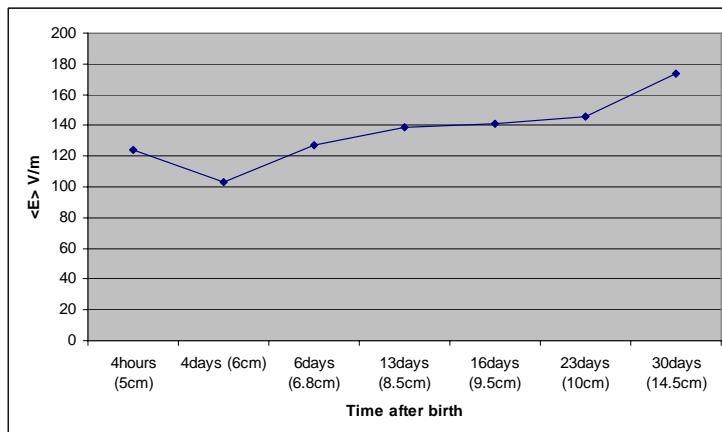


Figure 7.16 Necessary E level to achieve 4 W/kg for rats of different length

7.4.WBSAR vs. rats group

In exposure experiments, 3 small rats live with or without their mother in one container. Three small rats in one closed group without mother is one possible and frequently occurred configuration for exposure experiment.

Animal numerical models for the simulation are displayed in Figure 7.17.

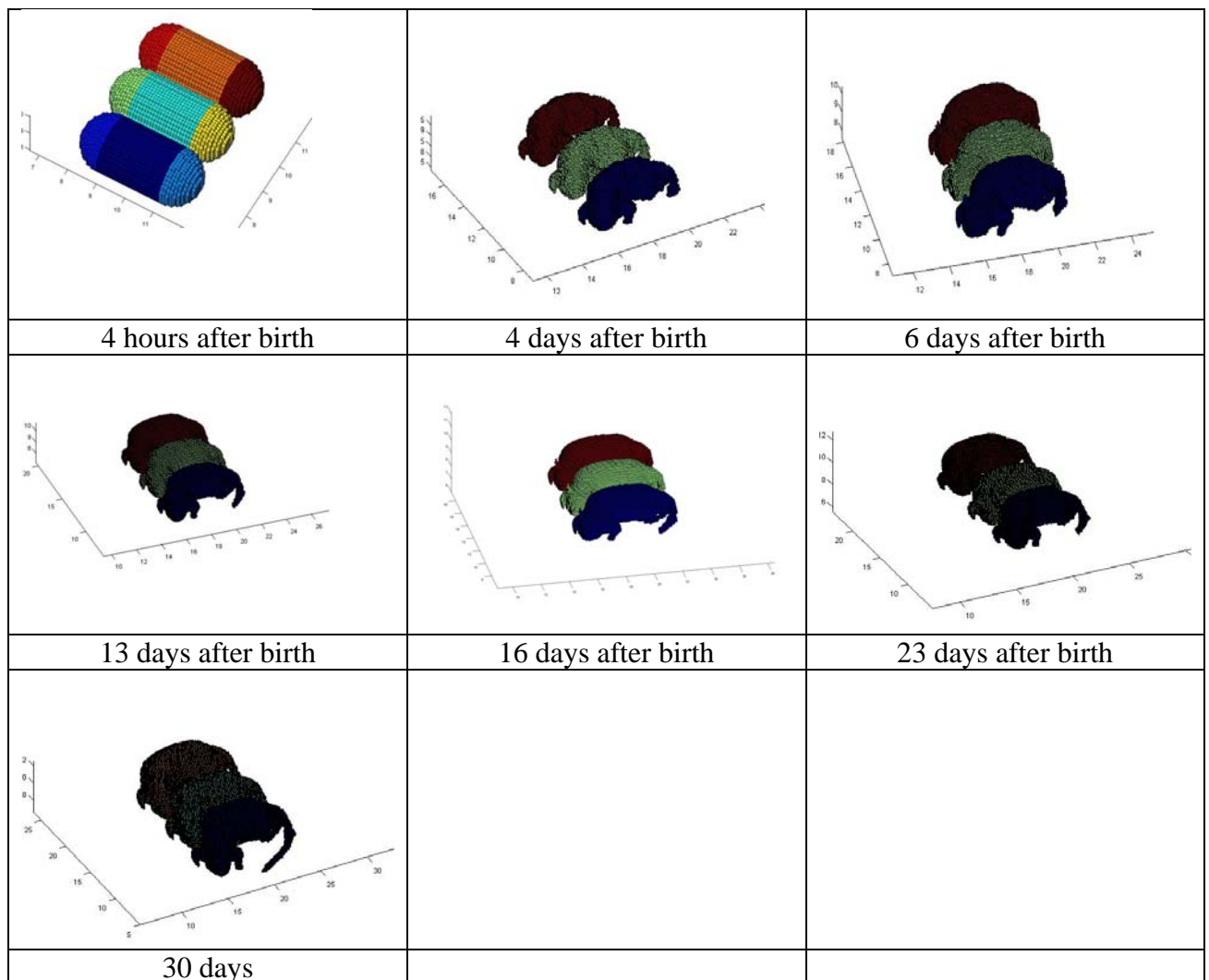


Figure 7.17 Numerical models for animals group

For this kind of configuration, central rat is covered by other rats on both sides. Its surface exposed to the radiation is the minimum among all 3-rat configurations. It is expected to absorb least power in the situation.

By RMPWM, WBSAR is calculated for different rat's models. The expected WBSAR for the rat group is shown in Figure 7.18 and Figure 7.19.

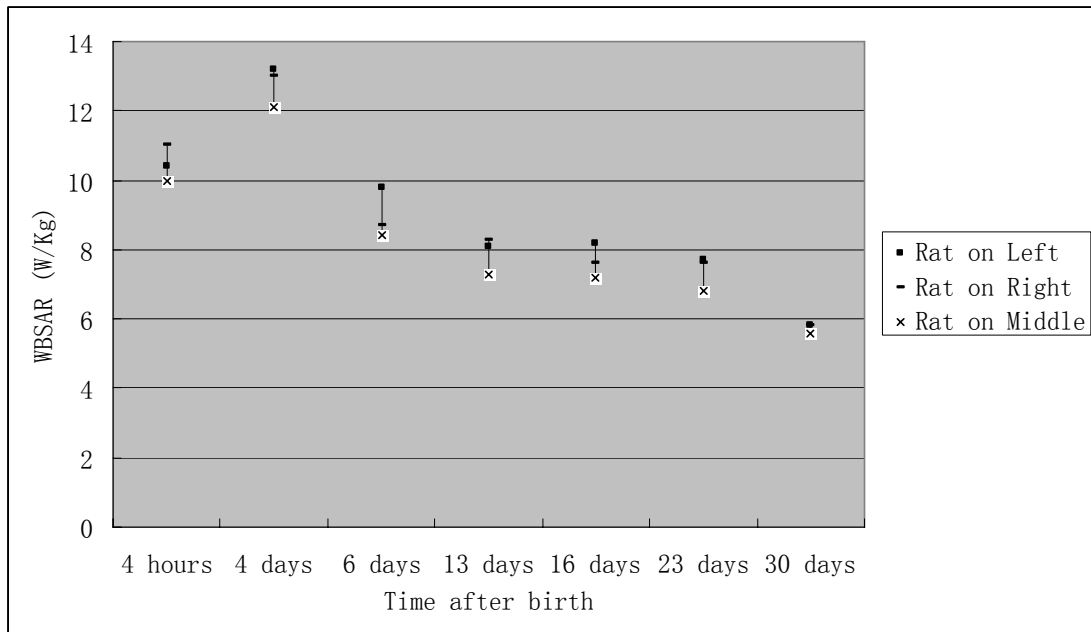


Figure 7.18 Expected WBSAR for rat group at $\langle E \rangle = 225 \text{ V/m}$

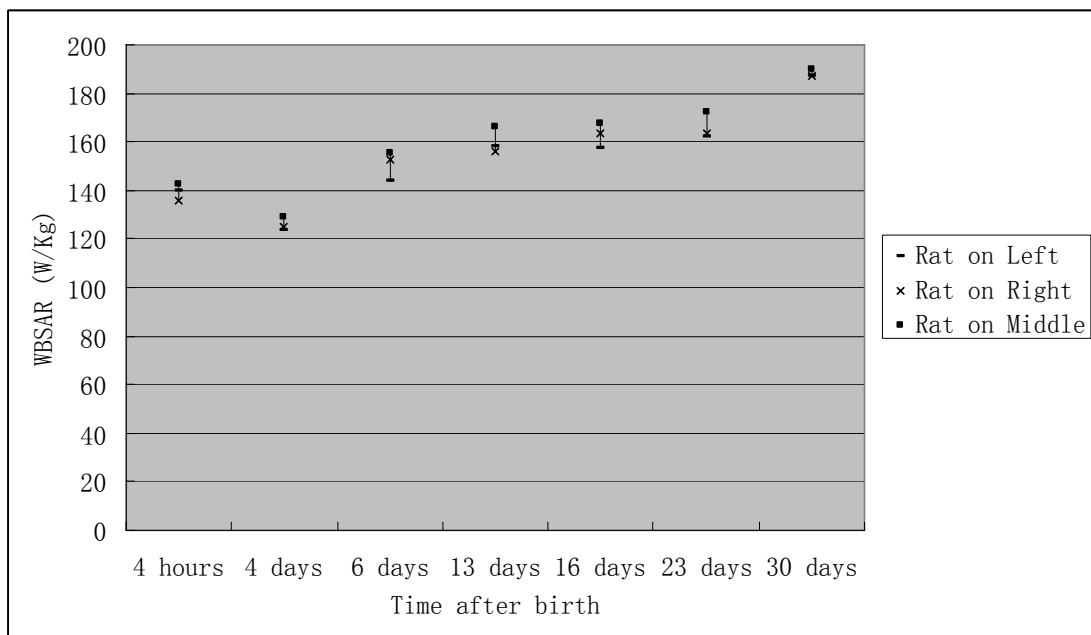


Figure 7.19 Target $\langle E \rangle$ for 4 w/kg whole body averaged SAR vs. time after birth

Thus, the difference of WBSAR for single (7.3) and group (7.4) rats can be concluded by Figure 7.20. Generally, the difference of WBSAR for the two configurations ranges from 20% to 25%.

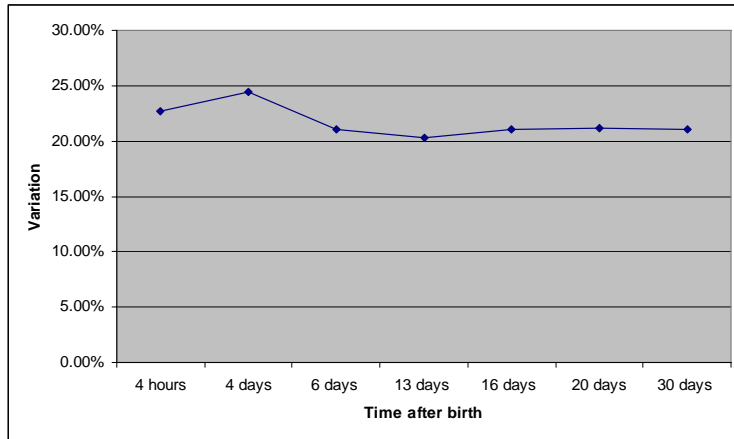


Figure 7.20 WBSAR variations between the single rat and rat group configuration

Conclusion: Influence by adjacent rats will induce lower exposure for the rat which is most likely to be covered by the other animals. Rat with resonance length can experience the maximal WBSAR if other conditions are the same. It inspires us that for the rat in the centre of the group and furthermore covered by the adult rat, it would potentially have less absorption surface and thus the minimal WBSAR can be expected.

In the above discussions, single animal configuration and animals in group configurations have been well presented. We will consequently research on the group with adult configuration to complete the study of the long term exposure result.

7.5.WBSAR vs. most frequent occurred animal configurations

7.3 and 7.4 have discussed two frequently occurred configurations: single rat and small rats in group without adult. In practical exposure configurations, three apparently different phases need to be discussed distinctively. By camera observation, rats tend to take some frequently occurred configurations. These frequently occurred configurations depend on the time after birth as Figure 7.21:

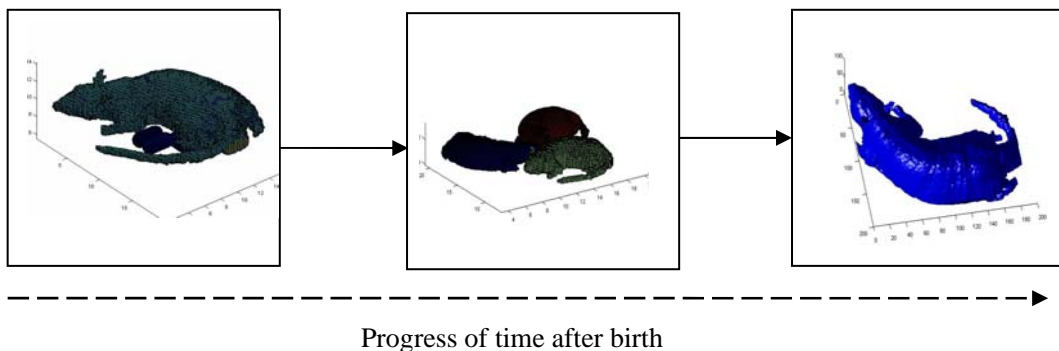


Figure 7.21 Most-likely happened relative positions

WBSAR assessment

Once born, three small rats form one group and are covered by adult during 0 to 6 days. Small rats can still incline to be in one group but will gradually acquire the independence and mobility at the end of the experiment. Adult would be taken out when the total weight overpasses the 375 g limit for each container. These configurations can be used in simulation to decide the most possible WBSAR for one general view of the exposure results.

Gestation period

Experiments start at embryo period. Exposure model is realized by the adult rat with several solid spheres in abdomen. Several key parameters of the embryo could be obtained by anatomic studies: they are diameters of the embryos, distance between the embryo and the skin of the adult and number of the embryos.

One pregnant adult is anatomized for analysis. It is the adult rat with 20-day pregnancy (just before birth). The embryos locate with 1.5 mm to the abdomen skin as shown in Figure 7.22.

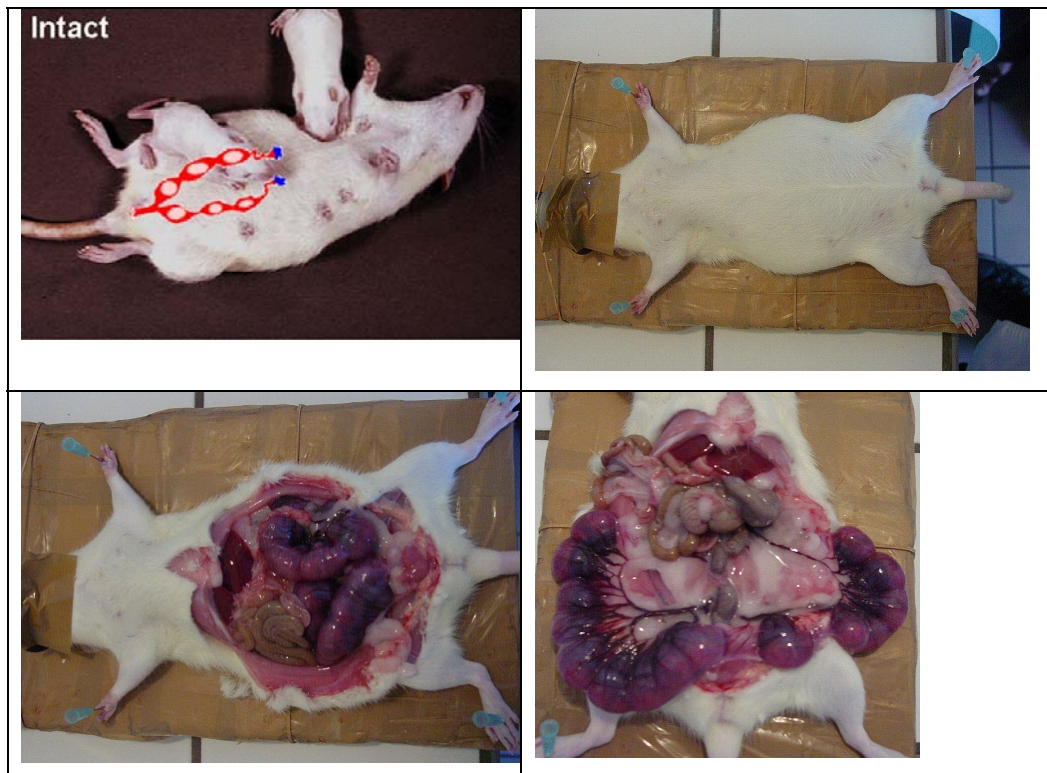


Figure 7.22 Position of the embryos

There can be as dozens of embryos in one ovary. Figure 7.23 shows ovaries which compose 10 and 6 embryos. To standardize the simulation, six embryos are realized for the ovary. Three embryos are on each side.



Figure 7.23 Layout of ovary

Embryo is covered by amniotic liquid. Size of the embryo is measured for purpose of numerical models. Figure 7.24 shows the different sizes of the embryo.

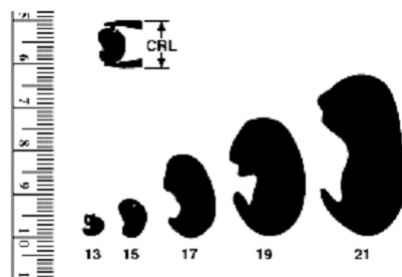


Figure 7.24 Size of the embryo*

* <http://www.taconic.com/wmspage.cfm?parm1=473>

Baby groups with mother

Once born, three babies are chosen for exposure experiment. Statistically, the baby rats seldom leave their mother. They tend to approach together and form the cluster with the coverage of their mother.

Independent rats group

When the total weight is over 375 g for one container, the mother rat is taken out. Only 3 small rats are left. Cluster is the favorite position of the rats.

Conclusion:

Configurations and results are introduced for the following experiments.

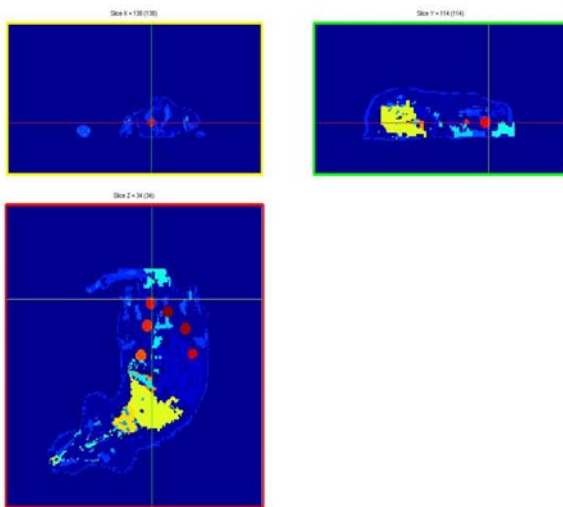


Figure 7.25 Configuration of adult rat with 6 fetuses (0.6 cm in diameter)

Figure 7.25 shows begin of the pregnant phase. There are totally six fetuses in the rats. Fetuses are realized by the sphere of 0.6 cm in diameter. The spheres are filled by homogenous liquid with dielectric parameters as $\epsilon=63$ and $\sigma=2.2$. The fetuses are covered by 1 mm layer of amniotic simulated fluid. Dielectric parameters of this fluid is set as the physiological saline ($\sigma=2.8$, $\epsilon=75$). The pregnant adult rat is realized by 250 g heterogeneous model. WBSAR is calculated in the pregnant rat and the fetuses.

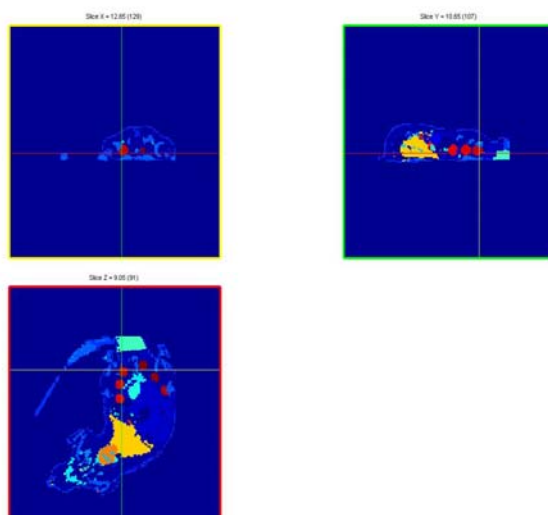


Figure 7.26 Configuration of adult rat with 6 fetuses (1 cm in diameter)

Figure 7.26 shows the progress of the pregnant phase. There are totally six fetuses in abdomen of adult rat. Fetuses are realized by sphere of 1cm in diameter. Spheres are filled by homogenous liquid with dielectric parameters as $\epsilon=63$ and $\sigma=2.2$. Fetuses are covered by 1 mm layer of amniotic fluid. Dielectric parameters of this fluid is set as the physiological saline ($\sigma= 2.8$, $\epsilon=75$). The pregnant adult rat is realized by 250 g heterogeneous model. WBSAR is calculated in the pregnant rat and the fetuses.

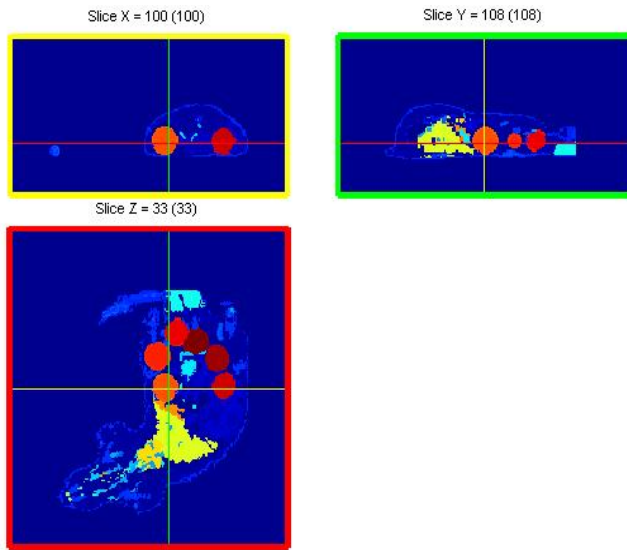
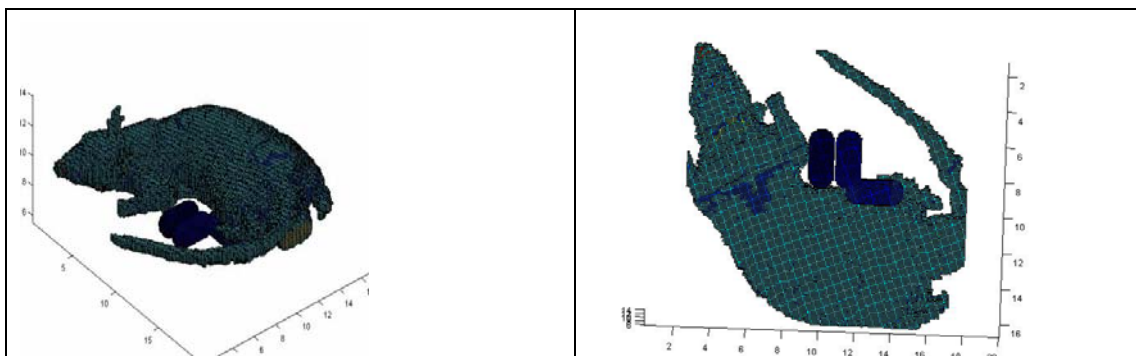


Figure 7.27 Configuration of adult rat with 6 fetuses (2 cm in diameter)

Figure 7.27 shows the end of the pregnant phase. There are totally six fetuses in the rats. Fetuses are realized by the sphere of 2 cm in diameter. The spheres are filled by homogenous liquid with dielectric parameters as $\epsilon=63$ and $\sigma=2.2$. These fetuses are covered by 1 mm layer of amniotic simulated fluid. Dielectric parameters of this fluid is set as the physiological saline ($\sigma= 2.8$, $\epsilon=75$). The pregnant adult rat is realized by 250 g heterogeneous model. WBSAR is calculated in the pregnant rat and the fetuses.



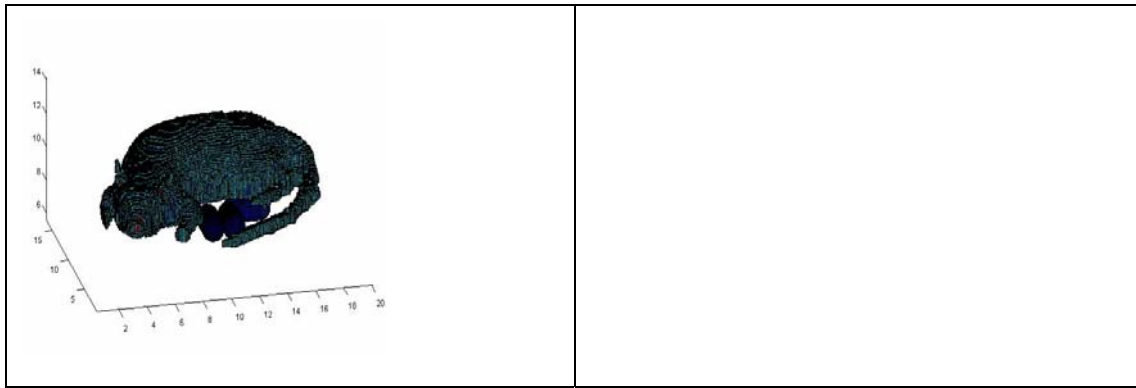


Figure 7.28 Configuration of adult rat with 3 babies (4 hours after birth)

Figure 7.28 shows the beginning of the birth. There are totally three new-born rats covered by one adult rat. New-born rats are realized by the cylinder of 4 cm in length. The cylinder are filled by homogenous liquid with dielectric parameters as $\epsilon=61$ and $\sigma=2.1$. The adult rat is realized by 255 g heterogeneous model. WBSAR is calculated in the adult rat and the baby rats.

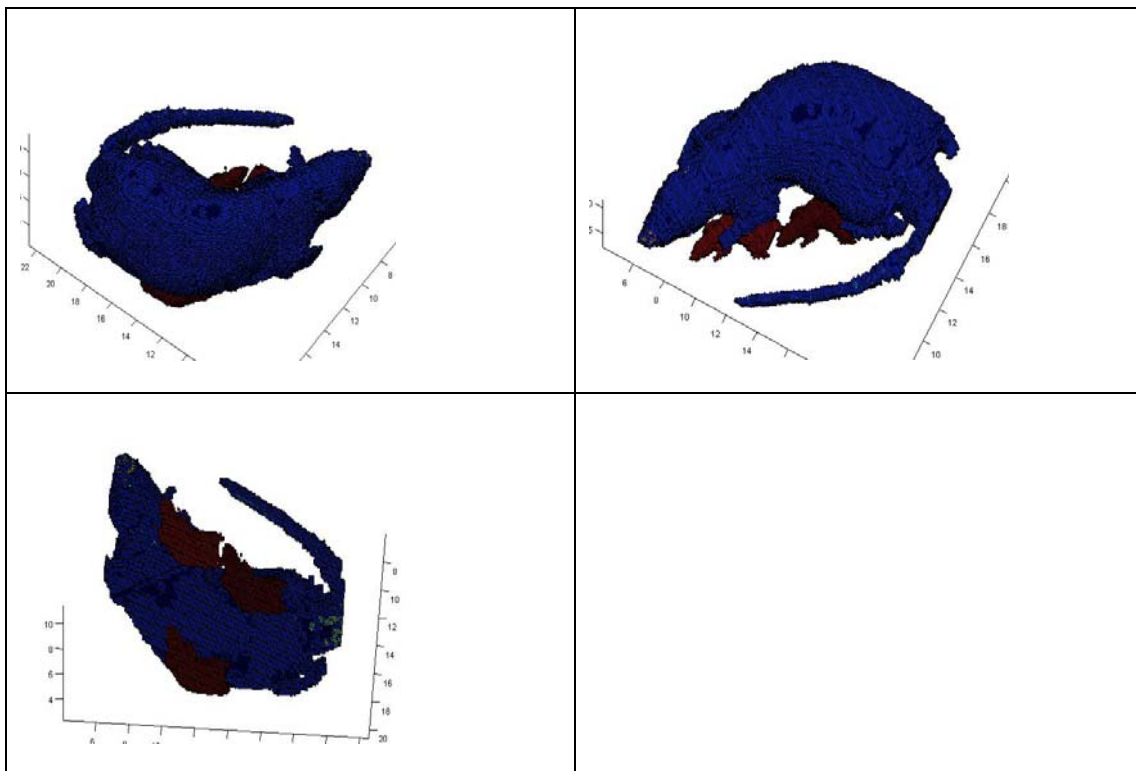


Figure 7.29 Configuration of adult rat with 3 babies (4 days after birth)

Figure 7.29 shows the development of the breeding period. There are totally three babies covered by the adult rat. Babies are realized by the reduced model of 10.51 g in weight. The reduced models are filled by homogenous liquid with dielectric parameters

as $\epsilon=60$ and $\sigma=2.05$. The adult rat is realized by 260 g heterogeneous model. WBSAR is calculated in the adult rat and the baby rats.

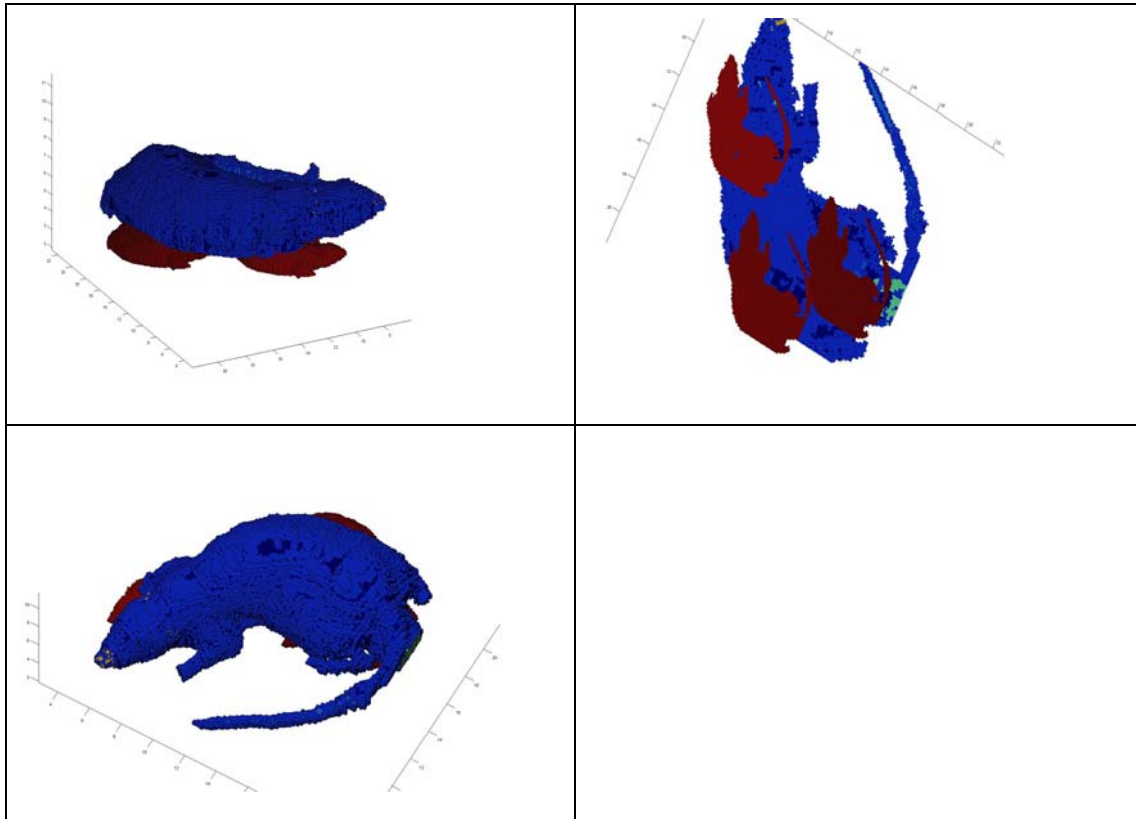
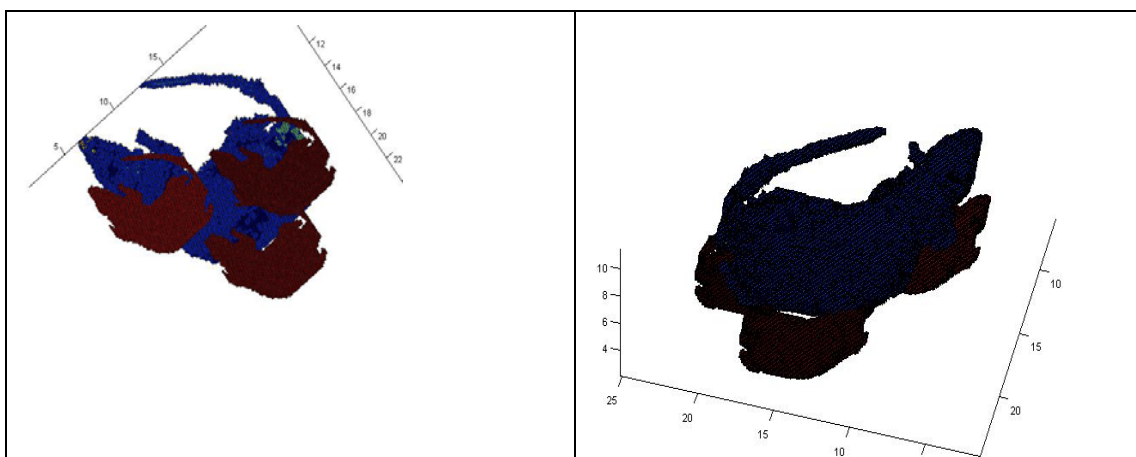


Figure 7.30 Configuration of adult rat with 3 babies (6 days after birth)

Figure 7.30 shows the development of the breeding period. There are totally three babies below the adult rat. Babies are realized by modified scaled model of 20.29 g in weight. The reduced models are filled by homogenous liquid with dielectric parameters as $\epsilon=59$ and $\sigma=1.9$. The adult rat is realized by 260 g heterogeneous model. WBSAR is calculated in the adult rat and baby rats.



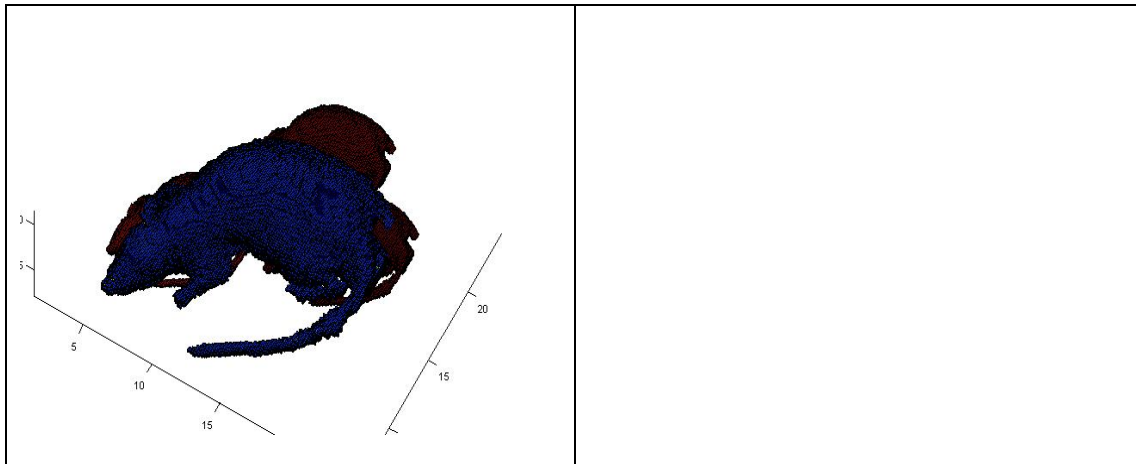


Figure 7.31 Configuration of adult rat with 3 babies (13 days after birth)

Figure 7.31 shows the end of the breeding period. There are totally three babies below the adult rat. Babies are realized by modified scaled model of 29.4 g in weight. The models are filled by homogenous liquid with dielectric parameters as $\epsilon=56$ and $\sigma=1.85$. The adult rat is realized by 260 g heterogeneous model. WBSAR SAR is calculated in adult rat and baby rats.

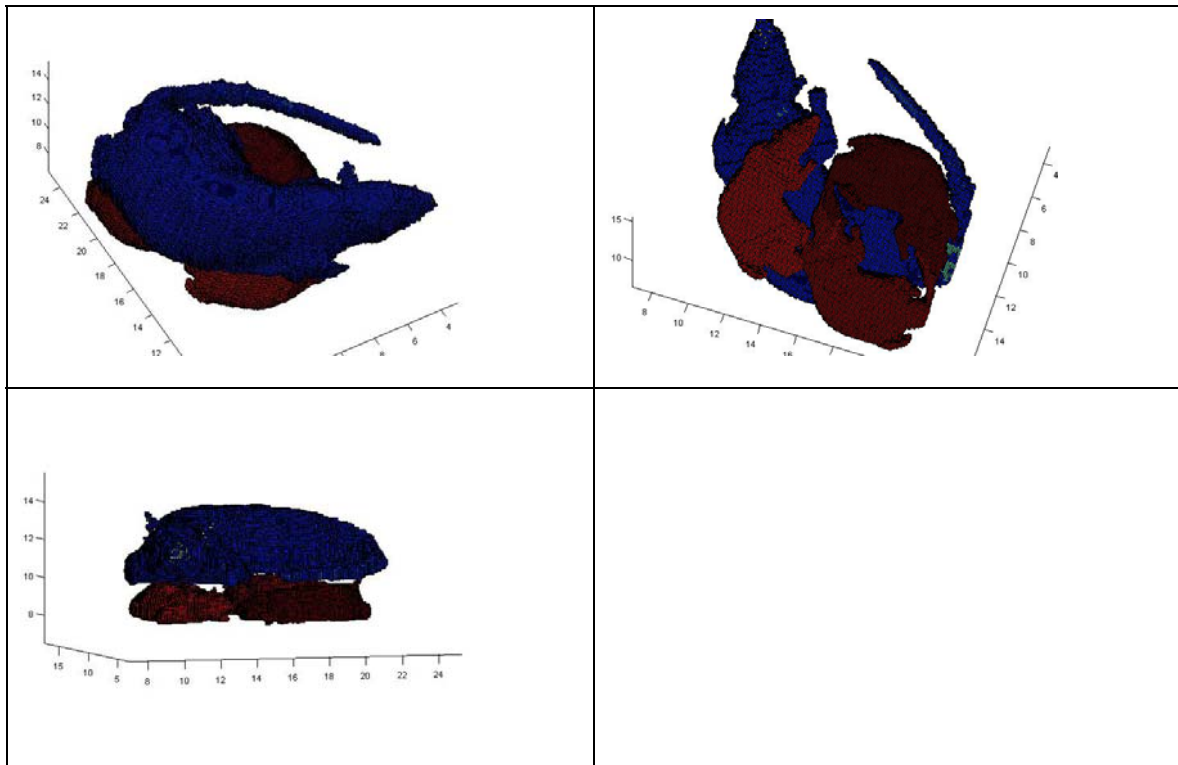


Figure 7.32 Configuration of adult rat with 3 babies (16 days after birth)

Figure 7.32 shows the end of the breeding period. There are totally three babies below the adult rat. Babies are realized by modified scaled model of 37.4g in weight. The models are filled by homogenous liquid with dielectric parameters as $\epsilon=52$ and

WBSAR assessment

$\sigma=1.8$. The adult rat is realized by 260g heterogeneous model. WBSAR is calculated in adult rat and baby rats.

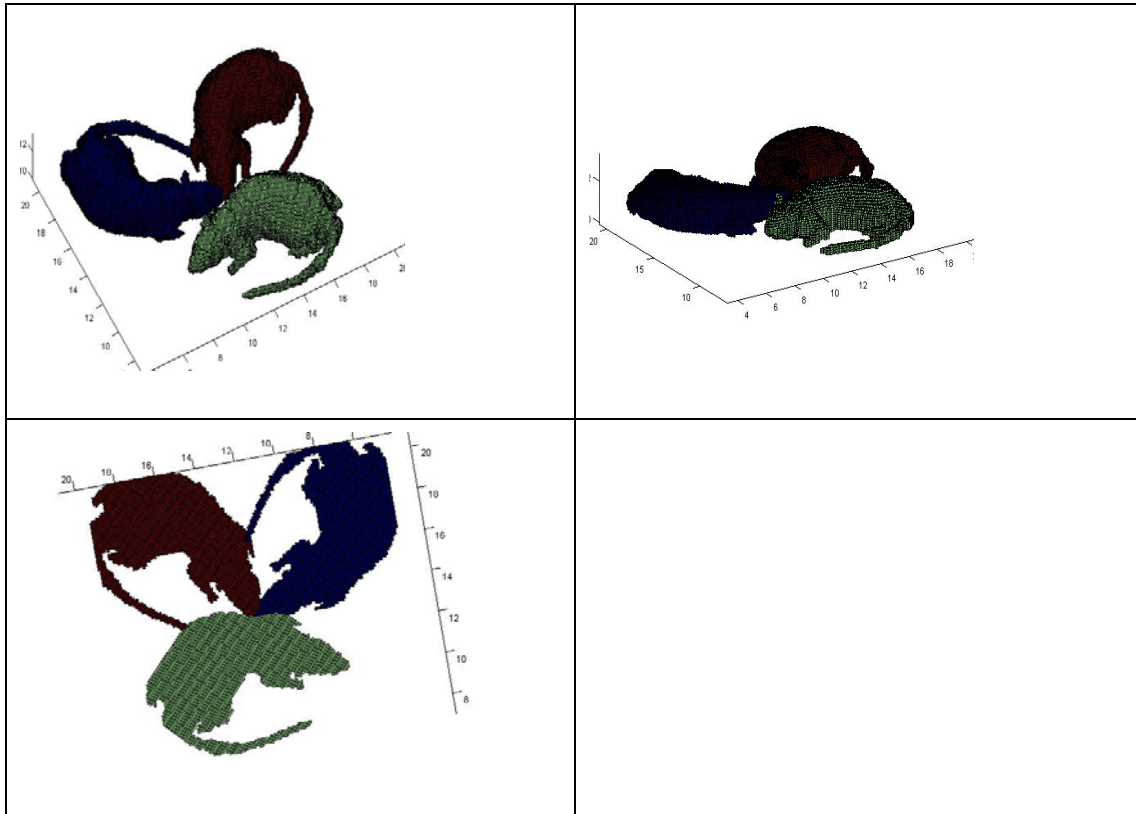
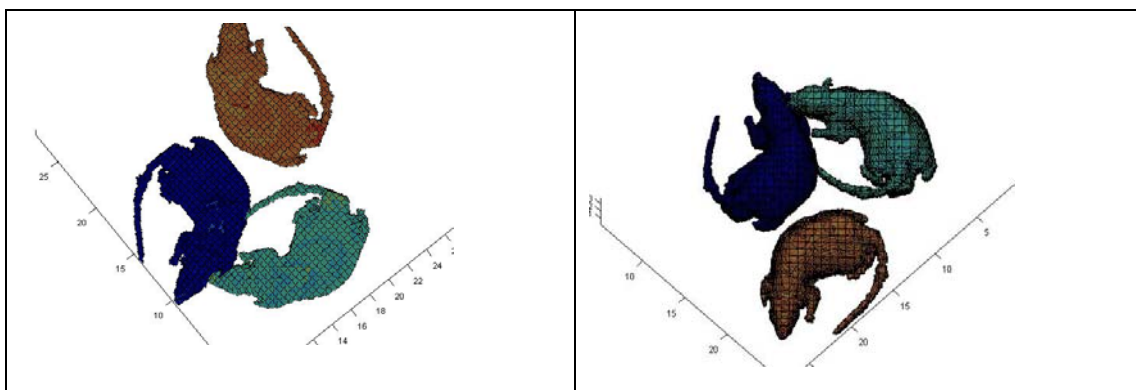


Figure 7.33 Configuration of baby rat group (23 days after birth)

Figure 7.33 shows the beginning of the independent living period. There are totally three small rats. Babies are realized by modified scaled model of 50.1 g in weight. The models are filled by homogenous liquid with dielectric parameters as $\epsilon=48$ and $\sigma=1.78$. WBSAR is calculated in the baby rats.



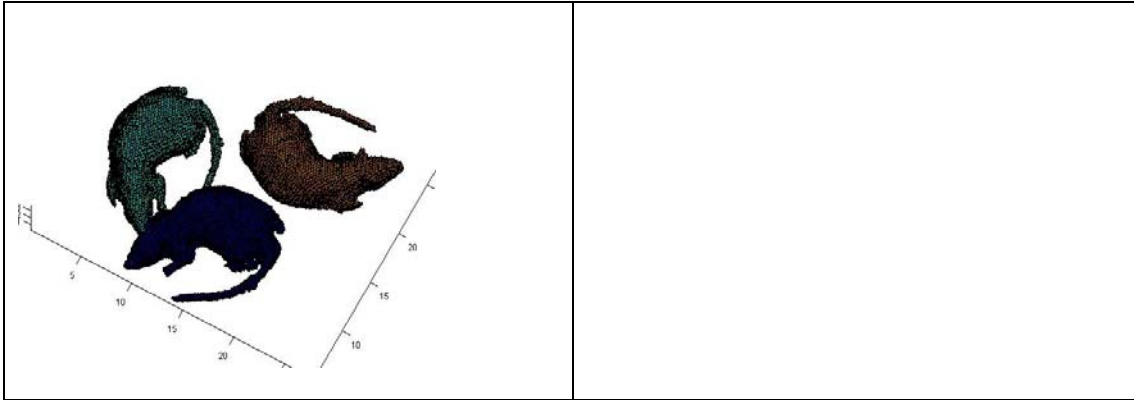


Figure 7.34 Configuration of baby rat group (30 days after birth)

Figure 7.34 shows development of the independent living period. There are totally three small rats. Babies are realized by the modified scaled model of 110.7g in weight. Both heterogeneous and homogeneous model are applied in the simulation. WBSAR is calculated in the baby rats.

By results from all the previous analysis, mean WBSARs (averaged over all the small animals in the same time simulation) by the most frequent occurred configurations are given in Figure 7.35 ($\langle E \rangle = 225 \text{V/m}$).

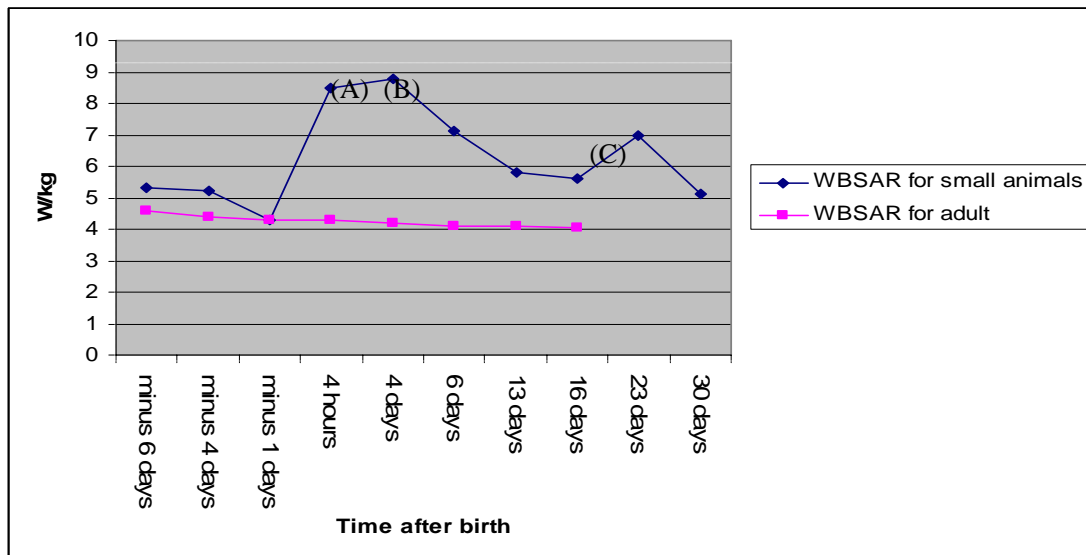


Figure 7.35 Mean WBSAR evolution on function of age

After the birth (A) the WBSAR of the baby rats increase until at the 4th day (B) after birth when body length reaches the resonance length. It continues to decrease due to growth of the body size and increase of the weight. It will encounter another sharp rise (C) due to the absence of the adult in experiment.

WBSAR assessment

In each experiment, if the different rats are considered respectively, detailed information about the WBSAR for small rats is displayed in Table 7.7 ($\langle E \rangle = 225\text{V/m}$).

WBSAR for small rats	WBSAR_max	WBSAR_min	WBSAR_mean	$\frac{WBSAR_{max} - WBSAR_{min}}{WBSAR_{min}}$
Embryos D=0.6cm	5.7	5	5.3	13.21%
Embryos D=1cm	5.9	4.7	5.2	23.08%
Embryos D=2cm	4.9	3.6	4.3	30.47%
Rats (4 hours after birth) +adult	9.5	7.4	8.5	24.90%
Rats (4 days after birth) +adult	9.9	7.2	8.8	31.03%
Rats (6 days after birth) +adult	7.7	6.1	7.1	22.64%
Rats (13 days after birth) +adult	6.3	5.3	5.8	16.95%
Rats (16 days after birth) +adult	6.2	4.7	5.6	26.63%
Rats (23 days after birth)	7.4	6.4	7	14.42%

WBSAR assessment

Rats (30 days after birth) heterogeneous model	5.5	4.6	5.1	17.65%
--	-----	-----	-----	--------

Table 7.7 WBSAR for different rats in experiments

WBSAR_min: WBSAR averaged over all the small rats in the same condition

WBSAR_max: Maximal WBSAR obtained for all the small rats in the same configuration

WBSAR_min: Minimal WBSAR obtained for all the small rats in the same configuration

The comprehensive results are generalized in Figure 7.36 ($\langle E \rangle = 225 \text{V/m}$).

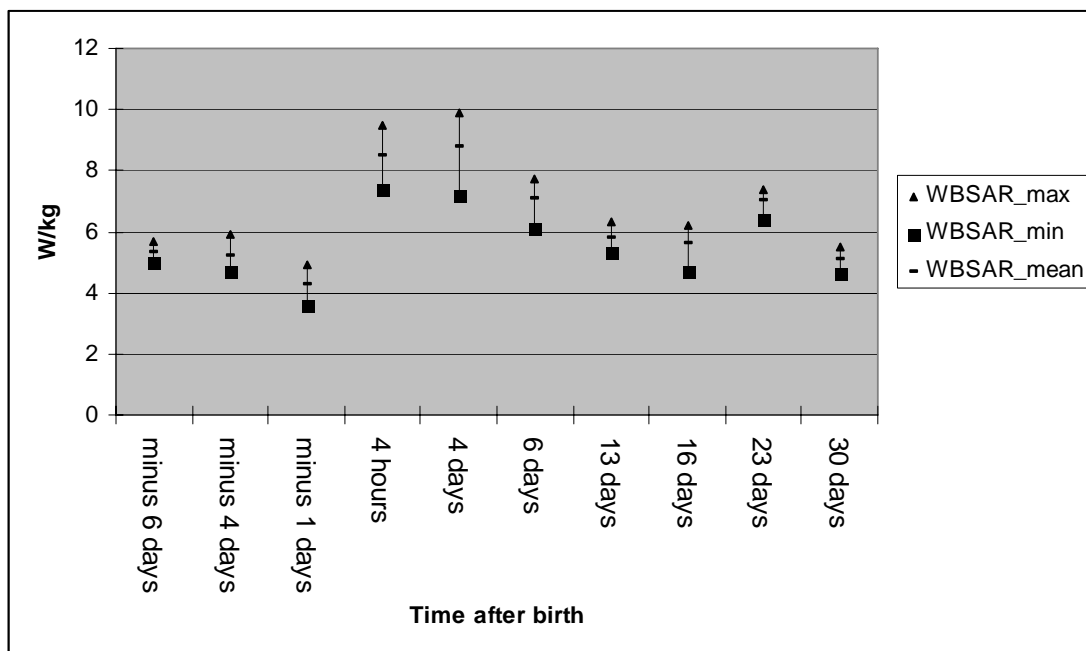


Figure 7.36 WBSAR of each small rat (embryo) for the most frequently occurred configurations

8. Exposure result and variability analysis

8.1.Objective

Exposure result and variability assessment are key parts of the project. Since the entire work can be classified as simulation and measurement. Variability contribution should also be at least divided as simulation, measurement and interface for these two parts. For the non-restrained animal exposure experiment, several factors will influence the measurement results, such as field homogeneity, postures, physical properties and proximity with the adjacent animals. At mean time, measurement with probe to characterize field distribution in RC can also introduce measurement uncertainty. Comprehensively, in the simulation-measurement hybrid method, what we used to measure and what we used to simulate can not be necessarily the same due to the difference between sham and the numerical model. All the aspects should be considered to describe the possible result range.

Single absolute and definitive result is less useful for the entire exposure period and for all the exposure species. Any results with fixed values are valid only for one special configuration. One feasible is to find the mean (or frequently occurred condition) WBSAR as well as the extreme configurations (or combinations of these configurations) for the maximal/minimal WBSAR. By this way, fluctuation range of WBSAR would be determined.

8.2.Assessment of variability for the simulation results

8.2.1 Objective

As we discussed above, even for the same time of experiment, WBSAR can vary greatly among animals due to numerous different configurations such as relative positions, postures, fluctuation of the incident power, field strength homogeneity, difference between animal samples, etc. It is infeasible to list all the possible combination of parameters even for one time configuration (e.g. 4 hours after birth). One advantageous approach is to delimit the results variability domain by several extreme cases. In short, it is to utilize the minimal numbers of the simulation results to present the most comprehensive results. Procedure can be defined as:

- 1) Define all the parameters in simulation which would influence the results
- 2) Define one reference configuration (the most frequently occurred configurations as we introduced in part 7 is set as the reference configuration)
- 3) Find out respective max-min WBSAR which are introduced by manipulation of one parameter while other parameters remain fix
- 4) Discuss the combined simulation variabilitys with the self-independent property
- 5) Conclusion for the WBSAR histogram information

8.2.2 Parameters in determining the results of simulation variability

There are apparently five parameters which will influence the simulation results significantly:

- Field variability in the experimental volume
- Variability of relative position (proximity) with the adjacent animals
- Variability of weight among the animals in the same exposure configuration
- Variability of dielectric properties among the animals in the same exposure configuration
- Variability of animal posture

8.2.2.1 Field variability

Purpose of exposure with RC is to produce environmental homogenous field and omni-direction exposure. However, with the imperfection of the reverberation in RC, field can not be ideally uniform. During the non-restrained *in-vivo* experiment, rats have the possibility to experience non-uniform field. In simulations, both RMPWM and DMPWM assume that the field distribution follows Rayleigh statistics. Waves from all the directions and uniform exposure are achieved in RC (It can be verified by field uniformity research of the test volume by simulation. Only 4% standard deviation is observed for the field generated by RMPWM). Actual field variability can not be represented in this part. It is appropriate to be classified as the divergence between the simulation model of RC and the real RC and it will be discussed in 8.4.

8.2.2.2 Interference with the nearby animals (proximity of peers)

In experiment, interference among the animals changes sharply upon different cases. Factors in deciding the interference with the adjacent animals could be the distance between the animals and the existence of the mother.

Study with heterogeneous model ([57]) has demonstrated that the existence of adjacent rat will affect the SAR for specific tissue in rats with unpredictable results (maybe higher or lower). In simulation with homogenous model, power absorption is determined by the effective mass and surface of exposure. Single rat can absorb maximum power under the condition that they are exposed by waves from all directions. On the contrary, it could be regarded as having less effective mass and surface when it is covered by the adult and his peers (in the middle of the group and under the body of mother) while all other parameters remain the same. In this case, waves from certain directions are absorbed by the other animals. Few or even no power from these given directions can arrive to the animal body. Comparative studies in 7.3 and 7.4 have also demonstrated the higher WBSAR could be observed in completely uncovered configuration. If coincidence of all the relative conditions could be calculated (for single rat, small rats in group without adult and small rats in group with adult), effect of proximate would be well estimated.

Activities of rats in experiment were recorded by camera. During the exposure period, great differences have been observed. The new-born rats tends to spend 95% of the time with their mother and to form one group. Gradually, they acquire much more mobility. For 6-10 days after birth, they spend 2/3 time with in the group and under the body of the mother, about 1/3 time within the group far from the mother. They are less likely to be with the mother and this trend continues until the mother rat is taken out at the 19th day after birth. From that point, only two relative positions are possible for the animals under exposure: rat in group and single rat far from the others. Coincidence of each relative position with ages is presented in Table. 8.1.

	0-4days	6-10 days	13-19 days	20-30 days
Group with adult	95%	65%	33%	/

Exposure result and variability analysis

Group without adult	5%	30%	33%	50%
Single	0	5%	33%	50%

Table.8.1 Coincidence of relative position with ages for rats after birth

Since we have already analyzed the respective configurations in 7.3, 7.4 and 7.5, they can be combined to deduce the possible fluctuation range. The most frequently occurred configurations which were applied in 7.5 are adopted as the mean WBSAR configurations. Other conditions are combined to study for the max/mim WBSAR.

8.2.2.3 Difference of weight

Animals in controlled experiments are selected by species and breeds. In the well controlled experiments, at each time point of growth in the exposure period, rats can keep very similar weight and difference among the animals is less than 20%.

Reference configurations for the weight could be chosen as Table 8.2 (as measured from one rat in exposure experiment), which are used in the simulation.

Days of birth	-6	-4	-1	4 (hours)
Weight (g)	0.12	0.54	4.35	5.9
Days of birth	4	6	13	16
Weight (g)	10.51	20.29	29.4	37.4
Days of birth	23	30		
Weight (g)	50.1	110.7		

Table 8.2 Weight of numerical model in simulation

The above information is adopted for mean WBSAR configuration.

8.2.2.4 Difference in posture

Rats in experiment can take different shapes. They can be curl or stretch to some extent. Posture is one important role in studying the heterogeneous tissue/organ specified SAR while it will less likely significantly influence WBSAR for homogeneous model (As will be proved by the following simulations). However, for the variability assessment, it should be studied.

Exposure result and variability analysis

Research has been made by simulation. One modified cylinder is bent as $\frac{1}{4}$ and half circle. Length of the cylinder is 12.9 cm with cross-section of $3\text{cm} \times 3\text{cm}$. With RMPWM of resolution of 1 mm, the results are shown in Figure 8.1.

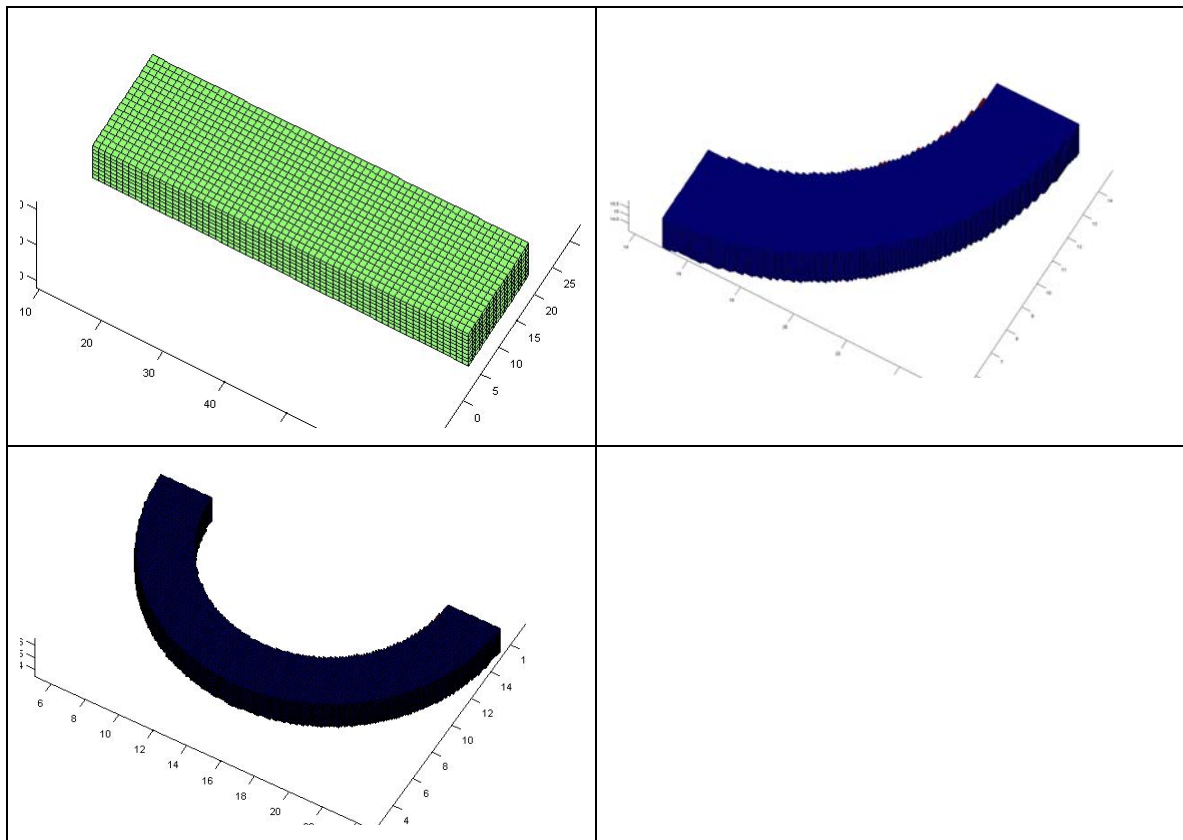


Figure 8.1 Models for posture research

Through averaged results of RMPWM with 1mm resolution, whole body averaged SAR among the three models is $\pm 3\%$. The result can be applied to rat numerical models of different sizes.

8.2.2.5 Difference in dielectric properties

Due to differences among the individuals, it is predicted that the dielectric properties can not be the same. Peyman and Gabriel [61] have demonstrated that for 5 rats in their dielectric parameters research, 5% variability could be observed.

Reference configuration for dielectric properties is defined by Table 7.4.

8.2.2.6 Discussion and combination for the variability components

The five factors have been analyzed separately. One question arising is whether they can be regarded as independent or not.

Exposure result and variability analysis

Among these parameters, exposure environment components can be independent to other variability components originated from the exposure animals. Different positions of the animals can incur reflection and diffraction and make the adjacent field irregular. $\langle E^2 \rangle$ may change in the volume adjacent to animals. However, in both the simulation and measurement, points to calculate $\langle E^2 \rangle$ are located at least 5 cm to the numerical model (simulation) and equivalent liquid sham (measurement). The influence by the distinctive position and posture can be neglected at this distance. $\langle E^2 \rangle$ fluctuation can be regarded as independent to all the other parameters.

Relative positions (proximate with peers) change with ages. It is recorded by camera. For each time after birth, it is fixed as the analysis from the video information. It is completely independent to the other aspects.

Weight and dielectric properties could be interrelated because for the same age, variability in weight means the composition of the animal body change. The dielectric properties which are based on the whole body averaged value could change. They are dependant. However, their respective variability contributions are about 3% to 5%. Inter-dependence between them can be deemed as trivial.

At each given time point, any posture that the rat can take is stochastic, it is completely independent to other parameters. And it will not influence other parameters.

When all the variability contributors are thought to be independent, the variability sources and their combined results in simulation part are estimated in Table. 8.3 and Figure 8.2:

Exposure result and variability analysis

	Embryo 0.6cm	Embryo 1cm	Embryo 2 cm	4 hours	4 days	6 days	13 days	16 days	23 days	30 days
Interference between animals (fetus)	±7%	±12.5%	±15%	±16.9%	±22.1%	±10.7%	±28.8%	±33.8%	±30%	±8.2%
Dielectric properties	0	0	0	0	0	±3%	±3%	±3%	±3%	±3%
Weight	0	0	0	±5%	±5%	±5%	±5%	±5%	±5%	±5%
Homogenous /heterogenous	±5%	±5%	±5%	±5%	±5%	±5%	±5%	±5%	±5%	±5%
Posture	/	/	/	±2%	±2%	±2%	±2%	±2%	±2%	±2%
Combined maximum Variability	±12%	±18.5%	±21%	±29.9%	±35.1%	±26.7%	±44.8%	±49.8%	±46%	±24.2%

Table 8.2 Variability of whole body averaged SAR for different rat model

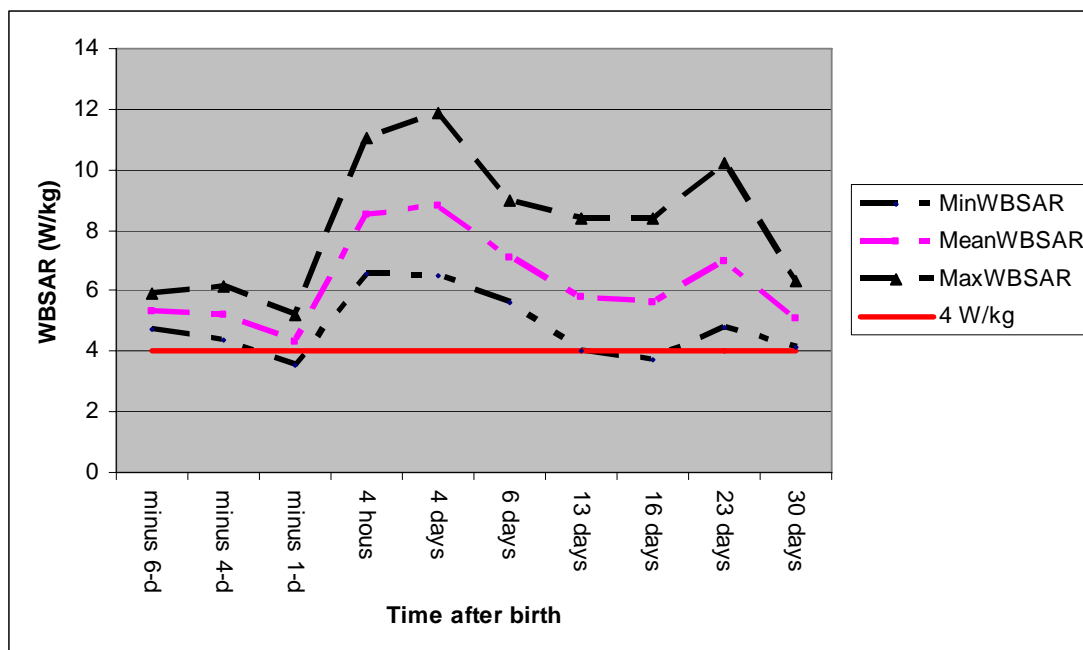


Figure 8.3 Histogram of WBSAR and possible variability by simulation part

$$\langle E \rangle = 225 \text{ V/m}$$

From the above figure, variability sources from different simulation configurations are discussed. Interference with adjacent rats (proximity) contributes dominant variability to the results. However, it can not be reduced greatly because the ability to move freely is just the character of non-restrained experiment. By video information, compartment of rats at each age can be recorded. Upon statistically analysis, coincidence of each configuration at each age can be determined. Then, either single rat, rats in group with adult or rats in group with adult configurations could be combined to calculate the WBSAR. By the means, precise results could be obtained.

8.3. Uncertainty from measurement part

8.3.1 Principle of measurement uncertainty

In the measurement part, measurement uncertainty can be introduced by instruments, measurement procedures, environment and operators. Uncertainty assessment for even the most sophisticated animal *in vivo* non-restrained exposure system is very complicated.

Measurement is seldom or even impossible to be exactly correct. Due to:

- 1) Measuring instrument is not calibrated precisely correctly
- 2) Repeated measurements of the same quantity yield slightly different values
- 3) Meter has only limited number of digits
- 4) Constants themselves are known only approximately
- 5) Change of some external variable changes the outcome of the measurement

There exist several studies on evaluating the measurement uncertainty in EMF exposure introduced by some specific instrument such as [63]. Very few studies exist for complicate system exposure result uncertainty analysis.

According to [64], [65] and [66], measurement uncertainty and its evaluation procedure are well defined. It can be classified as Type A and Type B uncertainty, which can be referred to Annex II.

In the following part, the possible measurement uncertainty sources will be discussed in details.

8.3.2 <E> field strength measurement

<E> field measurement is constituted by several single E field measurements. Uncertainty comes from the follows aspects:

- 1) Calibration for antenna factor of the 3-axis probe

Type B uncertainty. Calibration certification documents provides the detailed calibration information as well as the uncertainty.

- 2) Receiver readout

Power meter is used as the receiver in the measurement. This is type A uncertainty and could be evaluated by repeated measurement for the same standard source. Once the standard deviation is obtained, the uncertainty component could be calculated. Normally, the standard uncertainty for receiver readout seldom exceeds 0.5dB.

- 3) Receiver calibration

Type B uncertainty. Receiver (power meter) calibration information is available in the calibration documents.

Exposure result and variability analysis

4) Attenuation factor of the cable

Type A uncertainty. Attenuation of the cable is not always the same due to the thermal effect and linearity domain of the cable. The uncertainty can be evaluated by repeated measurement at given frequency point (working frequency). 20 measurements are made to calculate the standard deviation. Result is 5%.

5) Mismatch of the receiver and 3-axis probe

Type A uncertainty. Mismatch is very common in RF measurement. It depends on the voltage reflective coefficient (VRC). VRC is a frequency dependant factor. In the exposure experiment, operational frequency is selected.

6) Linearity of probe

Type B uncertainty. Different input E strength can provide different voltage output for the probe. Measurement results are preferred to be located in linear domain. The information can be found in the document.

8.3.3 Equivalent liquid dielectric measurement

In measurement, dielectric properties of human equivalent liquid are used to load the RC. Its dielectric properties don't play an important role in the experiment as we will show in 8.4.

8.3.4 Conclusion

Combined measurement uncertainty is listed as Table 8.4.

SN	A	Type	C	d	$e = f(d,k)$	F	$h = c \times f / e$	k
	Uncertainty Component		Tol. (\pm %)	Prob. Dist.	Div.	c_i	U_i (\pm %)	v_i
1	Probe Calibration	B	26	N	2	1	13	∞
2	Probe Linearity	B	10	R	$\sqrt{3}$	1	5.8	∞
3	Receiver calibration	B	1.0	R	$\sqrt{3}$	1	0.6	∞
4	Readout Electronics	A	1.0	N	1	1	1.0	∞
5	RF Ambient Conditions	B	3.0	R	$\sqrt{3}$	1	1.73	∞
6	Attenuation factor of cables	A	5	N	1	1	5	∞
7	Mismatch of receiver and probe	B	2.9	R	$\sqrt{3}$	1	1.7	∞
	Combined Standard Uncertainty			RS S			14.5	

Expanded Uncertainty (95% confidence interval)				K= 2			29	
---	--	--	--	---------	--	--	----	--

Table.8.4. Combined uncertainty for measurement

Measurement uncertainties have multiple sources. Probe calibration uncertainty is the most important component. Small probe with better performance will decrease measurement uncertainty dramatically. Other uncertainty sources such as environmental components are less likely to be changed.

8.4. Variability assessment for measurement-simulation interface

Other important variability source is the interface between the simulation and measurement. As we described in the previous parts, different models, measurement antennas are applied in simulation and measurement. Difference between measurement and simulation can introduce ambiguity to the final result.

Measurement is operated with the bottles of the human tissue liquid, while simulation is always carried with the rat model (either homogenous or heterogeneous). Difference in models results the difference between the calculated results and the real exposure result. Analysis should be made to study and correct the difference between the two cases.

8.4.1 Tissue equivalent liquid and measurement sham mismatch

Since no available rat tissue equivalent liquid is available for measurement in RC, large-band human tissue equivalent liquid is substituted as the measurement load. When charactering the RC with 4 bottles of 375 g human tissue equivalent liquid, by measurement, dielectric properties are $\sigma = 1.7$ S/m and $\epsilon = 40.4$. To estimate the possible variability induced by the difference, simulation and measurement are performed. Configurations with 4 bottles shams and 4 rats are shown in the Figure. 8.3.

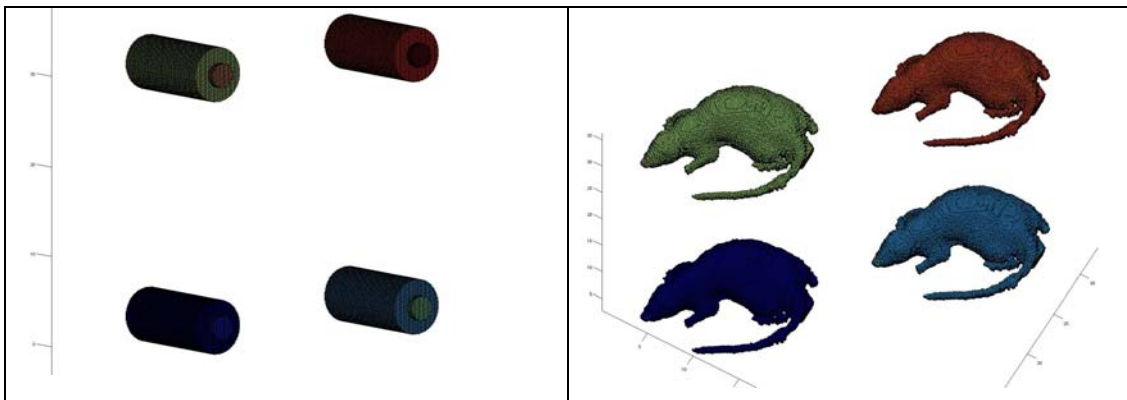


Figure 8.3 Configurations of the 4 bottles and 4 rats case

Simulation has been made with (1) rat heterogeneous numerical model and (2) equivalent liquid bottle sham of the same weight. By the same simulation condition (RMPWM, 200 rays, average upon 20 simulations), $\langle E \rangle$ are calculated in the central empty volume of about $20\text{cm} \times 20\text{cm} \times 20\text{cm}$. There are totally about 3.2×10^7 points to be averaged for $\langle E^2 \rangle$. $\langle E^2 \rangle$ for these two cases have only 0.47% difference. Considering RC has 3.37m^3 in volume while 4 small rats taking volume of about $3.75 \times 10^{-4}\text{m}^3$, the variability of absorbed power in the tiny animal body (and the bottle sham) can not influence the repartition of the stored power in the empty volume of RC greatly if the total mass of the absorber is the same. $\langle E^2 \rangle$ should not be changed greatly. It means that we can obtain a credible $\langle E^2 \rangle$ with the bottle sham in measurement to represent the rat numerical model in simulation. What we have measured can be normalized to what we could obtain in the simulation without any problem. No significant incoherence in $\langle E^2 \rangle$ will be produced by the application of bottle sham in measurement.

8.4.2 Perturbation of the measurement probe to field in RC

One of the incoherencies between the simulation and measurement is the existence of the measurement probe. In simulation, no measurement probe is realized while in measurement, existence of the probe in RC may perturb the field distribution.

Probe perturbation could be evaluated by simulation. Tri-axis probe is realized by three orthogonal dipoles. Each dipole has length of 4 cm as in the measurement.

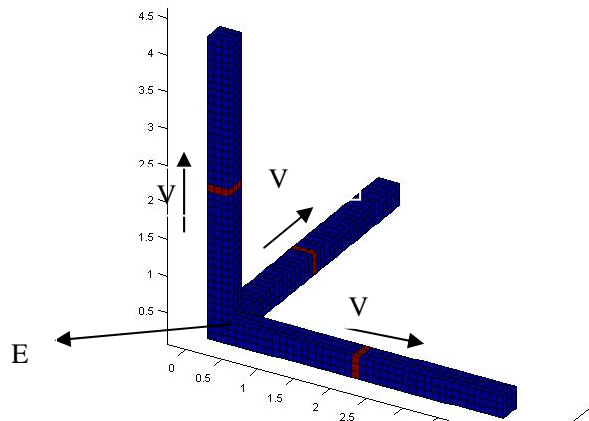


Figure 8.4 Numerical model of measurement probe

Two series of simulations have been operated with the metallic dipole in RC.

(1) Perturbation of the measurement probe to field distribution in RC

RC loaded with 4 adult rat models is realized. In the first case, there is no measurement probe in the RC. In the second case, above mentioned probe is placed in RC. By RMPWM, SEFR is calculated for both two cases with E value from the same volume. With 20 simulations for each method, results show that the existence of this measurement probe in RC will not change SEFR.

(2) E measurement error due to size of probe (displacements of the gaps to the central part of 3-axis antenna)

Measurement probe that we used in the experiment is not volume negligible. It has length of about 4cm on each dipole. The actual measured value is the voltage at gap of each dipole. With antenna factor, they can be converted in to E at direction X, Y and Z. Consequently, E can be calculated as:

$$E = \sqrt{E_x^2 + E_y^2 + E_z^2} \quad (8.4)$$

There will surely be some errors introduced by the deviation of the gaps to the center of probe (which is used as the E value in simulation).

The result could be compared with the E value directly obtained from the same position without the metallic probe.

Results show that the E by two different methods can produce about 5% difference.

8.4.3 Measured <E> and simulated <E>

As described in experiment part, measured <E> is obtained by limited points on the test bench in RC due to the considerable dipole size. By comparison, in simulation, <E²> results are obtained from mean value of enormous E² (4x10⁶ points) in the empty space of the loaded RC. These two distinctive approaches for interpreting <E> could lead to discrepancy on the results. The difference induced by the distinctive measurement methods should be evaluated.

Exposure result and variability analysis

Studies have been made by simulation. Entire simulation volume is meshed by 2 mm length cubes. 4 adult rats are placed on the test bench. 20 simulations have been made by RMPWM. We define the $\langle E^2 \rangle$ obtained from the entire empty volume in the loaded RC as Mea1 (as shown in Figure 8.5). $\langle E^2 \rangle$ obtained only on the test bench is defined as Mea2 (as shown in Figure 8.6) while $\langle E^2 \rangle$ obtained on the chosen points of Mea2 is defined as Mea3. In Mea3, all the sample points keep interval of at least 5 cm which is the same in the real measurement.

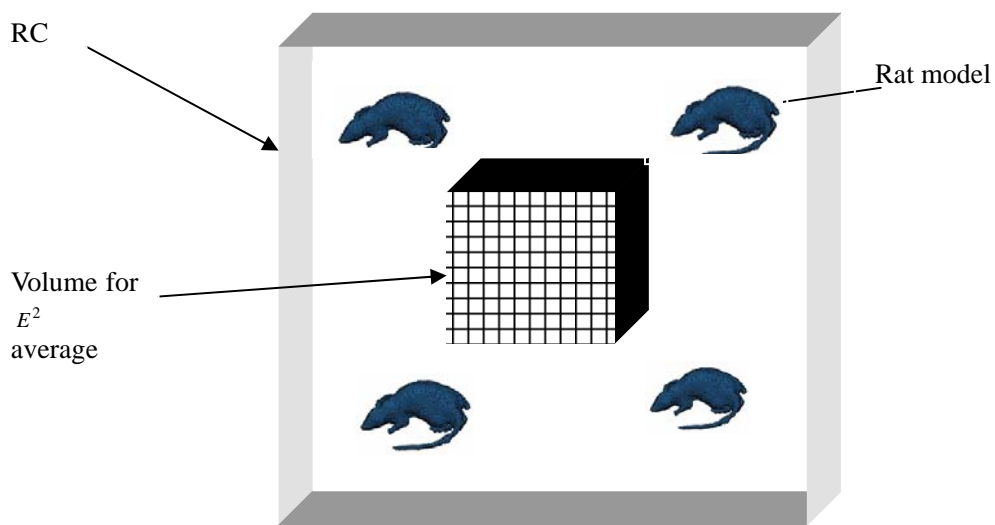


Figure 8.5 $\langle E^2 \rangle$ in the empty volume of loaded RC by simulation (Mea1)

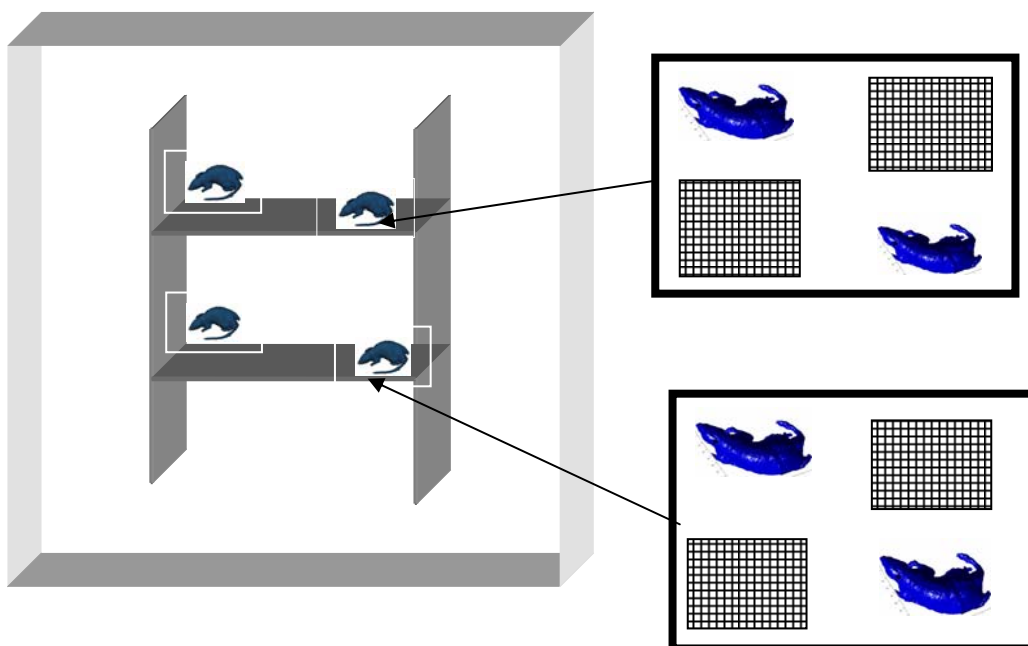


Figure 8.6 $\langle E^2 \rangle$ on two stage of the test bench (Mea2 and Mea3)

If $\langle E^2 \rangle$ obtained from the central empty volume (Mea1, 4×10^6 points) is taken as reference, averaged value on the test bench and on the test bench but with chosen points are compared with reference. The differences are shown in the following Figure 8.7.

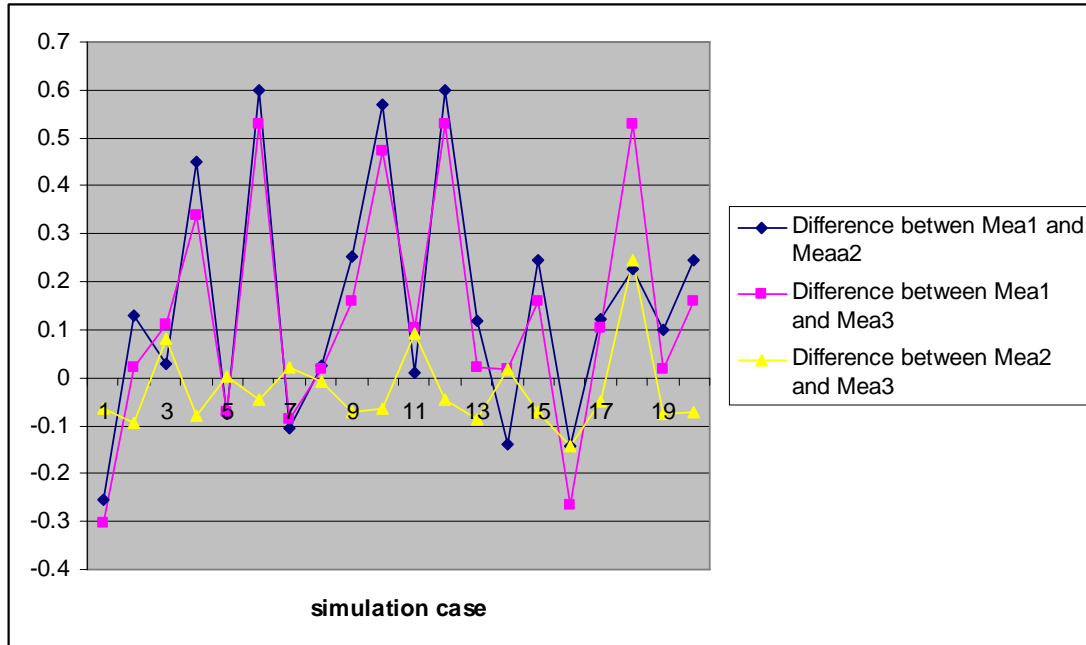


Figure 8.7 Variability of different measurement method

By calculation, standard deviation of difference in $\langle E^2 \rangle$ between Mea3 and Mea1 is 12%. Same value is observed between Mea3 and Mea2. There is insignificant standard deviation between Mea2 and Mea3. That means:

- If measured on the test bench, whatever points are chosen, no significant variability should be observed. Measurement on different points will only introduce trivial difference.
- Difference between $\langle E^2 \rangle$ in entire empty volume (as in simulation) and $\langle E^2 \rangle$ by chosen points on the test bench (as in measurement) can be compensated by $\pm 12\%$.

By previous analysis, the incoherence between the simulation part and measurement will influence the measured $\langle E^2 \rangle$.

If we decide to study how many measurement points can reconstructed $\langle E^2 \rangle$ with less error in comparison with the simulated $\langle E^2 \rangle$, we have added some extra points in the

Exposure result and variability analysis

central empty volume. Since simulation to decide $\langle E^2 \rangle$ is from the values in the central empty volume about $20\text{cm} \times 20\text{cm} \times 20\text{cm}$, some points in this part should be selected to find if any additional measurement points could ameliorate the discontinuity between simulation and measurement values.

The research can be performed by simulation. Rats of standard weight (375 g) are placed on two layers of the test bench. 18 points are recorded on two layers of the test bench as in the real measurement plus several points in the central empty volume of RC. Simulations are carried by 20 times of RMPWM. In each time of simulation, 200 rays are designed to be emitted from each point of Huygens box. Configurations for the two series of simulations are 18 points on two layers of the test bench (at least 5 cm interval just as in measurement) plus:

(1) 27 points (9 cm interval) in the central empty volume of the loaded RC ($20\text{cm} \times 20\text{cm} \times 20\text{cm}$)

or,

(2) 216 points (about 4 cm interval) in the central empty volume of the loaded RC ($20\text{cm} \times 20\text{cm} \times 20\text{cm}$)

Results are shown in Table 8.5.

	18 points on test bench +27 points in the central empty volume	18 points on test bench +216 points in the central empty
Variability to reference $\langle E^2 \rangle$	0.097	0.084
Standard deviation	0.089	0.055

Table 8.5 Results for different numbers of measurement points

18+27 points measurement conforms to the simulation results with about 8.4% error. Much more points measurement can achieve much closer approximation, however compared with the measurement task, 18 +216 points measurement will not be accepted as feasible measurement plan.

If we calculate uniquely the 27 points in the central empty volume and compared with the simulation value (reference value), we obtain variability to simulated $\langle E^2 \rangle$ as

0.097 with standard deviation of 0.089. It demonstrates that 27 measurements (uniformly distributed) in the central empty volume of the loaded PC can achieve very satisfactory results compared with measurements on the test bench.

8.4.4 Field homogeneity

Reported by measurement in RC, the field uniformity is 1.2dB. Field variability in the test volume is 15% which will introduce 22.5% variability in term of WBSAR (with the reference $\langle E \rangle = 225$ V/m), while other configurations remain the same.

8.4.5 Conclusion

By conclusion, variability from the measurement- simulation interface part will introduce variability of $\pm 39.5\%$ to the final result.

8.5. Conclusion for the result

Combining variability from the distinct three parts, variability of the system can be calculated as in Table 8.6.

Exposure result and variability analysis

Phase Source Of variability	Embryo 0.6cm	Embryo 1cm	Embryo 2 cm	4 hours	4 days	6 days	13 days	16 days	23 days	30 days
By simulation	±12%	±18.5%	±21%	±29.9%	±35.1%	±26.7%	±44.8%	±49.8%	±46%	±24.2%
By measurement	±29%	±29%	±29%	±29%	±29%	±29%	±29%	±29%	±29%	±29%
By interface of simulation and measurement	±39.5%	±39.5%	±39.5%	±39.5%	±39.5%	±39.5%	±39.5%	±39.5%	±39.5%	±39.5%
Combined maximum Variability	±80.5%	±87%	±89.5%	±98.4%	±103.6%	±95.2%	±113.3%	±118.3%	±114.5%	±92.7%

Table.8.6 Combined result variability for different time after birth

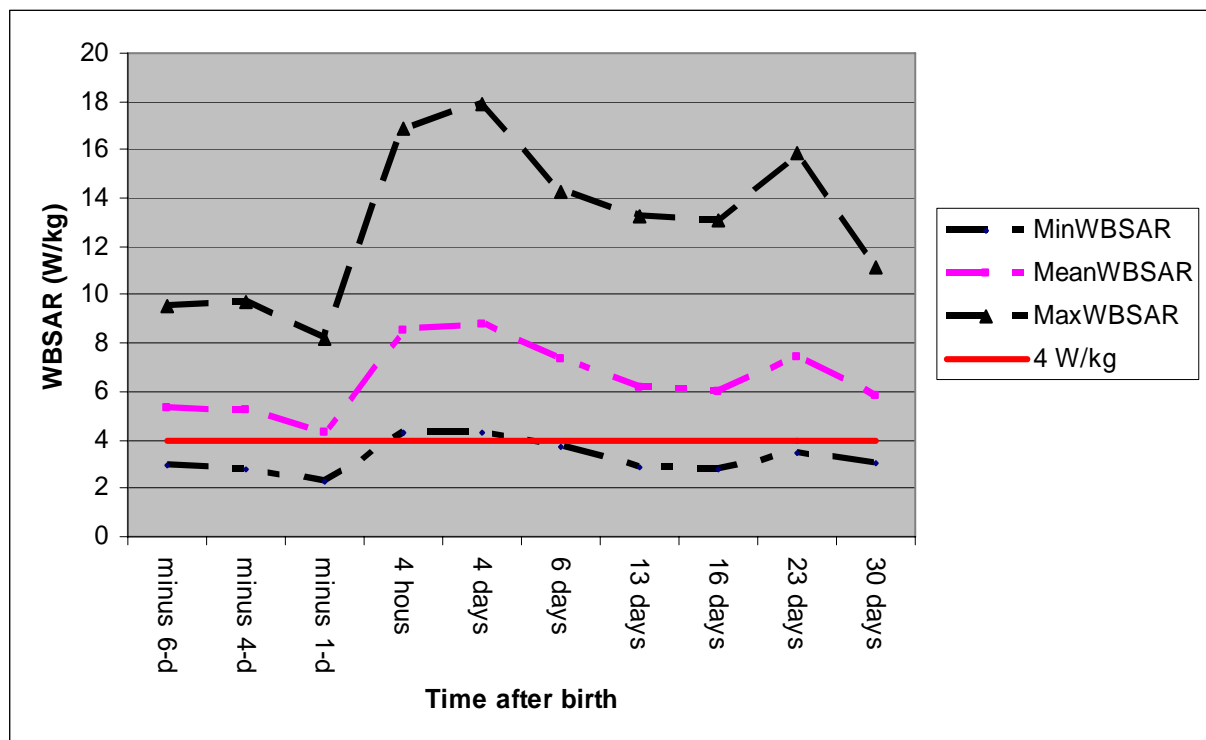


Figure 8.8 Combined variability for the whole exposure period ($\langle E \rangle = 225 \text{ V/m}$)

8.6. Discussion for the result

As a non-restrained animal *in vivo* exposure experiment, exposure dose can change a lot due to numerous configurations. Several methods could be applied to reduce the result variability greatly. Measurement probe and the statistical research on the habitude of the rats (proximity with other rats) are among the most influential factors. With the precise calculation for the coincidence of the different positions, result variability could be expected to be minimized.

Experimental rats should be selective in order that variability of weight is within the research range. Abnormal species (weight, size, sickness etc) are recommended to be eliminated from the experiment.

Variability produced from the simulation configuration can be very lightly reduced. Few aspects could be ameliorated. All aspects originate from *in vivo* non-restrained experiment itself. Variability diminution in this part is less possible.

Exposure result and variability analysis

Measurement part contributes the maximum uncertainty to the final results. If precise measurement instruments (tri-dipole probe is the key instrument in the experiment) can be applied, the uncertainty would be optimized.

Interface between the measurement and simulation introduces significant variability by the incoherent measurement points for $\langle E^2 \rangle$. It can be modified by enlarge the numbers of the measurement point in the empty volume of the loaded RC.

9. Conclusion

This thesis presents one system for non-restrained animal *in vivo* Wi-Fi frequency exposure as well as the work to characterize the field distribution in the system. Rats and mice are designed to have 4 W/kg WBSAR in the non-restrained experiment. Maximal weight of the rats is 1.5kg. Two requirements are interpreted from the experiment target. First, by estimation, about 6 W power should be absorbed by the animals with 1.5 kg mass. Second consideration is that homogeneous exposure for the animals whenever they move in the test bench.

According to analysis on the available non-restrained animal *in vivo* exposure experiment, RC has been chosen as the relevant system. RC has the possibility to provide one uniform exposure environment as well as considerable test volume for hosting up to 16 rats (4 adults + 12 small ones). One novelty antenna layout and excitation method is proposed in the work. There are six half wavelength dipole antennas on each internal surface of the RC. They function in one random pattern. Only one antenna is active for any time. It is designed to provide much better uniform field and omni-direction exposure. This design can also exempt the existence of large size stirrers in RC. Only three small size continuous mode stirrers are installed in the corner of the RC, which permit one much bigger test volume for the activity and thus much comfortable environment of animals.

Dimension of RC is determined by interaction of the emission antennas and the animal under exposure. Animal numerical model is realized by cube filled with 1.5 kg human tissue equivalent liquid. It can move in one $40cm \times 40cm \times 40cm$ volume. Variability for S_{11} of antenna is recorded on function of the different positions of the animal model. Result show, one cubic RC with length of $1.5m$ is sufficient.

By previous studies, RC is realized with aluminum wire-knot canopy-like materials which are often used for EMF protection. This kind of material permits the respiration of animals in RC. No addition air-exchange equipment is needed for the exposure system. It can also guarantee that the EM wave can be well reflected by the enclosure to generate theoretically omni-direction exposure.

Conclusion

Accessories such as test bench, EM lossless test container were prepared for the experiment. With the constructed RC, fundamental measurements were performed to calculate the field homogeneity as well as the Q estimation. Measured Q is based on the ratio of the power received by the reception antenna to the power transmitted by the emission antenna in RC. There are several factors which will reduce the received power by the measurement antenna, such as the power dissipation to the RC enclosure, power leakage from the aperture of the RC, power dissipation to the measurement equipment and etc. All these factors lead to a lower pseudo-readout of the measured power. Furthermore, it leads to a Q which is far lower than the theoretical value due to the neglect for these dissipative aspects. This Q can be called as one conservative value because it is inferior to the actual value and the conductivity deduced from this measured Q will also be less than the actual value (since all the dissipative factors are attributed to the conductivity of the RC enclosure) .

Characterizing the field distribution in RC is the key point to study the repartition of energy in RC and is essential to determine the WBSAR of animals. Attempt by tradition FDTD method on realizing all the details of RC (entire cavity, antennas, stirrers and accessories) was demonstrated as less capable in solving the power distribution in RC. Alternative methods such as pure measurement, pure simulation and simulation-measurement combined method in determining the animal power absorption were reviewed. One simulation-measured hybrid method is proposed. The assumption is that in RC, power absorption by animals depends on squared averaging E strength in the test volume. Much higher E in the test volume, much higher WBSAR will be observed in rats. Also averaging E can serve as the bridge to link the incident power (much higher the incident power to RC, much higher $\langle E \rangle$ in RC) and the WBSAR in rats.

With previous studies, field distribution in RC satisfying several criterions can be deemed as Rayleigh statistic if the Q is superior to 100. From our measurement in the constructed RC, measured Q (also the conservative Q as we introduced in previous paragraph) is in the order of 1000. Then we can borrow Rayleigh distribution to reconstruct the exposition in RC. Field distribution in RC can be simulated by one Huygens box emitting summation of plane waves on each point of its surface. Several parameters in construction of the wave propagation function are discussed in detail by simulation. Some trials were made to determine the minimal number of simulation that

Conclusion

will be needed to have a stable WBSAR in the animals. Another similar method was also tried and compared. In the method, only several plane waves with given vectors were chosen to radiated the animals. The effect of other waves was looked as trivial to WBSAR of animal. Results of the two methods are compared to mutually verify the validity.

With the measurement in RC on Q and field uniformity, the validity of application of the Rayleigh statistics to the field distribution is obtained. Simulation results can be consolidated.

When the typical configuration of 4 adult rats in RC is calculated, problem arises for the studies of exposure for rats of different ages. Numerical models of different ages are realized by proportionally reduced adult model modified by morphing technology according to the data measured from the animals in experiment. For each time point of the exposure period, several possible configurations are discussed. Several parameters which play important roles in the results such as dielectric properties, postures, etc are analyzed to present results in order to be utilized in variability research.

Uncertainty and variability research are provided for the result. Non-restrained animal *in vivo* exposure is very complicated. They may include multiple aspects and significant value in individual uncertainty sources. This part is divided into three parts as measurement, simulation as well as interface between these two parts. Combined variabilities were furnished at the end of part 8.

The entire system and the method to analyze the field distribution can be applied to the studies of characterization of Wi-Fi exposure in modern urban and domestic environment. Modern domestic and urban environments are featured as plenty of scatters or reflectors with multiple sources and multi-path situation. Wave propagation in such environments by measurement in Manhattan has been found near-Rayleigh fading [67]. It provides one assumption that real field distribution model in such complicated and broad modern environment could be determined by limited point field measurements. When any statistical model (not only Rayleigh, but also Rician, Gaussian or other else could be possible) is constructed, $\langle E \rangle$ could be served as the indicator for the SAR (WBSAR or local SAR in heterogeneous model). Holography for exposure in this environment can be estimated. There is no need to realize the

Conclusion

extremely changeable buildings or the quarter which permit the fast perceive to the environment exposure.

By comparison, in the office with several access points, tables, chairs, steel bar-concrete wall as well as office equipments, reflection and diffraction are great. Some similar studies [68] have been published on the Wi-Fi field distribution in the office with FDTD-subgridding technology to decide the installation of the AP access points. Considering the modern construction of the office, wave propagation introduced in it by multiple excitation points can be also much like in one reverberation cavity. Field strength attenuates but the reflection could be dominated if the reflective coefficient of the walls and scatters are significant and the waves may be coming from all directions. By E strength measurement, $\langle E \rangle$ could be obtained to reconstruct the possible exposure situation in the office with different mathematical models.

The work included in this project can be classed as three types:

- (1) Pre-conception for the exposure system
- (2) Measurement-simulation hybrid method to determine the power distribution for the rats
- (3) Long term exposition result and its variability discussion

This system can be extended for non-restrained exposure experiment for other species. Potential work in ameliorating the performance of the system and the result of exposure could be expected in:

- (1) Fabrication of the gel model of the rat for measurement. This model is used to load the RC for measurement task. The model would have the exactly same contour as the animals in exposure.
- (2) Choose the positions for the field strength measurement task to get precise measurement value with less measurement points.
- (3) Study for the activities of the rats on function of days after birth with statistically large number of rat samples. Then the variability of the results can be reduced.
- (4) Research on determination of the field distribution model based on analysis of the field value such as the method propose by Stéphanie Mengué *et al* [69].

Conclusion

- (5) Integration with other numerical methods such as subgridding or alternating direction implicit finite-difference time-domain (ADI-FDTD) [36] to save the calculation resources.

Annex I FDTD method

AI.1 Maxwell function and Yee's function

Law of the electromagnetism was elaborated in by James Clerk Maxwell [70]. The well-known Maxwell equations are:

$$\nabla \times \bar{H} = \frac{\partial}{\partial t} \bar{D} + \bar{J} \quad (\text{AI.1})$$

$$\nabla \times \bar{E} = -\frac{\partial}{\partial t} \bar{B} \quad (\text{AI.2})$$

$$\nabla \cdot \bar{D} = \rho \quad (\text{AI.3})$$

$$\nabla \cdot \bar{B} = 0 \quad (\text{AI.4})$$

where \bar{E} , \bar{B} , \bar{H} , \bar{D} , \bar{J} , and ρ are function of position and time.

\bar{E} electric field strength (volts/m)

\bar{B} magnetic flux density (webers/m²)

\bar{H} magnetic field strength (amperes/m)

\bar{D} electric displacement (coulombs/m²)

\bar{J} electric current density (amperes/m²)

ρ electric charge density (coulombs/m³)

Maxwell also point out:

$$\nabla \cdot \bar{J} = -\frac{\partial}{\partial t} \rho \quad (\text{AI.5})$$

$$\bar{D} = \epsilon_0 \bar{E} \quad (\text{AI.6a})$$

$$\bar{B} = \mu_0 \bar{H} \quad (\text{AI.6b})$$

Where

Annex I FDTD method

$$\epsilon_0 \approx 8.85 \times 10^{-12} \text{ farad / meter}$$

$$\mu_0 \approx 4\pi \times 10^{-7} \text{ henry / meter}$$

K. Yee [71] has published his remarkable research in 1966. When apply the (4.1) and (4.2) to the three dimension Cartesian coordination, we can get:

$$\frac{\partial H_x}{\partial t} = -\frac{1}{\mu} \left(\frac{\partial E_z}{\partial y} - \frac{\partial E_y}{\partial z} \right) \quad (\text{AI.7})$$

$$\frac{\partial H_y}{\partial t} = -\frac{1}{\mu} \left(\frac{\partial E_x}{\partial z} - \frac{\partial E_z}{\partial x} \right) \quad (\text{AI.8})$$

$$\frac{\partial H_z}{\partial t} = -\frac{1}{\mu} \left(\frac{\partial E_y}{\partial x} - \frac{\partial E_x}{\partial y} \right) \quad (\text{AI.9})$$

$$\frac{\partial E_x}{\partial t} = \frac{1}{\epsilon} \left(\frac{\partial H_z}{\partial y} - \frac{\partial H_y}{\partial z} - \sigma E_x \right) \quad (\text{AI.10})$$

$$\frac{\partial E_y}{\partial t} = \frac{1}{\epsilon} \left(\frac{\partial H_x}{\partial z} - \frac{\partial H_z}{\partial x} - \sigma E_y \right) \quad (\text{AI.11})$$

$$\frac{\partial E_z}{\partial t} = \frac{1}{\epsilon} \left(\frac{\partial H_y}{\partial x} - \frac{\partial H_x}{\partial y} - \sigma E_z \right) \quad (\text{AI.12})$$

Field components' configurations are shown in Figure AI.1.

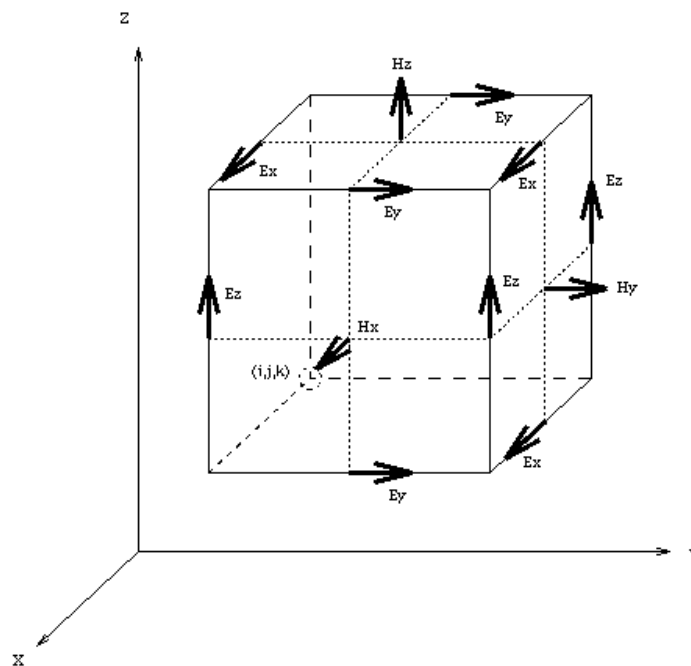


Figure AI.1 Configuration of the field components for Yee grids

The calculation volume is meshed by cubes. On each surface of the meshed cell, there are different components of the E or H. Each E component is encompassed by four H components and vice vice.

Temporal discretization can be explained in three-dimension case as follows

$$\frac{\partial}{\partial t} H_x(i, j, k, t) = \frac{H_x(i, j, k, t + \frac{dt}{2}) - H_x(i, j, k, t - \frac{dt}{2})}{dt} \quad (\text{AI.13})$$

In the same equation, the E and H are never on the same time point. They have the temporal difference of $dt/2$. This case can be well presented by the one dimension situation in Figure AI.2.

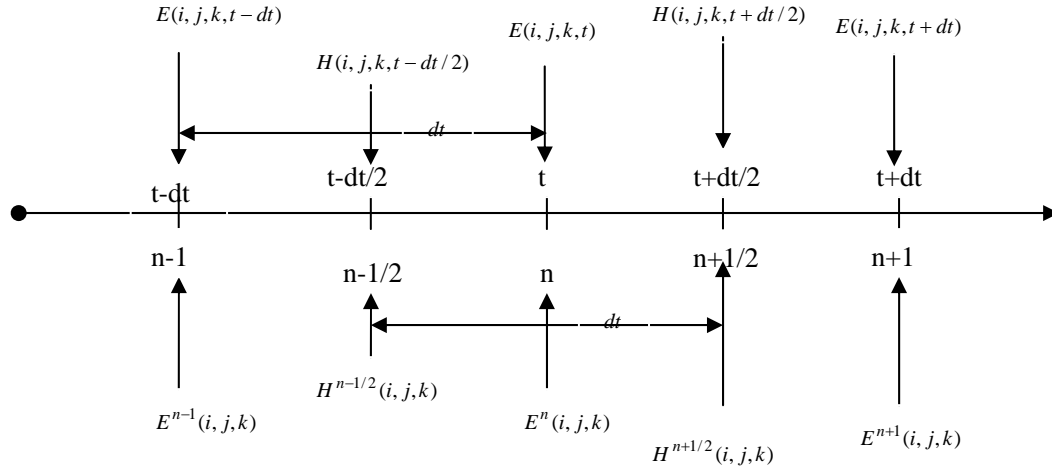


Figure AI.2 Configurations for Yee updates

When replacing all the temporal and spatial difference by temporal and spatial displacement, we obtain:

$$H_x^{n+1/2}(i, j, k) = H_x^{n-1/2}(i, j, k) - \frac{dt}{\mu_0 dy} [E_z^n(i, j+1, k) - E_z^n(i, j, k)] + \frac{dt}{\mu_0 dz} [E_y^n(i, j, k+1) - E_y^n(i, j, k)] \quad (\text{AI.14})$$

$$H_y^{n+1/2}(i, j, k) = H_y^{n-1/2}(i, j, k) - \frac{dt}{\mu_0 dz} [E_x^n(i, j, k+1) - E_x^n(i, j, k)] + \frac{dt}{\mu_0 dx} [E_z^n(i+1, j, k) - E_z^n(i, j, k)] \quad (\text{AI.15})$$

$$H_z^{n+1/2}(i, j, k) = H_z^{n-1/2}(i, j, k) - \frac{dt}{\mu_0 dx} [E_x^n(i+1, j, k) - E_x^n(i, j, k)] + \frac{dt}{\mu_0 dy} [E_x^n(i, j+1, k) - E_x^n(i, j, k)] \quad (\text{AI.16})$$

$$E_x^{n+1}(i, j, k) = E_x^n(i, j, k) + \frac{dt}{\varepsilon(i, j, k) dy} [H_z^{n+1/2}(i, j, k) - H_z^{n+1/2}(i, j-1, k)] - \frac{dt}{\varepsilon(i, j, k) dy} [H_y^{n+1/2}(i, j, k) - H_y^{n+1/2}(i, j, k-1)] \quad (\text{AI.17})$$

$$E_y^{n+1}(i, j, k) = E_y^n(i, j, k) + \frac{dt}{\varepsilon(i, j, k) dz} [H_x^{n+1/2}(i, j, k) - H_x^{n+1/2}(i, j, k-1)] - \frac{dt}{\varepsilon(i, j, k) dx} [H_z^{n+1/2}(i, j, k) - H_z^{n+1/2}(i-1, j, k)] \quad (\text{AI.18})$$

$$E_z^{n+1}(i, j, k) = E_z^n(i, j, k) + \frac{dt}{\varepsilon(i, j, k) dx} [H_y^{n+1/2}(i, j, k) - H_y^{n+1/2}(i-1, j, k)] - \frac{dt}{\varepsilon(i, j, k) dy} [H_x^{n+1/2}(i, j, k) - H_x^{n+1/2}(i, j-1, k)] \quad (\text{AI.19})$$

AI.2 Total field/scattered field technique

Total field/scatter field technique in FDTD origins from the idea to reduce the calculation effort in realizing any source in the simulation, the plane wave is introduced, the total field /scattered field technique method arises. It eliminates the need for modeling the long duration excitation signals and it brings the possibility for cutting down the simulation volume.

Theoretically, the total field and scattered field technique assumes that in the FDTD calculation volume, E and H can be decomposed as total field, incident field and scattered field:

$$E_{total} = E_{inc} + E_{scat}, \quad H_{total} = H_{inc} + H_{scat} \quad (\text{AI.20})$$

Where, the index *inc* represents the incident value and *scat* represents the scatter field.

They are assumed to be known at all points of the space lattice at all time steps. These values are actually the field distribution value in the free field without existences of the scatters. Scatter values are unknown and are the results of the interaction of the incident wave to the objects in the space lattice. On the boundary of the two regions, the field values can be deemed as either total field or scatter field. By the definition, the boundary interface can apply plane wave to the total region or scatter region (Figure AI.3).

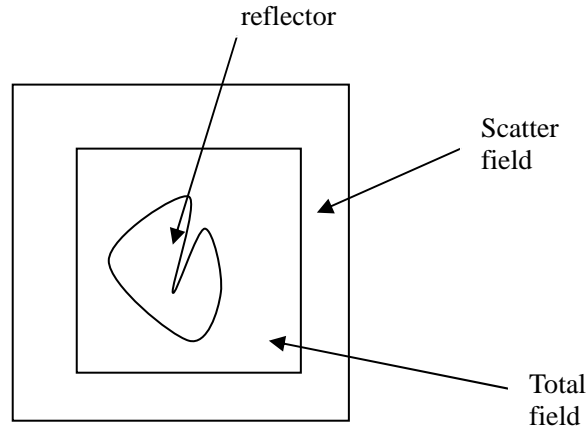


Figure AI.3 Total/ scatter field

One-dimension total field/scatter field configuration is displayed in Figure AI.4.

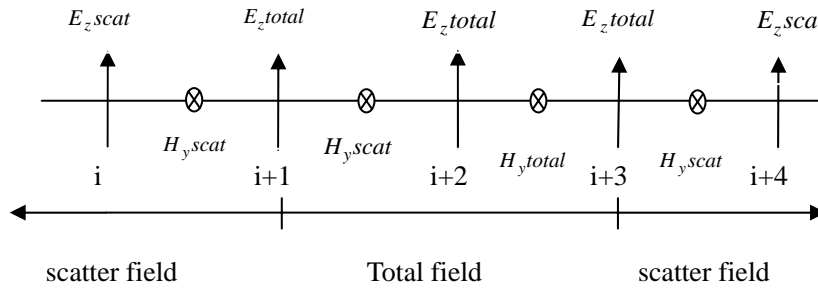


Figure AI.4 One-dimension of Total/ scatter field conception

The total field and scatter field are separated on position $i+1$ and $i+3$. Fields updates within the respective region with the same values (either all on scatter or on total). On the interface, we define it as total field, and then on the left interface, we have:

$$H_{y,scat}^{n+1}(i+1/2) = H_{y,scat}^n(i+1/2) + \frac{\Delta t}{\mu_0 \Delta d} (E_{z,scat}^{n+1/2}(i) - E_{z,total}^{n+1/2}(i+1)), \quad (\text{AI.21})$$

and

$$E_{z,total}^{n+1/2}(i+1) = E_{z,total}^{n-1/2}(i+1) + \frac{\Delta t}{\epsilon_0 \Delta d} (H_{y,scat}^n(i+1/2) - H_{y,total}^n(i+3/2)) \quad (\text{AI.22})$$

Since the field values are from different regions, it is inconsistent to perform the direct update. Modification should be made to the equations.

$$H_{y,scat}^{n+1}(i+1/2) = H_{y,scat}^n(i+1/2) + \frac{\Delta t}{\mu_0 \Delta d} (E_{z,scat}^{n+1/2}(i) - E_{z,scat}^{n+1/2}(i+1)) - \frac{\Delta t}{\mu_0 \Delta d} E_{z,inc}^{n+1/2}(i+1), \quad (\text{AI.23})$$

and

$$E_{z,total}^{n+1/2}(i+1) = E_{z,total}^{n+1/2}(i+1) + \frac{\Delta t}{\varepsilon_0 \Delta d} (H_{y,scat}^n(i+1/2) - H_{y,total}^n(i+3/2)) + \frac{\Delta t}{\varepsilon_0 \Delta d} H_{y,inc}^n(i+1/2) \quad (\text{AI.24})$$

By supplied with the incident values, the equations are consistent and fields in all the regions could be updated. On the left boundary, the same modification could be applied. For two-dimension and three-dimension cases, the same procedures are applied to all the fields' components.

AI.3 Huygens principle in FDTD

In propagation of the EMF, if plane wave is assumed, every point on the wave front can also be supposed to be sum of numerous EM wavelets [36]. If one virtual box could be constructed, on the entire surface, the tangential equivalent electric current and the tangential equivalent magnetic current at every point can be calculated using the DFTs applied to the FDTD-computed tangential H- and E-fields, respectively. Then these equivalent currents are integrated with the free-space green function to obtain far-field quantities. It is also the most common method in EMF computation for near to far field transfer.

AI.4 Non-uniform and sub-grids method in FDTD

In practical application, material and structure which need to be realized may have very different sizes. Precise modeling should simulate the delicate field distribution around tiny objects. If uniform coarse lattice is applied, some nuance structure may be neglected by the coarse mesh because the boundary can not be assured to coincide with the lattice. If the uniform fine lattice is applied, numbers of the cells are too enormous to be calculated. Also, for some places, the variability of the field is rather smooth and is unnecessary to utilize the fine lattice. One approach is to adopt the non-uniform grid, different resolution lattices are provided depending on the variability of the field distribution. There are two kinds of the non-uniform grids which are called as gradually changed non-uniform grids and local sub-grid techniques.

For the first method, the size of the grid varies gradually whilst the update time is the same. For the second method, the fine grids are only applied in local region. Update time for the local fine grid is $1/n$ for the coarse grid if ratio of the size of coarse grid to fine grid is n which is as shown in Figure AI.5

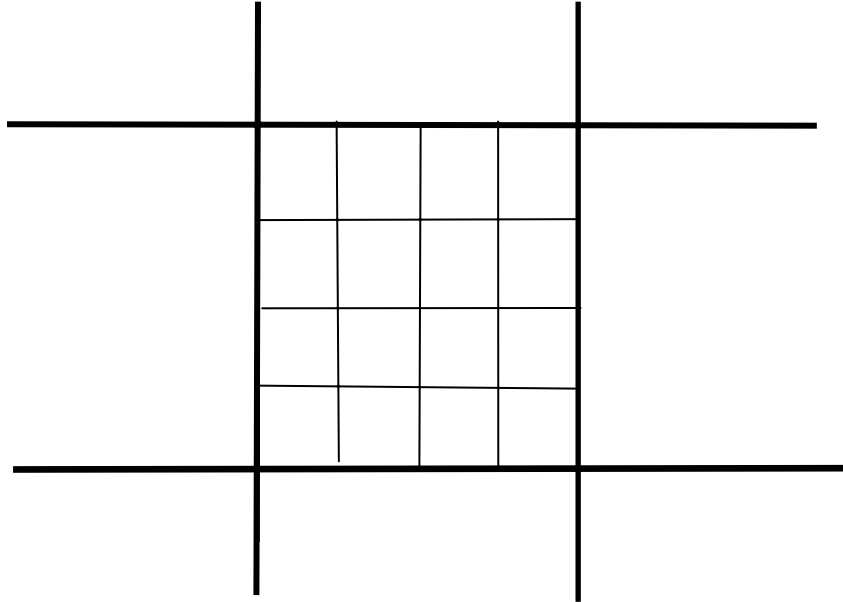


Figure AI.5. $n=4$ subgridding

Gradually changed non-uniform lattice have no obvious boundary among different sizes of lattices and it is easy to be realized. By comparison, the subgrid method has distinctive boundaries. Information transfer between the different sizes of grids is the key point in computation. Improper treatment between fine and coarse grid may result reflection. Several proposals are provided to eliminate the reflection from the boundaries. As shown in Figure AI.6..

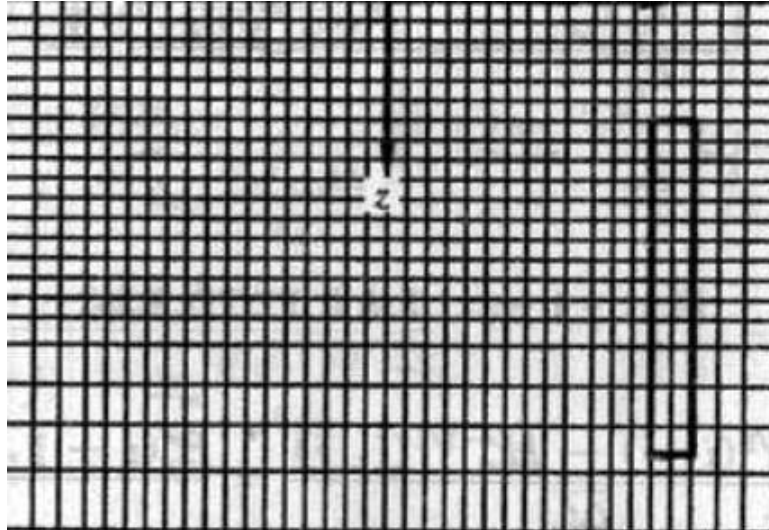


Figure AI.6 Gradually changed non-uniform lattice

Annex II Uncertainty evaluation principle

A Type A evaluation of standard uncertainty may be based on any valid statistical method for treating data. Examples are calculating the standard deviation of the mean of a series of independent observations; using the method of least squares to fit a curve to data in order to estimate the parameters of the curve and their standard deviations; and carrying out an analysis of variance in order to identify and quantify random effects in certain kinds of measurements.

Procedures for assessment of type A uncertainty can be concluded by the following example.

Consider an input quantity x_i whose value is estimated from n independent observations. $X_{i,k}$ of x_i obtained under the same conditions of measurement. In this case the input estimate x_i is usually the sample mean

$$x_i = \bar{X}_i = \frac{1}{n} \sum_{k=1}^n X_{i,k} \quad (\text{AII.1})$$

and the standard uncertainty $u(x_i)$ to be associated with x_i is the estimated standard deviation of the mean value:

$$u(x_i) = s(\bar{X}_i) = \left(\frac{1}{n(n-1)} \sum_{k=1}^n (X_{i,k} - \bar{X}_i)^2 \right)^{1/2} \quad (\text{AII.2})$$

Type B uncertainty is not measured statistically due to

- Measuring instruments not precisely calibrated
- Drift in a meter
- Constant offset, as due to background intensity
- Uncertainty quoted from manufacturer
- etc...

Type B evaluation of standard uncertainty is usually based on scientific judgment using all of the relevant information available, which may include: previous measurement data, experience with, or general knowledge of, the behavior and property of relevant materials and instruments, manufacturer's specifications, data provided in calibration and other reports, and uncertainties assigned to reference data taken from handbooks.

Procedure to analysis of type B uncertainty can be concluded as:

Annex II Uncertainty evaluation principle

- Convert an uncertainty quoted in a handbook, manufacturer's specification, calibration certificate, etc.
- Generally speaking, the uncertainty is either obtained from an outside source, or obtained from an assumed distribution.

Combined standard uncertainty

$$u_c = \sqrt{u_r^2 + u_1^2 + u_2^2 + u_3^2 + \dots} \quad (\text{AII.3})$$

Express experimental results in form

$$u \pm 2u_c \quad (\text{AII.4})$$

$U = 2u_c$ is called as expanded uncertainty

Factor 2 is called coverage factor, which means confidence interval is between

$u - 2u_c$ and $u + 2u_c$ with 95 % confidence interval

In the following part, the possible measurement uncertainty sources will be discussed in details.

Reference

- [1] Online (<http://www.ieee802.org/11/>)
- [2] Guidelines for Limiting Exposure to Time-varying Electric, Magnetic, and Electromagnetic Fields (up to 300 GHz), International Commission on Non-Ionizing Radiation Protection, 1998
- [3] WHO workshop on electromagnetic hypersensitivity (2004), October 25 -27, Prague, Czech Republic,
www.who.int/peh-emf/meetings/hypersensitivity_prague2004/en/index.html
- [4] COST244bis (1998) Proceedings from Cost 244bis International Workshop on Electromagnetic Fields and Non-Specific Health Symptoms. Sept 19-20, 1998, Graz, Austria
- [5] Bergqvist U and Vogel E (1997) Possible health implications of subjective symptoms and electromagnetic field. A report prepared by a European group of experts for the European Commission, DGV. Arbete och Hälsa, 1997:19. Swedish National Institute for Working Life, Stockholm, Sweden. ISBN 91-7045-438-8.
- [6] Rubin GJ, Das Munshi J, Wessely S. (2005) Electromagnetic hypersensitivity: a systematic review of provocation studies. *Psychosom Med.* 2005 Mar-Apr;67(2):224-32
- [7] Seitz H, Stinner D, Eikmann Th, Herr C, Roosli M. (2005) Electromagnetic hypersensitivity (EHS) and subjective health complaints associated with electromagnetic fields of mobile phone communication---a literature review published between 2000 and 2004. *Science of the Total Environment*
- [8] Staudenmayer H. (1999) *Environmental Illness*, Lewis Publishers, Washington D.C. 1999, ISBN 1-56670-305-0
- [9] Standard for Safety Levels with Respect to Human Exposure to Radio Frequency Electromagnetic Fields, 3 kHz to 300 GHz, IEEE Std C95. 1TM 2005
- [10] E Conil, A Hadjem, F Lacroux, M F Wong and J Wiart, 2008 Variability analysis of SAR from 20 MHz to 2.4 GHz for different adult and child models using finite-difference time-domain. *Phys. Med. Biol.* 53 1511-1525]
- [11] Chou, C. K., A. W. Guy, L. L. Kunz, R. B. Johnson, J. J. Crowley, and J. H. Krupp. 1992. Long-term low-level microwave irradiation of rats. *Bioelectromagnetics* 13:469-496.
- [12] Vijayalaxmi, and G. Obe. 2004. Controversial cytogenetic observations in mammalian somatic cells exposed to radiofrequency radiation. *Radiat. Res.* 162:481-496.
- [13] K.B Jung, T.H.Kim, J.L. Kim, H.J.Doh, Y.C. Chung, J.H. Choi, J.K.Pack 2008 Development and Validation of Reverberation-Chamber Type Whole Body Exposure

Reference

System for Mobile-Phone Frequency. *Electromagnetic Biology and Medicine*, 27:73-82, 2008

[14] Volkert W. Hansen, Member, IEEE, Andreas K. Bitz, and Joachim R. Streckert RF Exposure of Biological Systems in Radial Waveguides *IEEE TRANSACTIONS ON ELECTROMAGNETIC COMPATIBILITY*, VOL. 41, NO. 4, NOVEMBER 1999

[15] J. Streckert and V. Hansen, "Design of high-frequency exposure setups for the experiments in Bonn and Essen," in *Electromagnetic Compatibility of Biological Systems*, K. Brinkmann and G. Friedrich, Eds. Berlin, Germany: VDE-Verlag, 1997, vol. 5.

[16] A. Lerchl, H. Brendel, J. R. Streckert, A. K. Bitz, and V. W. Hansen, "Investigations on the effects of 900 MHz electromagnetic fields on growth, melatonin, and testicular cell composition in Djungarian hamsters," presented at BEMS Annu. Meet., St. Petersburg, FL, June 1998.

[17] V. W. Hansen, A. Bitz, and J. R. Streckert, "Electrically fully shielded, but mechanically easily accessible, rf-exposure system for a large number of small biological samples," presented at BEMS Annu. Meet., Long Beach, CA, June 1999.

[18] Mendes H.A. A new approach to electromagnetic field-strength measurements in shielded enclosures. In western Electronic Show and Convention(WESCON), Los Angeles, CA

[19] Slattery.K., Neal Jeffrey "A comparison of REVERBERATION CHAMBER and Semi-Anechoic Chamber Testing for Automotive Susceptibility" Digital Avionics Systems Conference, 1999. Proceedings. 18th, 10/29/1999

[20] Leo D. R., Primiani, M.V. "Radiated Immunity Tests: Reverberation Chamber vs. Anechoic Chamber Results" IMTC 2005-Instrumentation and Measurement Technology Conference, Ottawa, Canada, 17-19 May 2005

[21] Corona P., Ladbury J., and Latmiral G. Reverberation-chamber research- Then and now: A review of early work and comparison with current understanding. *IEEE Transactions on Electromagnetic Compatibility*, 44:87-94, 2002

[22] IEC 61000-4-21, " Electromagnetic compatibility (EMC)-Part 4-21: Testing and measurement techniques-Reverberation chamber test methods"

[23] M. Petirsche and A. Schwab, " Investigation on different methods to improve shielded room for EMO measurement," presented at the Proc. Mode-stirred chamber, Anechoic chamber and OATS Users Meeting, Vail, CO, 1997

[24] F. Leferink, J. Bourdenot and W. van Etten, "Experimental results obtained in the vibrating intrinsic reverberation chamber", *proc. IEEE Int. Symp. Electromagnetic Compatibility*, pp 639-644, 2000

[25] P. Corona, G. Latmiral, and E. Paolini "Performance and analysis of a reverberating enclosure with variable geometry", *IEEE Trans. Electromagn. Compat. Vol. EMC-22*, pp. 2-5, Feb. 1990

Reference

- [26] F.Leferink et al., "Test chamber," The netherland Patent WO 00/34 795, 1999
- [27] N.K.Kouveliots, P.T. Trakadas, and C.N. Capsalis, "FDTD Modeling of A vibration Intrinsic Reverberation Chamber", Progress In Electromagnetics Research, PIERS 39,47-59,2003
- [28] F.Leferink, D. Boerle, F. Sogtoen, G. Heideman, and W. van Eten, "In-situ EMI measurements using a vibration intrinsic reverberation chamber," in Proc. 14th Int. Zurich Symp. and Technical Exhibition on Electromagnetic Compatibility. Zurich, Switzerland: Swiss Federal Inst. Techol. Zurich, 2001,pp.653-658
- [29] D.A. Hill, "Electronic mode stirring for reverberation chambers," IEEE Trans Electromang. Compat., vol.36, no.4, pp.294-299,1994
- [30] J.S. Hong, "Multimode chamber excited by an array of antennas," Electronics letters, vol.29,no.19,pp.1679-1680,1993
- [31] D.Wu and D.Chang, "the effect of an electrically large stirrer in a mode-stirred chamber," IEEE trans, Electromagn. Compat., vol.31, no.2, pp.111-118,1989
- [32] J.S.Hong, "Effect of a modulated source on a multimode cavity," IEEE Microwave Guided Wave Lett. Vol.4,no.2, pp.43-44,1994
- [33] C. Bruns 2005 Doctoral thesis 2005 "Three-Dimensional Simulation and Experimental Verification of a Reverberation Chamber" Swiss Federal Institute of Technology, Zurich
- [34] J-S Rosnarbo, "Criteria of choice of mode stirred reverberation chamber" in Proc. 17th int. Wroc_law Symp. And Exhibition on Electromagnetic Compatibility. Wroc_law, Poland: Politechniki, Wroc_lawskiej, 2004, pp. 274-277.
- [35] Gibson, Walton C.:The Method of Moments in Electromagnetics Chapman & Hall/CRC, 2008. ISBN 978-1-4200-6145-1
- [36] Taflove A., Hagness S.C. 2005 Computational Electrodynamics: The Finite-Difference Time-Domain Method, 3rd ed. Norwood, MA: Artech House.
- [37] O. C. Zienkiewicz, R. L. Taylor, J.Z. Zhu : The Finite Element Method: Its Basis and Fundamentals Butterworth-Heinemann; 6 edition (March 21, 2005)ISBN 0750663200
- [38] <http://ww.feko.info>
- [39] <http://www.ansoft.com/products/hf/hfss/>
- [40] <http://www.cst.com>
- [41] Kane Yee. "Numerical solution of initial boundary value problems involving Maxwell's equations in isotropic media". Antennas and Propagation, IEEE Transactions on 14: 302–307. doi:10.1109/TAP.1966.1138693
- [42] F.Petit,"Modélisation et simulation d'une chambre réverbérante à brassage de modes à l'aide de la méthode des différences finies dans le domaine temporel", Ph.D dissertation, Université de Marne-la-Vallée, France, 2002

Reference

- [43] K.Harima and Y.Yamanaka,"FDTD analysis on the effect of stirrers in reverberation chamber," in Proc.Int .Symp.on Electromagnetic Compatibility.Tokyo, Japan: IEICE, 1999, pp.223-229.
- [44] K. Harima, "FDTD analysis of electromagnetic fields in a reverberation chamber," IEICE trans. Commun., E81-B, no.10,pp.1946-1950, Oct.1998.
- [45] L.Bai, L.Wang, B. Wang, and J.Song, "Reverberation chamber modelling using FDTD," in Proc. IEEE Int.Symp. on Electromagnetic Compatibility. Piscataway, NJ: IEEE, 1999,pp. 7-11.
- [46] F.Moglie, "Finite difference, time domain analysis convergence of reverberation chambers," in Proc. 15th Int. Zurich Symp. And Technical Exhibition on Electromagnetic Compatibility. Zurich, Switzerland: Swiss Federal Inst. Technol. Zurich, 2003, pp.223-228.
- [47] F.Moglie and A. Pastore, "FDTD analysis of reverberating chambers" in Proc. Int. Symp. On Electromagnetic Compatibility. Eindhoven, The Netherlands: Technische Universiteit Eindhoven, 2004, pp.6-11.
- [48] International Electrotechnique Commission 2001 EN 50361: Basic standard for the measurement of specific absorption rate related to human exposure to electromagnetic fields from mobile phones (300 MHz - 3 GHz)
- [49] Gati A., Wong M.F., Ibazizen A., Fouad Hanna V., and Alquie G. 1999, Combining neural networks and IIR filters for circuit microwave design and optimization in the time domain, IEEE MTT-S International Microwave Symposium Digest, Vol. 4, 1927-1930.
- [50] S. Haykin Adaptive Filter Theory, 4th Edition, Prentice-Hall, 2002
- [51] Ising H, Prasher D. "Noise as a stressor and its impact on health" Noise Health 2000; 2:5-6
- [52] Lagroye I. "Cancer, the immune system, differentiation, and the sensitivity of children: how supportive are the laboratory studies?" WHO Workshop, Istanbul, 2004
- [53] Balzano Q, Chou C , Cicchetti R, Faraone A and Tay R 2000 "An efficient RF exposure system with precise whole body average SAR determination for *in vivo* animal studies at 900 MHz" IEEE trans. Microw. Theory Tech. 48 2040-9
- [54] Sklar M. "Rayleigh Fading Channels in Mobile Digital Communication Systems Part I: Characterization" IEEE Communications Magazine 35 (7): 90–100, 1997
- [55] Kostas J.G. and Boverie B. "Statistical Model for a Mode-Stirred Chamber "EMC, IEEE Trans Vol33.4: 366-370, 1991
- [56] Kidal P.S., Orlenius C. 2005 18th International Conference on Applied Electromagnetics and Communications ICECom page:1-4.
- [57] Berdinas-Torres V. J. 2007 Exposure System and Dosimetry of Large-Scale *In Vivo* Studies Ed. Haartung-Gorre Verlag Kontanz
- [58] <http://www.brooks.af.mil/>

Reference

- [61] Hadjem A., Lautru D., Dale C., Wong M-F, Hanna V.F., Wiart J. "Study of Specific Absorption Rate (SAR) Induced in Two Child Head Models and in Adult heads Using Mobile Phones" IEEE Transactions on Microwave Theory and Techniques. Vol.53, No.1, January 2005
- [61] A. Peyman, A. A. Rezazadeh and C. Gabriel, "Changes in the dielectric properties of rat tissue as a function of age at microwave frequencies", Phys. Med. Biol. 46 1617-1629 doi: 10.1088/0031-9155/46/6/303, 2002
- [61] Uzman, L.L., and M.K. Rumley. 1958. Changes in the composition of the developing mouse brain during early myelinization. J. Neurochem. 3: 170-184.
- [62] Gabriel C. "Review Dielectric Properties of Biological Tissue: Variation with Age " Bioelectromagnetics supplement 7:S12-S18, 2005
- [63] Wang J., Saito T and Fujiwara O. "Uncertainty Evaluation of Dosimetry Due to Plastic Holder for Restraining Small Animal *in Vivo* Near Field Exposure Setup", IEEE, Transactions on Electromagnetic Compatibility Vol. 46, NO.2, May, 2004.
- [64] Anonymous, Guide to the Expression of Uncertainty in Measurement, International Organization for Standardization, Geneva, 1993.
- [65] Barry N. Taylor and Chris E. Kuyatt, Guidelines for Evaluating and Expressing the Uncertainty of NIST Measurement Results, Natl. Inst. Stand. Technol. Tech. Note 1297, Washington, 1994. Available on the Web at <http://physics.nist.gov/Pubs/guidelines/outline.html>. This is sort of a guide to the GUM.
- [66] John Taylor An Introduction to Error Analysis: The Study of Uncertainties in Physical Measurements, University Science Books, Mill Valley, California, 1997. (This excellent book does not teach or conform to the methodology of the GUM.)
- [67] Dmitry Chizhik, Jonathan Ling, Peter W. Wolniansky, Reinaldo A. Valenzuela, Nelson Costa, and Kris Huber (April 2003). "Multiple-Input–Multiple-Output Measurements and Modeling in Manhattan". IEEE Journal on Selected Areas in Communications 21 (3): 321–331. doi:10.1109/JSAC.2003.809457
- [68] Louis-Ray Harris, Takashi Hikage, Toshio Nojima, Masahiko Hirono, "A Numerical Estimation of Human Effects on Electric Field Distribution in Wireless Office LANS Using the FDTD Method", Proceedings of Progress In Electromagnetics Research Symposium(PIERS) 2008, p.635, Hangzhou, China, March 24-28
- [69] Stéphanie Mengué, Elodie Richalot and Odile Picon "Comparison Between Different Criteria For Evaluation Reverberation Chamber Functioning Using a 3-D FDTD Algorithm", IEEE Transactions on Electromagnetic Compatibility, VOL, 50, NO.2, May 2008
- [70] James Clerk Maxwell, "A Dynamical Theory of the Electromagnetic Field", Philosophical Transactions of the Royal Society of London 155, 459-512 (1865)
- [71] Kane Yee. "Numerical solution of initial boundary value problems involving Maxwell's equations in isotropic media". Antennas and Propagation, IEEE Transactions on 14: 302–307. doi:10.1109/TAP.1966.1138693

Résumé : Ce travail de thèse consiste en la conception et l'analyse d'un système d'exposition des animaux *in vivo* avec les signaux Wi-Fi dans une chambre réverbérante. La nouvelle méthode d'excitation est appliquée avec 6 antennes qui fonctionnent aléatoirement pour avoir un champ plus homogène et des ondes venant de toutes les directions. Cette configuration permet d'éviter une grande taille du brasseur de la chambre réalisée.

La répartition de puissance chez les rats est étudiée par la méthode hybride de simulation-mesure. La puissance incidente est enregistrée de même que le champ au centre de la chambre. Le rapport de la puissance incidente sur E carré moyenné est déterminé. La méthode FDTD est choisie pour la simulation et permet d'analyser la répartition de la puissance absorbée par les rats. La distribution du champ dans la chambre suit une statistique de Rayleigh comme il a été prouvé par les études et les mesures. Donc, la boîte de Huygens est utilisée pour émettre des ondes planes aléatoires (avec les paramètres suivant distribution Rayleigh) et exposer les rats. On peut alors obtenir le rapport de DAS pour le corps entier chez les rats sur E carré moyenné dans la chambre. Donc il est possible de relier le DAS corps entier chez les rats et la puissance d'entrée dans la chambre à E carré moyenné. Une autre méthode de simulation est aussi appliquée pour vérifier ce résultat.

L'évaluation de la variabilité des résultats pour plusieurs paramètres à différents âges des rats est effectuée. En générale, les sources de variabilité sont classifiées selon trois parties : simulation, mesure, et interface entre les deux. Le DAS corps entier chez les rats pendant toute la période d'exposition avec le domaine de variabilité sont présentés dans ce travail.

Cette étude pourra être utilisée afin d'évaluer des résultats d'une exposition à long terme des animaux. Elle pourra aussi servir à caractériser le champ dans des environnements domestiques et urbains.

Mots clés : *in vivo* exposition, Wi-Fi, DAS corps entier, chambre réverbérante, statistique Rayleigh, simulation, mesure, variabilité

Abstract: This thesis dedicates to design and analysis for the animal *in vivo* Wi-Fi exposure system by reverberation chamber. 6 random functioned antennas are deployed in the reverberation chamber to radiate the rats with homogenous field and Omni-direction waves. So, there is no significant size stirrer in the system.

Power absorption by rats is studied by the simulation-measurement hybrid method. In this method, by measurement, incident power and the mean squared E in the system are recorded. The ratio these factors are obtained. For simulation, FDTD is chosen to analyse the power absorption by the rats. E distribution in reverberation chamber is proved as Rayleigh statistics by studies and measurements. One Huygens box is constructed to radiate the rats. There is no need to realise the wall, the antennas and the accessories of the system. So the whole body averaged SAR can be obtained with the mean squared E in the chamber. Then whole body averaged SAR is linked with the incident power. One other method has also been applied to verify the results.

Evaluation of the result variability depending on different parameters of rats with different ages is performed. The variability comes from simulation, measurement and interface between these two parts. Whole body averaged SAR with the variability domain on function of the rat's age is presented in this thesis.

This work can be used to evaluate the long term animal exposition. It can also serve to characterise the field in modern domestic and urban environments.

Key words: *in vivo* exposure, Wi-Fi, whole body averaged SAR, reverberation chamber, Rayleigh statistics, simulation, measurement, variability